Offshore Pile Drilling from a Floating Vessel

A Dynamic Heave Compensation Assessment

Youri Thomas Ursem

Delft University of Technology

Offshore Pile Drilling from a Floating Vessel

A Dynamic Heave Compensation Assessment

by

Youri Thomas Ursem

Student number:	4440846	
Project duration:	February 2022 - December 2022	
Thesis committee:	Ir. A.C.M. van der Stap	TU Delft, Chair
	Dr. ir. P. van der Male	TU Delft, Supervisor
	Dr. ir. R.L.J. Helmons	TU Delft, Supervisor
	Ir. I.K. van Giffen	Boskalis NV, Supervisor
	Ir. R.J. van der Wal	Boskalis NV, Supervisor

Abstract

To fulfil the ever-increasing need for wind energy, European offshore wind farm sites are selected in deeper waters with seabed conditions which can consist of hard consolidated sediments or even rock. The deeper sites require the use of floating wind turbine foundations that are moored off to anchor piles in the seabed. For rock seabed sites, the anchor piles must be drilled. As the water depth of these sites increases, commercially available jack-up vessels are no longer able to operate. Therefore, the anchor pile drilling operation must be performed from the deck of a floating vessel. An extensive techno-economic analysis has led to the finding that a topside-operated drilling rig mounted on a large construction support vessel with heave compensation (HC) added is the most cost-effective configuration. The performed research focuses primarily on the determination of which HC method is most effective at changing water depths of 50 m up to 200 m. Leading to the understanding which site requires the use of active HC, limiting the resources required to construct future floating wind farms. The configurations are tested for relevant wave conditions, determined by assessing potential European floating wind farm sites.

Firstly, the research assesses the maximum allowable topside displacements before the drilling column reaches either the operational limits of plastic failure or bottom hole assembly lift-off. Secondly, the operational vessel motions are determined for the relevant environmental conditions. By comparing the results, the need for HC in the drilling configuration is determined. Third and finally, the passive and active HC methods are assessed for a 3-hourly time simulation under the before-mentioned environmental conditions. The assessment is performed using two performance criteria; weight on bit variation and the occurring drill-string stresses.

The performed analyses and simulations show that the vertical upward vessel motion is the limiting factor for the operations workability. Also, HC is required in every considered environmental condition. Further, the system operating with passive compensation shows a decreased stiffness with respect to the active system, most noticeable at 50 m water depth. This leads to higher frequency vibrations and stress variations being present in the drill-string of the active system. This effect is no longer noticeable for water depths larger than 50 m.

For locations with a water depth of 50 m, the active system shows favourable workability results. The active system shows a larger sensitivity to wave conditions with larger wave heights, as the stiffness is larger and more stress variations occur as a response. However, the results remain more favourable in comparison to the passive system as the lift-off percentage is significantly smaller. The passive and active systems show similar results when considering short waves in 50 m water depth, this is best witnessed in the weight on bit and lift-off percentages.

For locations with a water depth of 100 m and 200 m, the active and passive HC systems show comparable results for the performance criteria, for all considered wave conditions. The stresses remain within the ultimate limit state, the fatigue damage is negligible in comparison to the time required to perform the drilling operation, and the lift-off percentage for both configurations are in the same order. Therefore, as the workability of the two systems are so comparable for a water depth of 100 m and 200 m the availability, day-rate, and mobilisation complexity of the equipment will determine which HC system is most effective per project.

Preface

The past few months have been both challenging and rewarding. Finally, the result is a paper that I present with pride. A final accomplishment during my time at the Technical University of Delft, a place where I have had the chance to develop and grow both academically and personally. I have learned to push boundaries and have surrounded myself with loving friends who supported me to the end.

I would like to thank Ike van Giffen and Remmelt van der Wal for having the patience and energy to guide me through the jungle of performing a thesis research. Our weekly meetings and long sessions helped me to get the progress I wanted to achieve, even though I could be stubborn at times. My time at Boskalis has truly been great.

I would also like to thank my graduation committee, André van der Stap, Pim van der Male, and Rudy Helmons. The input I received on my work and the critical questions that were asked during our meetings sparked more interest in the topic and finally led to the improvement of the research and analysis of the work. Leading to a report which I present with pride.

Finally, to all my friends and family, thank you for sticking with me! You all know how much this means to me.

Enjoy every second you have ahead of you, Ciao!

Youri Thomas Ursem *Rotterdam, December 2022*

Contents

List of Figures

List of Tables

Nomenclature

Abbreviations

Abbreviation	Definition
AHC	Active Heave Compensator
BHA	Bottom Hole Assembly
BTS	Brazilian Tensile Strength
COG	Centre of Gravity
CSV	Construction support vessel
DCD	Direct Circulation Drilling
DDC	Dutch Drilling Contractors
DOF	Degree of Freedom
DP	Dynamic Positioning
DS300	300mm Drill-string
ESP	Specific energy
FEM	Finite Element Method
FLS	Fatigue Limit State
GSI	Geological Strength Index
JONSWAP	Joint North Sea Wave Project
KC	Keulegan Carpenter number
LDD	Large Diameter Drilling
MCA	Multi Criteria Analysis
NDOF	Multiple degree of freedom
NOAA	North Oceanic and Atmospheric Administration
PHC	Passive Heave Compensator
RAO	Response Amplitude Operator
RCD	Reverse Circulation Drilling
RMR	Rock Mass Rating
ROP	Rate Of Penetration
RQD	Rock Quality Designation
Std.	Standard deviation
UCS	Unconfined Compressive Strength
ULS	Ultimate Limit State
VIV	Vortex Induced Vibration
WOB	Weight On Bit
WTG	Wind Turbine Generator

Symbols

Symbol	Definition	Unit
A	Surface drill head	m^2
A	Cross-sectional area	m^2
A_{indent}	Surface indenter	m^2
c	Damping coefficient	Ns/m
$c_{critical}$	Crititical damping coefficient	Ns/m
C_D	Drag coefficient	-
d	Diameter	m
E	Young's modulus	N/m^2
e_r	Rotary specific energy	N/m^3
e_t	Thrust specific energy	N/m^3
F	Thrust	N
F_{cr}	Critical buckling load	N
f_d	Drag force	N
F_H	Horizontal component of thrust force	N
f_i	Inertial force	N
F_V	Vertical component of thrust force	N
f_y	Yield stress	MPa
H_s	Significant wave heigh	m
I	Moment of inertia	m^4
k	Wave number	m^{-1}
k	Spring coefficient	N/m
K	Effective length factor	-
k_{DS}	Spring coefficient drill-string component	N/m
L	Length	m
M_{BHA}	Mass bottom hole assembly	kg
M_{ds}	Mass drill-string component	kg
M_{rig}	Mass drill-rig	kg
m_L	Mass load	kg
N	Rotational peed	rpm
P	Tensional load	N
P_{max}	Maximum power	W
$P_{op.}$	Operational power	W
r	Radius	m
T	torque	Nm
T	Kinetic energy	J
$T_{max.}$	Maximum torque	Nm
$T_{op.}$	Operational torque	Nm
T_p	Peak period	s
u	Penetration rate	m/min
u	Current velocity	m/s
x_H	Heave displacement	m
x_L	Load displacement	m
ω	Wave frequency	rad/s
ω_d	Damped natural frequency	rad/s
ω_n	Natural frequency	rad/s

Symbol	Definition	Unit
ρ	Volumetric weight	kg/m^3
σ_c	Compressive strength	MPa
ζ	Wave function	m
ζ	Damping ratio	-
ζ_a	Wave amplitude	m

1
Introduction

1.1. Current state & problem statement

Following the Paris agreement, a large increase in sustainable energy is required. Sustainable energy comes in many forms, one type is the use of Wind Turbine Generators (WTG). As is visible in Figure 1.1, the amount of installed European turbines and the future ambitions are increasing rapidly. The Dutch government only has increased its installed capacity goal to 10.7 GW before the end of 2030.

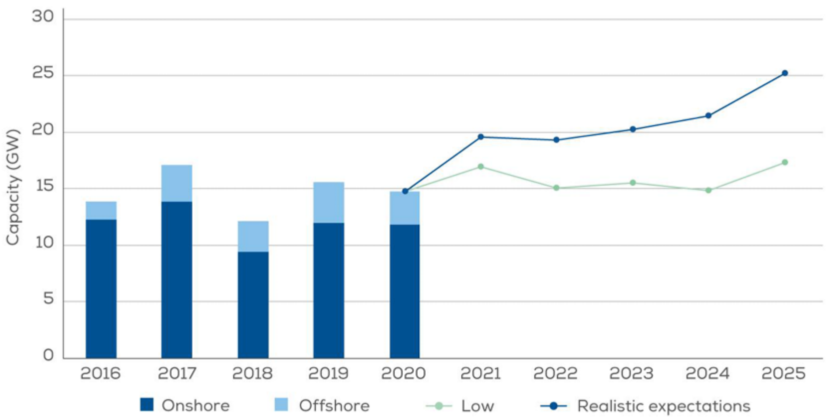

Figure 1.1: Yearly installed offshore wind capacity in Europe [78], expressed in Gigawatts.

The demand for wind farms is not only increasing in the Netherlands but in the whole of Europe, both onshore and offshore. This increase in installed capacity over the whole of Europe comes together with technological challenges, of which the most dominant challenge for the offshore sector is the shift to deeper waters. Due to the large number of wind farms already built, the potential wind farm sites which are still available are selected at harsher and, most importantly, deeper locations. These deeper locations require the technological revolution of the floating wind turbine foundation. These floating wind turbine foundations are expected to become more cost-effective in comparison to bottom fixed foundations when moving to water depths larger than 50 m [27], which makes it interesting for these future wind farms. For a floating turbine to maintain its position, it is secured to the seabed using long mooring lines. These mooring lines are connected and fastened to anchor points on the seabed. Anchor points can be created in multiple ways, one of them being by drilling a hole in the seabed and securing a foundation pile in the seabed. This option is most often used when the seabed consists of hard material such as rock.

To install such an anchor pile in rock seabed, a slightly oversized borehole is drilled to the desired depth. In the next step, the pile is placed inside the borehole and the spacing between the anchor pile and borehole is filled with grout, cementitious material which creates a strong connection between pile and rock. A drill rig would be installed on a Jack-up vessel in a shallow scenario due to its stability and low interaction with waves. However, due to the water depth increasing over 50 m these jack-up vessels can no longer operate, creating a need for floating vessels to take over. In the deep-sea oil and gas industry, drilling from a floating vessel has become a general approach. However, due to the larger number of boreholes required and the lower revenue per drilled hole, the use of drill ships is not an economically interesting option for such an operation. As a construction vessel is much smaller than an oil and gas drill-ship, wave excitation plays a more dominant role. Making it harder or even unable to drill in a safe and controlled manner without the use of motion compensation. A schematic representation of the drilling configuration and the components that come into play is provided in Figure 1.2.

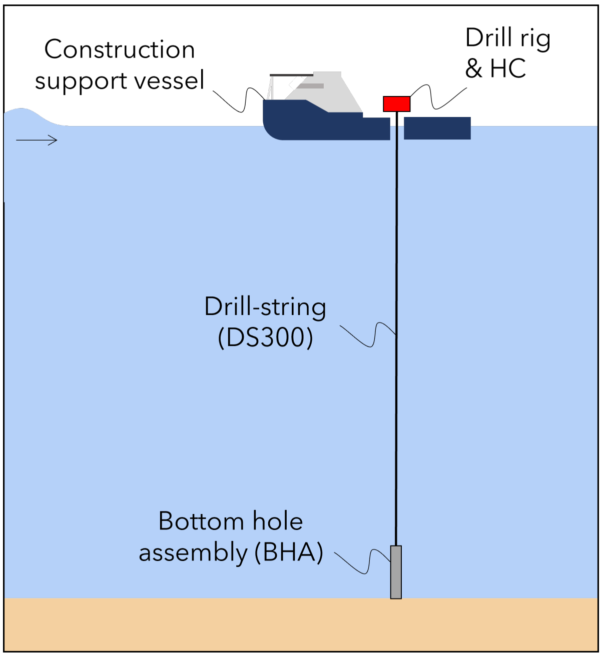

Figure 1.2: A schematic overview of each component in the drilling configuration.

When operating from a floating vessel, the drill-string dynamics play a critical role in the workability of the operation, these dynamics have been described by [25] [18] [34]. The drill-string stresses and drill head motions following these dynamics limit the operations workability. These occurring drill-string stresses can lead to plastic failure or, eventually, to fatigue failure [82]. Also, due to upward or horizontal vessel motions, the drill head can lose contact with the seabed described by [21] and [79]. The use of heave compensation is proven to increase workability for offshore lifting and installation operations from a floating vessel. The effect of heave compensation on drilling operations has already been described by [44], [16], and [17]. However, the applicability to the shallow water situation combined with a large bottom hole assembly mass (more than 30 tonnes) is to be assessed. Therefore, further research into the effect of heave compensation on the specific drilling situation is to be performed, and in particular the effect of heave compensation on the drill-string and drill head dynamics.

1.2. Research motivation & objective

This research is of commercial relevance for Boskalis. Researching the possibilities to compete with proven pile drilling methods and to discover the possibilities which go beyond the current operational limits, opening new opportunities to exploit. The social relevance is within the construction of deeper-lying floating wind farms to meet the demand for renewable energy while limiting the size and footprint of resources. The scientific relevance is to fill the knowledge gap on an optimised heave-compensated pile-top drilling installation operated from a floating vessel.

For the research into anchor pile drilling from a floating vessel, an initial literature study has been performed, presented in Appendix A. Finding the problems, future possibilities, and unknowns in the subject field. This literature review has been followed up by a market study and a techno-economic analysis which led to the most cost-effective drilling configuration, presented in Appendix D. This configuration consists of a large construction support vessel (length of more than 100 m and a crane capacity of more than 100 t) equipped with a topside-operated drilling rig, combined with a form of heave compensation. Following the previous work, the research question for the technical analysis can be formulated as:

What is the most effective heave compensation method for anchor pile drilling from a construction support vessel?

To answer this research question, specifications are made in the form of sub-questions:

1. Is the use of heave compensation a requirement within the drilling configuration, under the relevant design criteria?
2. Which operational characteristics limit the workability of the drilling operation?
3. What is the effect of water depth on the workability of the heave-compensated drilling configurations?
4. What is the effect of the present wave conditions and current on the workability of the heave-compensated drilling configurations?
5. What is the effect of the seabed conditions on the heave-compensated drilling configurations?

1.3. Research method

The research focuses on the application of a drilling methodology operated in European waters. Europe is selected specifically due to the high demand for floating wind farms and the extensive experience and information on offshore operations in the North Sea, Baltic Sea, and the near Atlantic Ocean. Following from the proposed European floating wind farm sites, the relevant water depths, environmental conditions, and seabed characteristics are determined. The research focuses on the use of drilled anchor piles in rock seabed and the use of alternative foundation methods will not be discussed.

The research scope is on the combination of a Boskalis vessel and existing and commercially available drilling and motion compensation assets to form a new drilling configuration. As mentioned, the selected drilling method follows from a techno-economic analysis that has been performed in previous research. The drilling methodology which is further researched is a pile-top drill rig that is mounted on a large construction support vessel, combined with a form of heave compensation. This research focuses on determining which form of heave compensation is best fitted in this drilling configuration. As a driving criterion, the effect a heave compensation method has on the operations workability. In its turn, the workability of the operation relates to the cost-effectiveness of the total drilling operation.

This research will first assess the maximum allowable topside displacements, both vertical and horizontal, before the drill-string exceeds the established operational limits. These operational limits consist of the occurring drill-string stresses reaching the ultimate limit state, or the bottom hole assembly reaching its lift-off point. The lift-off point is the equilibrium point at which the drill head loses contact with the seabed. Next, the operational vessel motions under selected environmental conditions will be assessed to prove the requirement of heave compensation in the drilling configuration. Finally, the passive and active heave compensation methods will be assessed using the performance criteria, during a 3-hourly time simulation under the before-mentioned environmental conditions.

2
Background

As mentioned in the introduction, an elaborate techno-economic analysis has been performed in previous work, which focused on finding the most cost-effective method to perform offshore anchor pile drilling from a floating vessel. In this chapter, this techno-economic analysis is summarised to provide the necessary background information. First, the market study is summarised per configuration component. Being the drilling concept, the available Boskalis vessels, and, finally, the heave compensation methods available. Next, the configuration selection process is presented, using both economic and non-economic criteria. Finally, the design criteria for this research are presented. Here the relevant pile design is presented and the European floating wind farm sites are assessed to form generalised environmental conditions. These conditions are further used to assess the difference in workability between the heave compensated drilling configurations. The actions which limit the workability are elaborated further in the research.

2.1. Market study

In this market study, only Boskalis vessels were considered. Also, only the equipment providers which are actively present on the market with proven technology were considered. Thus it can not be guaranteed that all globally available methods and/or prototypes have been considered. These providers are companies with which Boskalis has had contact in the past, or has worked with in the past but also companies that have performed similar operations for competitive contractors. The types of drilling equipment provided vary widely between the providers, which gives a broad view of what is available on the market. The Boskalis fleet gives a representative view of the available floating vessels on the whole market. Next to vessels and drilling equipment, also heave compensation methods have been assessed.

2.1.1. Drilling concepts

Following the performed market study, three drilling techniques have been selected for further analysis; the pile-top drill, the in-pile drill, and subsea drill. The pile-top and the in-pile drill, most likely, require a form of heave compensation due to the rigid installation on the operating vessel. The subsea drill is a self-operating drilling concept. Which is only connected to the operating vessel using flexible umbilicals. Considered providers of the pile-top drill are [61], [60], [22], and [64]. For the in-pile drill, the methods provided by [55] and [32] are selected. Finally, the subsea drill is assessed and the method of [56] is chosen. All methods are proven technology, however, the subsea drill has only been used in test operations.

2.1.2. Vessels

All information on the vessels in provided by [31] and is further presented in Appendix A. The available vessels for the drilling operation are;

- barge
- sheerleg
- heavy-lift barge
- construction support vessel
- heavy lift vessel.

The drilling configuration requires a crane with a capacity of at least 20 tonnes. Therefore, a barge can also be equipped with a crawler crane when no crane is mounted on the deck. Within the construction support vessels, a subdivision is made for *small* construction support vessels, and *large* construction support vessels. The distinction between *small* and *large* is based on the vessel length in combination with the available crane capacity. The *small* construction support vessel is found not to be able to provide enough deck space for the drilling spread and the foundation piles. It must therefore be combined with a barge to increase the available deck space and perform the operation. Every barge mentioned above is not able to displace itself from location to location, thus it must be accompanied by multiple tugs to be able to position itself correctly. Also, a barge is not able to actively keep position during operation, thus anchors and anchor handling tugs are required to operate.

2.1.3. Heave compensation

As discussed in the previous subsection, the pile-top and in-pile drilling methods require heave compensation to operate. Heave compensation is split into active, passive, and hybrid compensation. Only active and passive compensation are considered. Active heave compensation works through the measurement and processing of displacements, velocities, and accelerations. By counteracting these motions a stable position can be achieved through a designed feedback system. An example of a full active compensation method is a 3-degree of freedom (DOF) compensating platform. Passive heave compensation is heave compensation that works in a reactive and passive sense. This could for instance be through the use of a spring and damper, to dampen a system or change the resonance frequency and therefore minimise the motion for certain vessel motions or over the whole conditions. In this market study, two active heave compensation providers ([5] and [7]) have been selected which provide a compensating platform. For the passive heave compensation, [20] provides extensive information on the working and specifications of their assets.

2.2. Configuration selection

The *cost-effectiveness* of a concept was driving the configuration selection. Thus each criterion used in this assessment is linked to the cost or total duration of the operation. For these economic criteria, a multi-criteria analysis (MCA) has been performed. An MCA is a qualitative decision-making framework. When desired, the outcome can be substantiated quantitatively in further research. Balanced and weighted scores were given to multiple criteria to come to a final ranking [23]. Next, the non-economic criteria were compared per configuration in addition to the scored economic criteria. To give a broader view of the impact each configuration has.

2.2.1. Economic criteria

As the *cost-effectiveness* of a concept was driving the decision which configuration would be further analysed, each criterion was linked to the cost or total duration of the operation. For every individual scenario, an individual analysis was performed. The criteria and their weights are presented in Table 2.1.

Table 2.1: Economic criteria ranked on the effect the criterion has on the total costs of the operation.

#	Criterion
1	Cost per pile
2	Cycle time
3	Risk of operation
4	Logistical complexity
5	Vessel response
6	Required deck space
7	Mass ratio

2.2.2. Non-economic criteria

Next to the economic criteria, some non-economic criteria play a role in the methodology selection. The environmental risks are a driving factor, consisting of environmental damage due to noise, spillage, or physical interaction with flora and fauna. Also, the high emissions of the considered vessels can play a role.

In the field, fully electric and renewable propulsion options are developed. However, as the scope of the research is limited to the fleet of Boskalis NV these options are discarded from the consideration. Some of Boskalis' construction support vessels feature a hybrid engine, which can be used during peak power output. Making it interesting from an environmental point of view. As stated in [52], the engine noises of offshore construction vessels are all in the same order of magnitude. Not making a clear distinction as to which vessel has a higher negative impact on the environment.

When assessing the emissions of each vessel, both the emissions during transport and drilling operations can be considered. As stated above, no fully electric or renewable vessels are present in the considered fleet. Hybrid solutions are present, which have lower emissions and are thus more favourable. More detailed research into the emissions of each considered vessel is recommended in further research.

When assessing the drilling assets, each drilling asset is expected to emit a comparable amount of noise during drilling. The majority of the noise is emitted through ground-borne vibrations, therefore, the use of a bubble screen is not expected to have a large impact on the total noise. However, once a casing is required during drilling the pile-top and in-pile drill use a vibro-hammer to fasten the casing. This emits more noise into the environment than a subsea drill which rotates the casing. The in-pile and subsea drills have a higher risk of substance spillage, as the hydraulic fluids are connected to the drill using umbilicals. When an umbilical leaks or breaks, the surrounding water is exposed to the hydraulic fluid. When using a pile-top drill, the hydraulic hoses are situated on the deck.

2.2.3. Final selected configuration

Following the morphological chart presented in Figure D.2, multiple configurations are constructed. When considering all criteria, the configuration consisting of a **large construction support vessel combined with a pile-top drill and a form of heave compensation** scores best for all scenarios, due to the relatively high rate of penetration combined with relatively low risks and low operational costs. As a result of the cost-effectiveness analysis, the day rate of a heave compensation system is relatively very small in comparison to the day rate of the construction support vessel. The difference in day rate between active and passive systems thus has little effect on the cost-effectiveness of the operation when considering a similar workability outcome. Therefore, the system which shows favourable operational conditions is governing the cost-effectiveness of the operation.

2.3. Design criteria

To form possible configurations, the design criteria for the drilling configuration must be determined. First, the generalised pile design for which the methodology is developed is stated in Section 2.3.1. Finally, based on the ongoing trend towards floating wind farm sites, the reference sites will be discussed in Section 2.3.2.

2.3.1. Borehole dimensions

To determine the borehole size, the dimensions of the anchor pile are relevant. In this research, the pile design is considered to be fixed. The pile dimensions are constructed for a semi-submersible floating wind turbine foundation with a capacity of 8.0 MW positioned in water depths between 90 and 100 m, which must bear 13 MN. This floating foundation concept is moored using a catenary mooring system to the anchor pile. As result, the pile is dominantly loaded in the horizontal direction. The borehole dimensions are found by adding a spacing distance of 0.1 m around the circumference of the pile design. This spacing distance is required to fasten the pile in the seabed using grout. A schematic pile design together with the final borehole dimensions is presented in Figure 2.1.

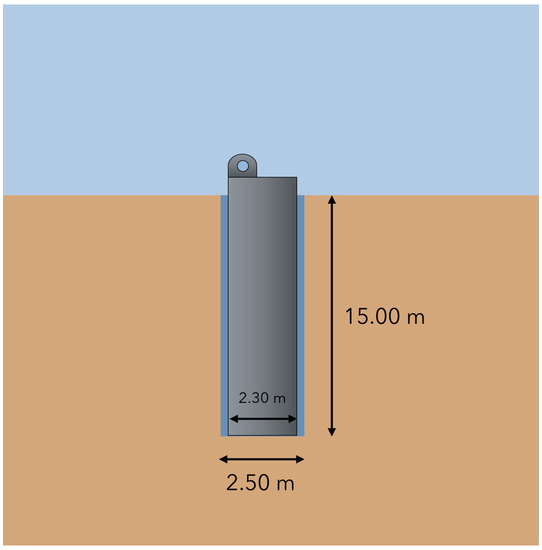

Figure 2.1: Schematic pile design and borehole dimensions

2.3.2. Considered locations

To come to a correct methodology, relevant environmental conditions are assessed for potential European floating wind sites. Using metocean and geological data, the following relevant criteria can be determined;

- water depth range
- significant wave height
- peak period
- bedrock strength

In total six proposed European floating wind sites are selected. European sites are chosen due to the large number of floating wind farms that are planned for construction (10 GW by 2030 [78]). Each selected site is publicly tendered by the local government as a floating wind farm site, creating relevance for mooring anchors at these locations. All sites are selected using software developed by 4COffshore [1]. In Figure 2.2 both the metocean and seabed sites are presented spread across Europe. In more detail, all characteristics per site are summed up in Tables E.3, E.2, and E.1. This data is used to determine the generalised scenarios used to assess each configuration.

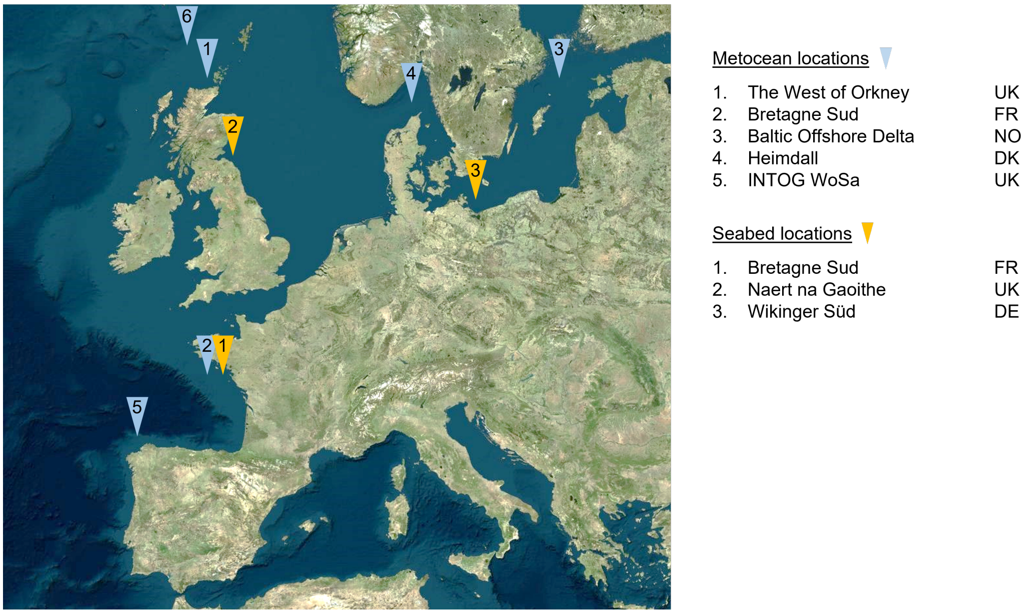

Figure 2.2: Map containing all metocean and seabed sites selected in Europe, modified from [49]. The metocean sites are potential floating wind farm sites that are to be built up to 2050.

Water depth

The selected sites mentioned above, are assessed for their bathymetry. In Table E.1 it is visible that the water depths and their ranges vary widely between the different sites. Generalised scenarios are defined to test the methodology for relevance. To define these scenarios, the sensitivity to the operation of a change in water depth must be assessed. Water depth influences the logistical deployment of equipment, the total loading on the drill-string or umbilicals by current, and the manner soil or rock react to an excavation device. When considering the combination of sites and the mentioned theoretical and practical changes, three relevant water depth scenarios can be distinguished. These scenarios are presented in Table 2.2.

Table 2.2: Generalised water depth scenarios used in further research.

Scenario	Water depth
WD_{50}	50 m
WD_{100}	100 m
WD_{200}	200 m

Metocean conditions

Next to water depth, the selected sites are assessed for their wave conditions. The specific parameters of the wave conditions determine the workability range for which lifting or drilling operations can be performed. Also, the DP system on a vessel is influenced by the wave specifics. The peak period is most interesting as this period holds the largest energy in the JONSWAP wave spectrum. This is determined using data from Aktis database [4], this data is next processed following the Wavewatch III method of NOAA [80]. The average significant wave height and the peak period for the summer months are presented in Table E.2, further, the conditions for two selected sites are presented in Figure 2.3.

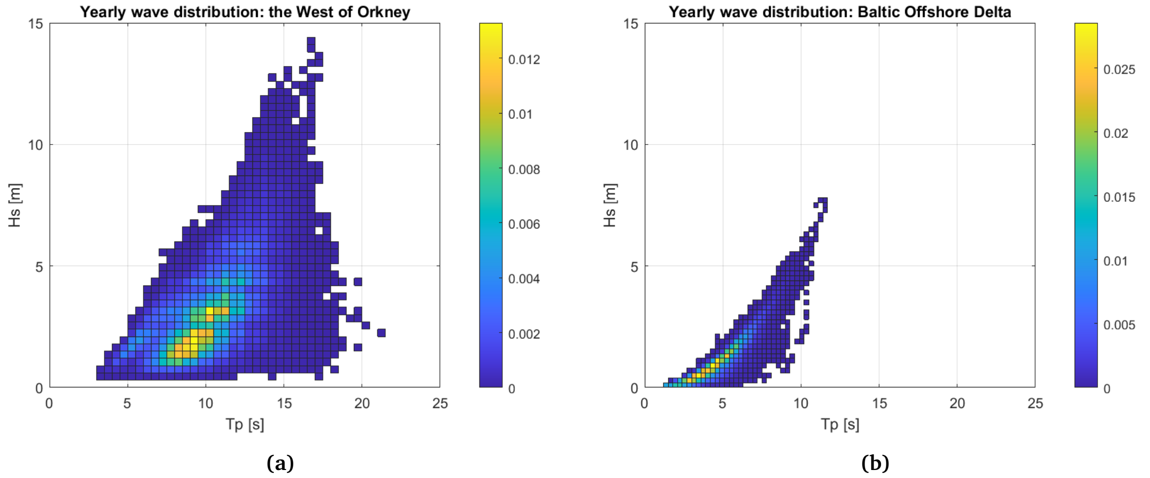

Figure 2.3: Two wave condition scatter plots presented for FOW site *The West of Orkney (a.)* and *Baltic Offshore Delta (b.)*, color-scaled per probability of occurrence. The sites in, the open, Atlantic Ocean (a.) and, sheltered, in In-land sea (b.) show a large difference in occurring waves. Using the conditions of all five selected sites, the generalised wave conditions are constructed.

When assessing the wave characteristics, three wave scenarios are formed. A single current velocity is selected, interchanging the peak period between 4.0 and 8.0 s and the significant wave height between 1.5 and 2.0 m. The characteristic values of the wave conditions are selected as criteria for the operational assessment and presented in Table 2.3.

Table 2.3: Generalised metocean conditions, relevant for potential European floating wind sites. The wave conditions are implemented in a JONSWAP wave spectrum during simulation.

Scenario	T_p	H_s	U_c
S1 - Short wave	4.0 s	1.5 m	0.0 m/s
S2 - Base case	8.0 s	1.5 m	0.0 m/s
S3 - High wave	8.0 s	2.0 m	0.0 m/s
S4 - Base case + current	8.0 s	1.5 m	0.5 m/s

Seabed conditions

Finally, the bedrock conditions at the selected sites are assessed. In the tendering phase, geological data is most often unknown. The scope of this research focuses on rock drilling, with or without an overburden layer. These two parts of the seabed conditions are split to come to relevant seabed scenarios. The scenarios are described using general parameters. The bedrock conditions for the three sites are presented in Table E.3.

When comparing the sites, it can be observed that both the UCS and RQD differ. To derive normative generalised bedrock conditions, two generalised scenarios can be formed. The methodology must be able to withstand peak UCSs in the bedrock, therefore the UCS range of the bedrock scenarios is chosen as higher than in the sites. Also, an extra bedrock scenario is added as a fictive possible scenario. Testing the possibilities for future projects in highly fresh and strong bedrock. The results of this derivation are stated in Table 2.4.

Table 2.4: Generalised bedrock conditions, relevant for potential European floating wind sites.

Scenario	UCS_{min}	UCS_{max}	RQD
Weak bedrock	5.0 MPa	10.0 MPa	Low (20% - 25%)
Medium strong bedrock	30.0 MPa	50.0 MPa	Medium (60% - 70%)
Very strong bedrock	100.0 MPa	150.0 MPa	High (80% - 90%)

For the overburden, the three sites all have multiple meters of overburden present. The composition of the overburden varies widely and is strongly location dependant. Here no generalised scenario is formed, only the presence of overburden is considered an extra scenario.

3

Model definition

To understand the working of the used model, some theoretical background is provided in the following subsections. Here also the modelling choices are presented and the assumptions and simplifications done in the modelling are discussed.

3.1. Geometric non-linear relation

To perform the geometric non-linear analysis, the OrcaFlex software (11.2) package by Orcina Ltd. is used to run simulations and perform extensive time analyses. In detail, the modelling of the vessel and drill-string are important to assess. As the vessel is excited by incoming waves, and the drill-string will be analysed for the occurring stresses and forces. The drill-string is modelled as a chain of elements. By increasing the number of elements, realistic results can be achieved. These nodes interact with each other and are solved numerically by iteration position, velocity, and acceleration for each degree of freedom over each time step. As geometric non-linearity is incorporated in this model, during each time step the local axes and coordinate system are updated for every degree of freedom. An axial displacement can lead to a transverse response. For this reason, the geometric non-linear analysis will contribute to a better understanding of the drill-string response. In Figure 3.1 the relation between nodes is presented. Here it is visible that the rotation (θ) is related to the axial position of the node with respect to the other nodes. Also, the axial spring holds both the z and x relation of the two interacting nodes. In this sense, all three degrees of freedom are related to one another.

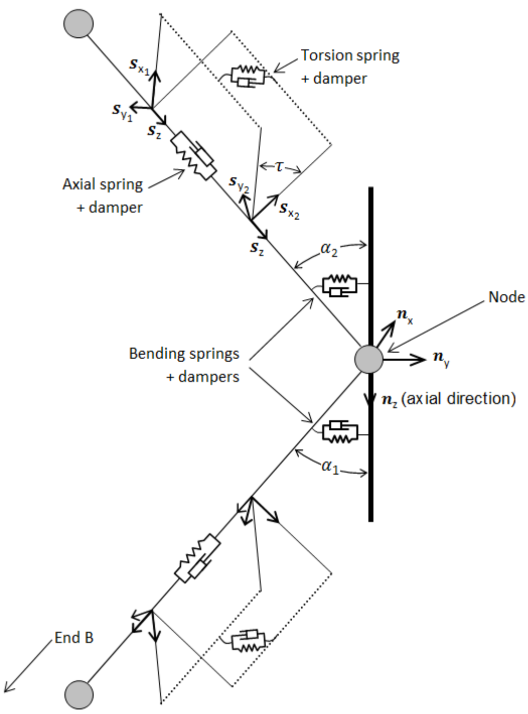

Figure 3.1: Geometric non-linear relation between nodes in the dynamic FEM analysis. Retrieved from Orcina Ltd. [57].

3.2. Researched parameters

In the creation of the model, certain parameters are set as constants and others vary per scenario. In this subsection, the relation between these parameters and the effect of a change in value is discussed. Figure 3.2 shows a schematic overview of all parameters investigated in this research.

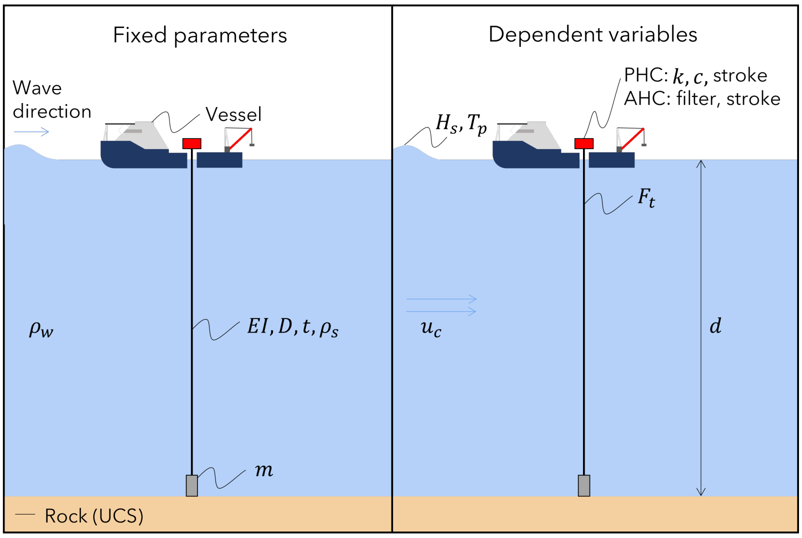

Figure 3.2: Parameters used in research, either fixed or variable per simulation.

3.2.1. Fixed parameters

The fixed parameters in the model are seen as the boundaries which the model operates within. Below the fixed parameters are described and the relevance to the research is discussed.

- Vessel design; the design of the vessel determines the response to wave loading and ultimately determines the motions of the topside. The design influences this response in two manners; the actual hull design and the draft at which the vessel operates. In this research, the vessel experiences wave loading head-on. The cross-sectional area of the vessel is one of the characteristics which influences the response, therefore, the operational draft is of relevance. A larger draft leads to a larger contact surface between the hull and waves and more loading. However, a larger draft is the result of heavier loading of the vessel. Which results in larger inertial forces required to excite the vessel. In the research, the design draft and loading condition of the vessel is considered.
- Position drill-rig on the vessel; in this research, the drill-rig is positioned at the moonpool. The moonpool is positioned on deck at the vessel's center of flotation. The displacements experienced at the position are a combination of multiple vessel motions and rotations. Thus selecting this position is relevant for the operational motions of the drill rig. By choosing this position at the CoF, the effect of pitch is minimised. When placing the drill rig at the stern of the vessel, the effect of pitch would be maximised and the absolute z-displacements will also increase during operation. Also when positioning the drill rig on the port or starboard side, the roll motion will have large effects on the absolute z-displacements experienced during operation (when the vessel is also loaded under an angle and roll occurs).
- Drill-string cross-section; in this research, the diameter and wall thickness are set to be constant. These characteristics are selected following in-field information. When increasing the wall thickness, pipe diameter, or both, the stiffness of the drill-string increases.

Leading to a larger sensitivity for stresses as a result of bending moments. This stiffness is represented by the moment of inertia (I). Further, the value EI that is presented in Figure 3.2 is the moment of inertia multiplied by Young's modulus, a constant parameter.

- Rock UCS; in this research, a rock strength of 30.0 MPa is selected. This rock strength is determined by assessing European wind farm sites which are constructed on a seabed consisting of rock. Following the rock strength and a penetration depth of 1.0 mm, the weight on bit (WOB) required to maintain production is found to be 20 tonnes. The determination of this required weight on bit follows the theory presented in Appendix A. When increasing the rock strength, the required WOB also increases.
- Mass bottom hole assembly; in this research, the mass is fixed for every simulation. In reality, the mass of the BHA is larger than the required WOB. As a result, the drill-string is pre-tensioned to obtain the required operational WOB. By changing the BHA mass and keeping the WOB constant, the pre-tension in the drill-string can be altered. By increasing the pre-tension in the drill-string the sensitivity to compressive failure is decreased.
- Wave direction; in this research the wave direction is considered fixed. This wave angle is set at 180°, which is the head angle of the vessel. This is the design wave angle, which leads to favourable vessel excitation. By considering this angle, the roll of the vessel is disregarded. Due to the positioning of the drill rig at the moonpool, the effect of roll is minimised in the absolute z displacements. However, larger displacements are expected when including a directional spread of the incoming waves, with respect to the single wave angle used in the research.

Table 3.1: Fixed parameters used in the model, meaning that these parameters stay constant over all simulations performed.

Parameter	Value	Unit
D	310	mm
t	14.5	mm
M_{BHA}	30	t
E	211	GPa
I	31.2 e3	kNm^2
ρ_s	7850	kg/m^3
ρ_w	1025	kg/m^3
UCS	30	MPa

3.2.2. Dependant variables

Next to the fixed parameters, there are variable parameters that differ per simulation. By changing these parameters, the response of the considered system can be analysed. The variables parameters are presented below.

- Water depth (d); in this research three water depths are assessed. These water depths are 50 m, 100 m, and 200 m. The selection of these water depths is presented in Section 2.3.2. By changing the water depth, the slenderness ratio of the drill-string differs. Also, following a performed linear analysis, the stiffness of the drill-string decreases for an increasing drill-string length. Therefore, the response to induced motions is different per water depth and this parameter is interesting to research further.
- Wave conditions (H_s & T_p); in this research, three wave conditions in a JONSWAP spectrum are used to perform time analyses. The wave conditions determine the vessel excitement by the peak period (T_p) and significant wave height (H_s). The selection of these

wave conditions is presented in Section 2.3.2. When investigating the heave response amplitude operator (RAO) of the considered vessel for the wave angle (head, 180°), it can be seen that for an increased peak period the response also increases (presented in Figure F.12). Also, a larger wave height leads to a larger excitation of the vessel for the same wave period and length.

- Current (u_c); in this research current is only added to one scenario. Here a current with a constant velocity of 0.5 m/s is added to the base case wave spectrum. The current works constantly over the whole length of the drill-string. This is a simplification as in reality, the current may differ in magnitude and direction over the length of the drill-string. A multi-directional current can lead to the drill-string being deformed in multiple directions over the length. Which can trigger a deformation in this shape when loaded compressive.
- Heave compensation; as the research question focuses on determining the most effective heave compensation method, the heave compensation is altered between passive and active heave compensation. The working of each system is described in the following subsection.
- Pre-tension (F_t); as mentioned the pre-tension is used to maintain a constant WOB per simulation. The pre-tension is dependent on the water depth, as the total self-weight of the drill column increases for a larger water depth. Therefore, a larger pre-tension must be applied at the top of the drill-string to experience the same WOB. In reality, this pre-tension can be altered during operation to increase or decrease the WOB, if required to increase production. However, during the simulations, this pre-tension is kept constant.

Table 3.2: Dependant variables used in the model, the environmental inputs are not included in this Table but presented in Section 2.3.2.

Parameter	Value	Unit
$F_{t,50}$	15	t
$F_{t,100}$	20	t
$F_{t,200}$	30	t

3.2.3. Independent variables

Finally, the independent variables are determined. These form the criteria which are used to assess the working of each simulation or scenario. These independent variables are thus the outcome of a scenario created using the above-mentioned fixed parameters and dependent variables.

- Maximum allowable stress; in this research, the ultimate limit state is assessed as the maximum allowable stress before plastic deformation occurs. Following the DNVGL-OS-C101 guidelines (Chapter 4, page 19), the ultimate limit state corresponds with a stress of 265 MPa. Which is the factorised yield strength of the drill-string material (S345 steel).
- Lift-off; in this research, the serviceability limit state is assessed as the point at which the bottom hole assembly is lifted off the seabed. As this is a limiting operational phenomenon. This is translated to the lift-off percentage which is determined over the time-series simulations. Lift-off is influenced by the weight on bit. As the weight on bit represents the load that acts on the seabed, in the static situation this is equal to the load required to lift the bottom hole assembly of the seabed. A tensional stress of 21.64 MPa

is required in the drill-string just above the bottom hole assembly to realise the lift-off of a bottom hole assembly weighing 30 tonnes.

- Weight on bit variation; in this research, the operational parameter weight on bit determines the production efficiency. Variations in weight on bit lead to decreases in production efficiency and increases in local stress as the combination of compressive and shear stress act simultaneously. This stress increase is unfavorable for the operation.
- Fatigue damage; in this research, the fatigue damage is used to compare the simulations. As large fatigue damage leads to a larger downtime of the operation as a result of material maintenance. Here only the fatigue in the drill-string is assessed at the point where the largest stresses occur.
- Workability; the workability of an operation is determined by the most limiting actions during the operation. As in this research, only the operational section is considered where the drill has contact with the seabed. This workability is limited by the first two variables mentioned in this section: the maximum allowable stress (ULS) and lift-off (SLS).

3.3. Modelling of drilling method components

In this section, the modelling of each drilling method component is discussed. Here also the assumptions and limitations which are connected to the modelling approach are presented. The effect of these assumptions and limitations is further discussed in the discussion of the results in Chapter 5. A general overview of the two heave compensation methods used is presented in Figures F.1 and F.2.

3.3.1. Vessel

In this research, the BOKA Ocean [31] is considered as the operational vessel. This is a large construction support vessel that is often used for comparable offshore installation operations. This vessel is modelled using the panel method and this model is provided by Boskalis Westminster NV. During the simulations, the vessel is loaded by head waves only. Thus meaning that the waves all have a direction of 180°. In this way, the drill-string motions can be analysed in 2D, this also has as result that only heave, pitch, and surge are relevant vessel DOFs. This is under the assumption that the vessel is perfectly longitudinally symmetric, in reality, this will never perfectly be the case. However, the magnitude of forces following these imperfections is neglectable. Also in reality the vessel will not experience loading perfectly from the head direction, waves under an angle will also be present. The loading by these waves can lead to larger absolute motions at the drill-rig position. When considering waves under an angle, a combined motion of roll and sway can become relevant for the drill-rig motions. Figure 3.3 shows a schematic representation of the drill-rig positioning on the vessel and the direction of the incoming waves.

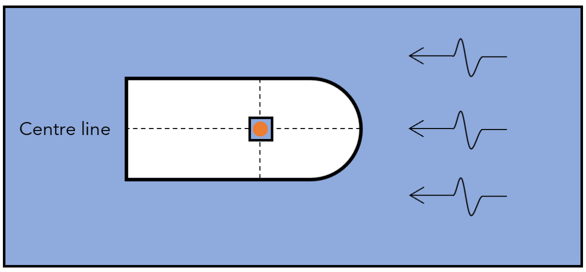

Figure 3.3: Schematic representation of the drill-rig position on the vessel, and the direction of the incoming waves.

3.3.2. Heave compensation

The passive heave compensator is modelled using a spring-damper system. Here the spring and damping coefficient (k and c respectively) are tuned to maintain the pre-tension and are non-constant values. Meaning the value of k and c are dependent on the displacement and velocity respectively. By adding this component to the total drilling methodology, the stiffness of the whole system is affected. The stroke of the passive heave compensator is 4.0 m, during operating in the considered wave conditions the maximum stroke is never reached. The efficiency of the heave compensator is determined using empirical data provided by [20]. Using this information, the most realistic working and efficiency of the system is simulated. Further optimisation of this system is out of the research scope.

The active heave compensator is modelled by modifying the vessel RAOs for the compensated DOFs. Information provided by [7] is used to determine the filtering efficiency of the heave compensator. The filtering percentage is determined by considering a similar drilling operation in deep water performed in the Gulf of Mexico. Here the vessel motions and platform motions have been compared over the full operational period. Following these results, a compensation of 95% is guaranteed as efficiency for wave spectra with a significant wave height of up to 2.0 m. As the operations are researched within the stated boundaries, this filter percentage is implemented in the heave, pitch, and roll RAOs. The expectation is that, in reality, the active heave compensation system has a smaller efficiency for waves with smaller periods, as the response time becomes limiting in the reaction to short waves. However, the RAO of the considered vessel shows little response to waves with short periods. The absolute excitation of the vessel will be small for short waves. These small motions lead to an extremely small contribution to the total stresses experienced by the drill-string. Therefore, the efficiency is chosen to be constant over all peak periods and significant wave heights researched. The modified vessel RAOs are presented in Figure F.9.

Assumptions

When modelling the heave compensation systems, the following assumptions are made;

- the active system operates within the boundaries of its stroke length
- the active systems damping efficiency is constant at 95% for all wave periods and wave heights researched
- the passive systems tuning is representative in the provided information by [20].

3.3.3. Bottom hole assembly

As lift-off is a limit for the operation, the bottom hole assembly can be modelled as fully clamped in the model. Here the mass of the bottom hole assembly thus is not relevant for the drill-string motions and stresses. However, to determine the lift-off point and the weight on bit experienced during operation the mass plays a role. The mass of the bottom hole assembly (BHA) is set to be constant at 30 tonnes for every simulation. This mass is used to construct the weight on bit experienced during operation. The mass of 30 tonnes is determined using the information provided by [61], [62], [64], and [22] combined with the required weight on bit to drill the selected rock.

Assumptions

When modelling the bottom hole assembly, the following assumptions are made;

- the lift-off point is determined disregarding the added mass, inertial component, and hydrodynamic dampening experienced during the actual lift-off of the BHA.

3.3.4. Drill-string

When determining the detail in which the model must represent reality as closely as possible. In this research, a DS300 drill-string is used. Which is constructed with 3.0 m segments which are connected using a bolted connection. The drill-string is modelled as a homogeneous pipe with a constant cross-section of 310 mm and a wall thickness of 14.5 mm, as presented in Figure 3.4. Here imperfections in the material and pipe design are assumed to be non-present. In reality, imperfections can lead to increased sensitivity to stability issues such as buckling or local plastic deformation due to stress hot spots. The flanges used for the bolted connections increase the local bending stiffness of the drill-string, which is not taken into account in the homogeneous pipe model. As described by [66] a result the local stresses due to bending moments near the bolted connection can increase. The amount of modelled nodes must be determined to correctly model the drill-string. The research focuses both on large displacements and higher frequent vibrations. The number of nodes is kept constant per water depth scenario. In the analyses, simulation time becomes limiting, due to the large number of simulations that are performed. By varying the number of nodes and comparing the results, an optimum is found for 200 nodes, presented in Table G.1. The amount of nodes is kept constant between all simulations. The nodes interact with each other in a geometrical non-linear relation. Updating the position of each node and therefore updating the local coordinate system during the simulation. This relation is incorporated in the OrcaFlex model provided by Orcina Ltd. The applied pre-tension combined with further tensioning or relieving due to vessel motions determine the actual tension during operation. This tension stiffening influences the eigenfrequencies of the system. Also, structural damping is incorporated in the OrcaFlex model.

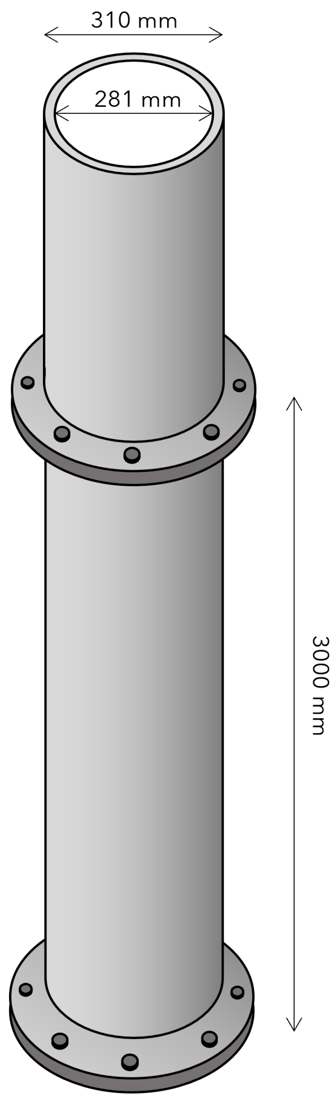

Figure 3.4: Schematic representation of the DS300 drill-string segment, *schematic is not to drawn to scale*.

Assumptions

When modelling the drill-string, the following assumptions are made;

- the drill-string is assumed to be flooded with seawater up to the sea level
- the drill-string is expected to experience dynamic effects due to topside displacements, therefore, added mass and hydrodynamic damping are incorporated in the model
- VIV are not incorporated in the dynamic drill-string model but assessed separately
- the drill-string is modelled as a homogeneous pipe with a self-weight and buoyancy
- the local increase of stresses around the bolted flanges is neglected and not researched
- the torque required to operate the drill head can be delivered during the entire simulation.

4

Research method

To answer the research question, multiple steps are taken. First, a decoupled analysis is performed to assess the requirement for heave compensation in the drilling method. Here the limiting topside displacements are determined and compared with the maximum vessel motions which occur during operation. Next, the validation of this decoupled analysis is presented. Further, the operational stresses and motions of the drilling components are analysed. Finally, the relevance of a static, eigenvalue analysis is presented. A flowchart of the steps leading to answering the research question and its sub-questions is presented in Figure 4.1.

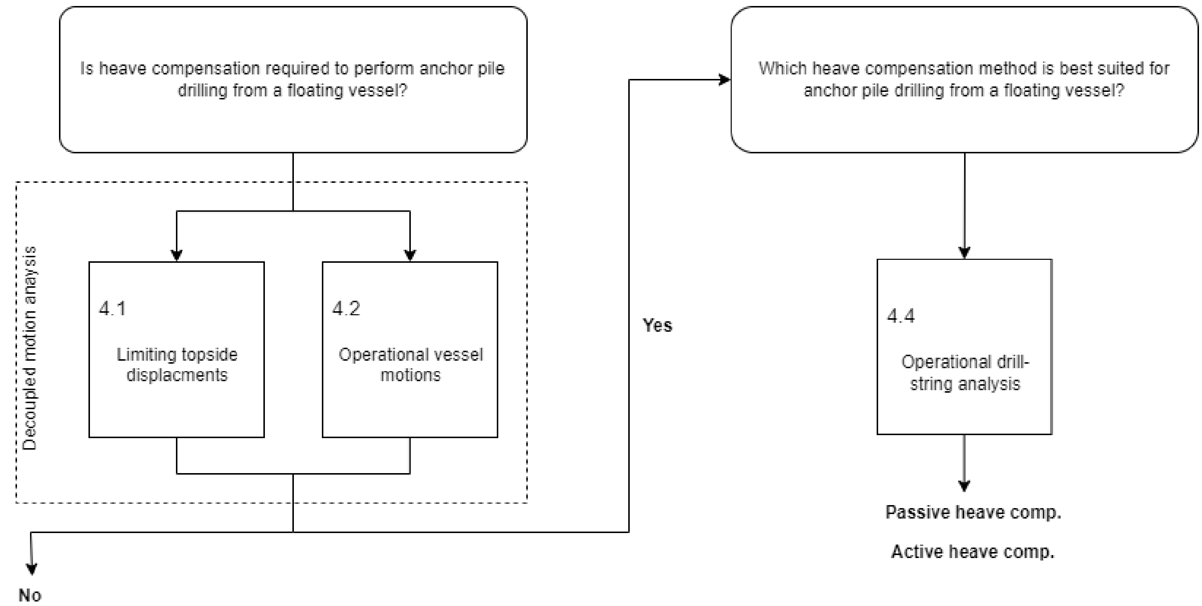

Figure 4.1: Research method deconstructed per section and presented in the form of a flowchart. The steps lead to the answering of the research question.

4.1. Limiting topside displacements

First, the limiting topside displacements must be determined at which the configuration is no longer operable. To find these limiting topside displacements, in both vertical (z) and horizontal (x) directions, criteria must be formulated. The first criterion is the ultimate limit state which may not be exceeded, described by DNVGL-OS-C101 guidelines (Chapter 4, page 19). The second is the lift-off point. Summed up, the criteria are;

- drill-string stresses may not exceed the ULS
- bottom hole assembly must remain in contact with the seabed.

As stated both the horizontal and vertical directions are assessed, and both are tested against the above-mentioned, criteria. The resilience of the drill-string is described as the geometric flexibility of the drill-string and is determined using the geometric non-linear dynamic approach. By displacing the top (clamped) of the drill-string in either the vertical downward, vertical upward or horizontal direction, the stress can be monitored per topside displacement. Depending on the direction, the limiting criteria are selected. The three directions and the matching criteria per mode are schematically presented in Figure 4.2. This simulation is performed for multiple drill-string lengths of 50 m, 100 m, and 200 m.

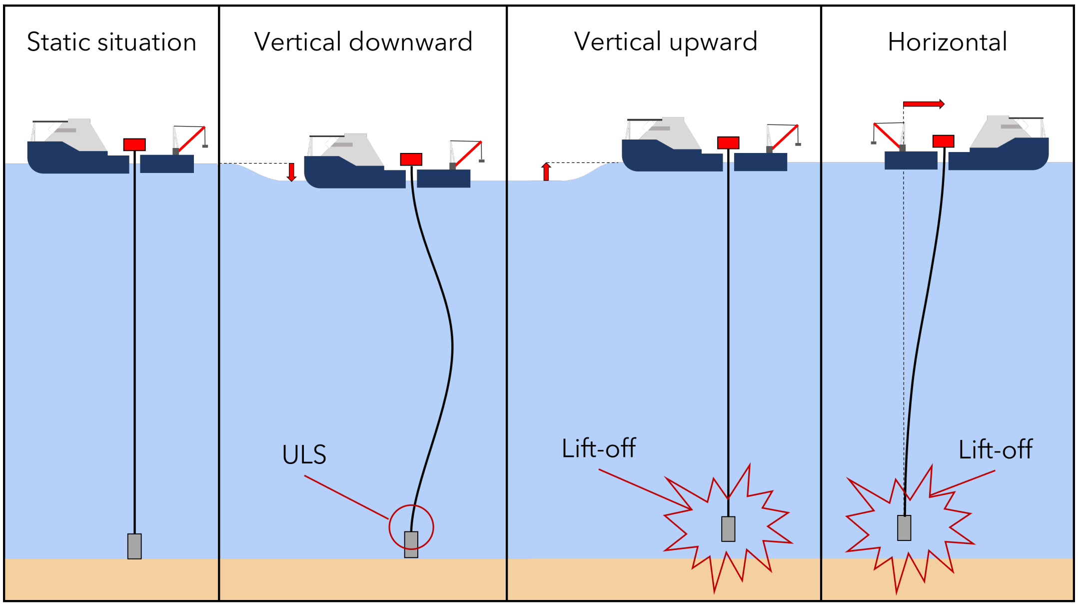

Figure 4.2: Limits determined per vessel motion, each motion has an individual criterion which determines the limiting motion.

The maximum allowable vertical downward displacement simulation is performed for multiple constant velocities. Following a dynamic Orcaflex simulation, the topside velocities are derived for the BOKA Ocean under the base case wave conditions. The mean downward velocity can be determined to be 6.25 m/s. The velocity plays a role in the numerical determination of the displacements and stresses during the simulation. To assess this influence of velocity, multiple velocities are assessed. The governing compressive measuring point for ULS is selected just above the clamped bottom hole assembly. Quantitative validation for this approach is presented in Appendix G. As the largest stresses occur at this location for all the buckling shapes (modes) and the self-weight of the drill-string is maximum at this location.

For the vertical upward and horizontal simulation, a single velocity of 0.25 m/s is set. Because these simulations are tensional, the numerical determination and the following instability issues do not play a role. The lift-off point is determined by measuring the stresses just above BHA and determining the equilibrium point where the tensional stress equals the stress as a result of a freely hanging bottom hole assembly (30 tonnes). At the point where these stresses are equal, the drill head loses contact with the seabed, and lift-off is achieved. This is a static equilibrium and dynamic effects are not taken into account in this assessment of the lift-off point, meaning this is a conservative approach

4.1.1. Assumptions and simplifications

In the method determining the limiting topside motions, the following modelling assumptions are made;

- the vessel and drill-string are present in still water and experience no current or wave loading
- both the top and bottom of the drill-string have a clamped connection to the seabed and vessel.

4.2. Operational vessel motions

The operational vessel motions in the vertical (z) and horizontal (x) are determined for the wave spectra described in Section 2.3.2. The selected wave spectra are each unique and must be assessed individually. In this analysis, the vessel is modelled as freely floating and only experiences loading of the incoming waves in the head direction (180°). Here the second-order wave drift force is not incorporated and the vessel moves around its mean position. In reality, the vessel will maintain its position through dynamic positioning to withstand this drift force, this drift force will vary over time and a small horizontal motion will stay present. This horizontal motion is not incorporated into the model. The motions are determined at the drill-rig location, as described in Figure 3.3. To compare the motions with the limiting topside displacements, these are translated to the vertical (z) and horizontal (x) displacements at the drill-rig position. These displacements are a result of the heave, pitch, and surge motions of the vessel. To determine these values, the considered vessel is loaded by the three selected wave spectra for a time series of 3 hours. Which statistically leads to the determination of the occurring maxima.

4.2.1. Assumptions and simplifications

In the method determining the operational vessel motions, the following modelling assumptions are made;

- the vessel only experiences loading as a result of the determined wave conditions
- current loading is not taken into account in the determination of the operational vessel motions
- the influence of water depth is disregarded, as the vessel operates in deep water
- wind loads are not taken into account in the determination of the operational vessel motions
- the second order wave drift force is not taken into account in the determination of the operational vessel motions.

4.3. Validation decoupled approach

To determine if heave compensation is required at all, the allowable topside displacements are compared with the operational vessel motions. Here a decoupled approach is used, in the sense that the vertical (z) and horizontal (x) motions are assessed individually. In reality, the vessel will displace in a coupled manner, meaning that the vessel simultaneously shows a displacement in z, x, and θ (pitch). In this assessment, the rotation (θ) and resulting stresses are not considered. Once the decoupled motions are all within the maximum allowable displacements, the rotation and coupled displacements are considered. From analysing the vessel motions in the time analysis, the maximum vertical (z) and horizontal (x) displacements do not occur simultaneously. However, the maximum stress which could occur in the drill-string is during a simultaneous maximum vertical and horizontal displacement.

The stresses following from vertical and horizontal topside displacement can be superpositioned to determine the total stress in the drill-string when the stresses have a linear relation to the topside displacement. This is only the case for vertical upward motion. However, to assess the requirement for motion compensation, all possible combinations of the vertical and horizontal motions must be within the criteria, thus all individual motions must also be within the criteria. As the stresses due to vertical downward and horizontal motion are not linear with the displacement of the vessel, the combination of vessel motions can only be superpositioned by linearising the stresses at the desired point.

4.4. Operational drill-string analysis

In this section, the operational drill-string analysis is elaborated. This analysis is again performed using OrcaFlex software provided by Orcina Ltd. First, the performance criteria are discussed on which the heave compensation methods will be tested and compared. Next, the drill-string dynamics and possible occurring dynamic phenomena are discussed. The dynamic effects are incorporated in the interpretation of the results obtained from a 3-hourly time analysis.

4.4.1. Assumptions and simplifications

In the operational drill-string analysis, the following modelling assumptions are made;

- the vessel only experiences loading as a result of the determined wave conditions
- wind loads are not taken into account in the determination of the operational vessel motions
- the second order wave drift force is not taken into account in the determination of the operational vessel motions.

4.4.2. Performance criteria

To determine the most effective heave compensation method, the operational stresses and weight on bit are analysed in a dynamic analysis. Using these simulations, the effect of water depth, wave conditions, and current can be investigated. The heave compensation methods can next be compared on the assessment criteria described in the previous chapter, being;

- lift-off of the bottom hole assembly
- maximum occurring stress
- weight on bit variation
- fatigue damage in the drill-string.

The assumptions made in the modeling of each component of the drilling method are presented in the previous Chapter. The stresses are measured just above the bottom hole assembly, as the largest stresses occur at this point, the validation is presented in Appendix H, Figure H.1, H.2, and H.3.

4.4.3. Resonance analysis

Following a static drill-string analysis, the eigenvalues of the drill-string can be determined using the Euler-Bernoulli beam theory. By solving the eigenvalue problem of the stiffness matrix, the resonance frequencies of the system can be derived for static unloaded situations. This resonance character could be used in the interpretation of the observed stresses during operation and also in the interpretation of the operational parameters as weight on bit. This approach is described in the following subsection. The resonance frequency is interesting, because of the relation to the loading wave spectrum. If the frequency of the loading wave has a frequency equal to or very close to the resonance frequency of the system, the drill-string can resonate. Which leads to larger displacements of the drill-string and larger occurring stresses during operation.

Assumptions and simplifications

In the resonance analysis, the following assumptions are made;

- constant current velocity over full length and time-series
- drill-string is assessed under the target pre-tension
- drill-string is assessed without the incorporation of a rotation.

Eigenvalue problem

In this research, the first step was to approach the drill-string reaction to topside displacements in a geometric linear analysis. Here the drill-string was modelled as an Euler Bernoulli beam, as the drill-string is highly slender for all considered water depths. In a geometric linear analysis, small displacements and rotations were assumed. Over the considered water depths this assumption is valid. The geometric linear analysis is useful to determine the resonance frequency of the drill-string under zero pre-tension. However, this is not the case for the operational analysis. This approach does not suffice in the determination of the operational resonance frequencies. Therefore, the model choice is made to shift to a geometric non-linear model (OrcaFlex) to find the resonance frequencies of each system under operational conditions.

Modal analysis using OrcaFlex

As mentioned, the resonance frequencies with the operational pre-tension for the systems can be derived using the dynamic OrcaFlex model. By understanding the resonance characteristic, the operational stresses can be better interpreted. In the operational model, pre-tension is applied, and as a result tension stiffening occurs. An increase in drill-string tension thus leads to an increase in stiffness, which leads to an increase in the resonance frequency. The pre-tension is used to determine the resonance frequency under the target pre-tension, i.e. the *static* situation.

Vortex Induced Vibrations

Vortex-Induced Vibrations (VIV) play a role in slender structures which experience flow along the circumference of the structure. As the drill-string is a cylindrical structure, the flow around the pipe can create vortexes when the flow detaches from the structure's surface. Due to this vortex shedding, the pipe can experience vibrations which can become motions due to constant excitation.

In this assessment, it is assumed that the drill-string is stationary and does not experience rotation from the topside. The rotational effects are thus disregarded. The relevance of vortex-induced vibration is assessed using the dimensionless Strouhal number. The Strouhal number at which vortex-induced resonance occurs is dependent on the Reynolds number. For the assessed current, with a velocity of 0.5 m/s around the drill-string with a diameter of 0.31 m, the Reynolds number is 1.55e5. Following this Reynolds number, a value of 0.198 [14] is used to determine the frequency at which vortex-induced vibration may occur in the drill-string. The critical velocity range within lock-in could occur is empirically described by [43] as velocities within a bandwidth of 35%.

5 Results and discussion

In this chapter, the results of all simulations, further analysis, and a discussion of these results are presented. First, the limiting topside displacements in the vertical and horizontal direction are determined following two criteria in Section 5.1. Secondly, the occurring operational vessel motions are assessed in Section 5.2. By comparing the occurring stresses and limiting motions, the need for heave compensation can be determined. Finally, an operational drill-string analysis is performed to determine the motions and stresses in the drill-string for three hours. This is performed for multiple wave spectra. Further analysis of the results is presented in each section.

5.1. Limiting topside displacements

First, the maximum downward displacement is determined at which the measured drill-string location reaches ULS. Next, the lift-off point is determined due to both an upward vessel motion and a horizontal vessel motion.

5.1.1. Maximum downward displacement

As discussed in the previous chapter, the topside is displaced downward with a constant velocity. The stresses in the drill-string per downward displacement are presented in Figure 5.1. The constant velocity used in this assessment is 20 mm/s, as this velocity shows a constant result without numerical calculation issues. The effect of the velocity on the results is presented in Appendix G, Figure G.2, G.3, and G.4.

In Figure 5.1 it is observed that an increase in water depth and drill-string length leads to larger allowable downward displacements before ULS is reached. This is attributed to the decrease in lateral stiffness of the drill-string. As the model incorporates geometric non-linearity, the drill-string will mobilise in the direction of least resistance, being a lateral deflection over the length.

A small disturbance is visible on the stress signal for a water depth of 200 m in the first 0.5 m of displacement. During this phase of the simulation, higher-order mode shapes are observed, and in particular the drill-string skipping from one mode shape to the other. This leads to sudden increases in the local stress at the measuring point. This is a dynamic effect of the drill-string mobilisation and is more present for large water depths and large downward velocities. This relation is attributed to the ratio of drill-string stiffness over the drag force generated by the motion through the seawater. The drag force and inertial force both counteract the mobilisation of the drill-string and can increase the sensitivity of the drill-string to take a higher-order mode shape. Higher-order mode shapes have smaller absolute displacements over the length.

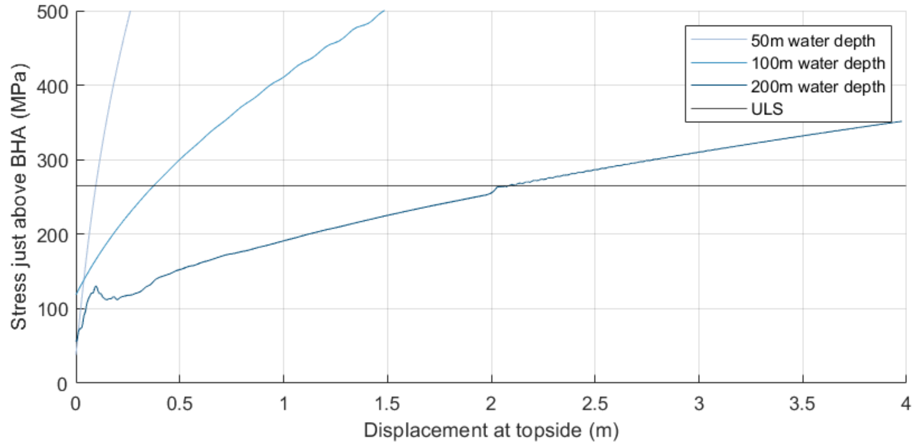

Figure 5.1: The local **compressive** stress of a DS300 drill-string above the bottom hole assembly as a result of a vertical downward displacement at the topside, intersecting the factorised yield strength of the drill-string material (steel).

Sensitivity to topside displacement velocity

To assess the influence of the displacement velocity, i.e. the effect of dynamics on the analysis, a sensitivity analysis is performed. This sensitivity analysis is presented in Figure 5.2. The figure only shows the displacement at which the drill-string reaches ULS. It is visible that the water depth of 200 m shows the largest sensitivity for large velocities within the analysed range. As described in the previous section, this is attributed to the ratio of drill-string stiffness over the drag force generated by the motion through the seawater.

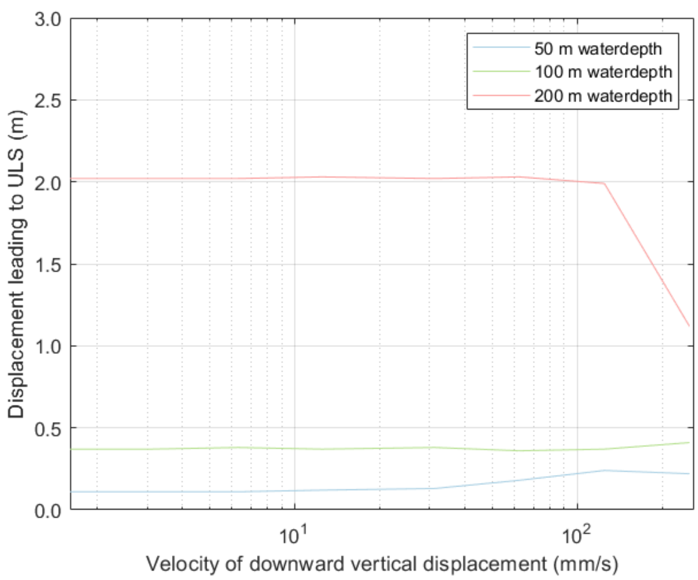

Figure 5.2: Allowable axial displacement of the topside before the DS300 drill-string reaches the factorised yield stress. A simulation was performed for multiple topside displacement velocities.

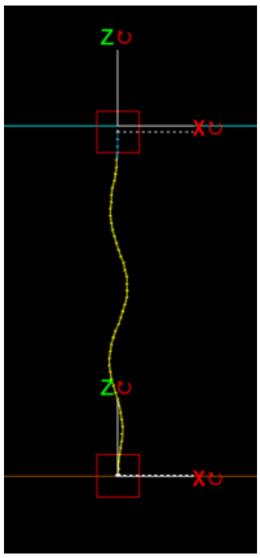

Figure 5.3: Higher order buckling shape observed during topside displacement.

When assessing the relation between lateral stiffness and the drag and inertial force qualitatively, it can be found that the magnitude of the analysed drag force scales with the velocity of the drill-string node through the seawater. The ratio is dependent on the water depth and the sensitivity increases for increasing water depths. All simulations are performed using the dynamic OrcaFlex model. Here the drag coefficient in the Morison drag force working on the tubular is increased for every water depth until a third-order mode shape is visible during the full simulation. Figure 5.3 shows the third mode shape for 50 m water depth and an extremely increased C_D value (2000). This value is not representative of reality. When performing the same simulation for 200 m water depth a C_D value of 300 leads to the same result. Showing that the sensitivity is larger for larger water depths.

5.1.2. Maximum upward displacement

The limiting criterion for the maximum upward displacement is the point at which lift-off occurs. This point is dependent on both the total weight of the drill column and the water depth. Figure 5.4 shows the displacements leading to lift-off for multiple bottom-hole assembly weights. Important to note is that no pre-tensioning is applied for the drill-string, thus the figure illustrates the relation between drill-string length and increased BHA mass. It can be observed that the relation between the required upward displacement and the water depth is non-linear. This is the result of the simultaneous increase in total drill column weight and the decrease of the drill-string stiffness over an increasing water depth. Also, it can be observed that longer drill-strings, which operate at larger water depths, require a larger displacement to lift the bottom hole assembly of the seabed. Here the dynamic effects of lift-off are not taken into consideration.

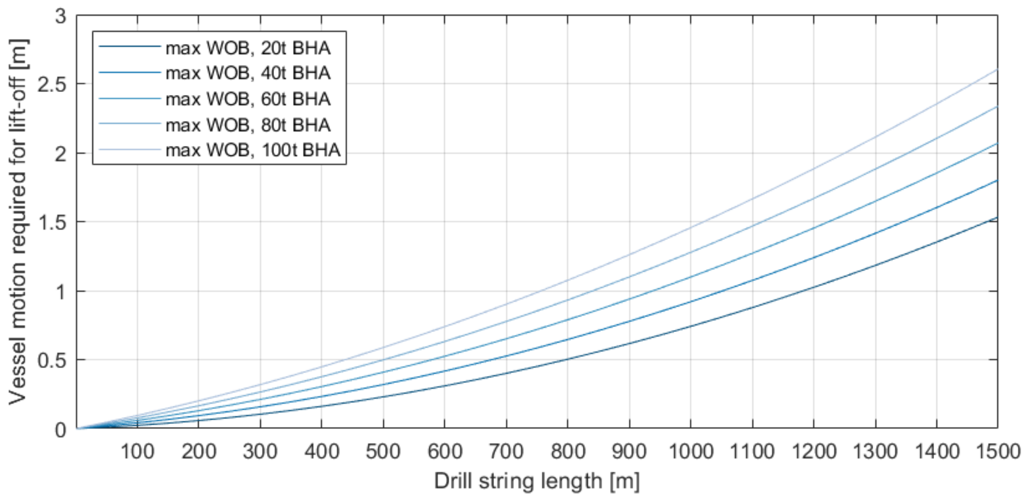

Figure 5.4: Vessel heave displacement required for lifting the bottom hole assembly of the seabed, performed for multiple BHA weights and plotted against the drill-string length. The total mass increases for larger water depths due to the increasing length of the drill-string.

In the research, a bottom hole assembly mass of 30 t is assessed, which is a real operational value for the specific drilling operation. For clarity, the topside displacements required for lift-off for the operational situation are presented in Table 5.1. Meaning that the pre-tension is applied in the drill-string which leads to the target weight on bit of 20 tonnes.

Table 5.1: Topside displacement required for lifting the bottom hole assembly of the seabed, performed for a drilling column with a drill-string pre-tension leading to a target weight on bit of 20 tonnes.

Drill-string length	Upward displacement required for lift-off required for lift-off
50 m	6.1 mm
100 m	18.5 mm
200 m	89.0 mm

5.1.3. Maximum horizontal displacement

The limiting criterion for the maximum horizontal displacement is the point at which lift-off occurs. A horizontal topside displacement leads to both shear stresses and stresses due to bending moments. These stresses are translated to a vertically oriented stress vector, which is tested to the stress required for lift-off. The bending moment is the result of the drill-string design, clamped at the top and bottom. Figure 5.5 shows the stresses as a result of a horizontal topside displacement. In the simulation, a constant velocity is used for the displacement and no currents or waves are present. The velocity equals 20 mm/s, this displacement simulates the drift velocity of the vessel during operation. The efficiency of the dynamic positioning system used on the construction support vessel is not assessed in the determination of the used velocity.

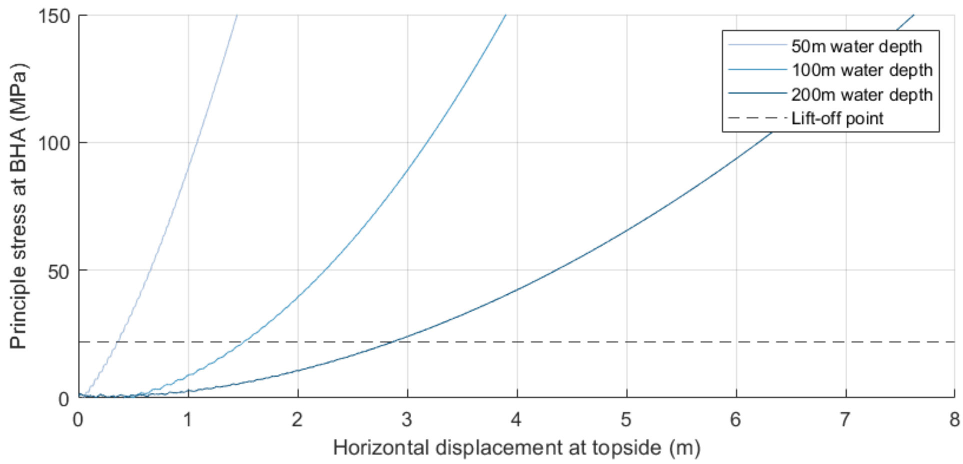

Figure 5.5: The local **tensile** stress of a DS300 drill-string above the bottom hole assembly as a result of a horizontal displacement at the topside, intersecting the factorised yield strength of the drill-string material (steel).

It can be observed that the allowable horizontal displacement increases for an increasing water depth. An additional simulation that shows interesting results is the effect of passive heave compensation on the lift-off due to horizontal displacement presented in Figure G.1. The passive heave compensator only works in the vertical direction and is tuned to keep a constant tension in the spring-damper. Once the drill-string is horizontally displaced, the spring is elongated as result. As the stiffness of the drill-string is larger than that of the passive heave compensator, the passive heave compensator spring is elongated. This elongation leads to an added tensile load to the drill-string. Therefore, the total tensile stress in the drill-string increases faster than without a damper.

5.1.4. Summary of limiting displacements

Below an overview of the found maximum displacements is summated. The maximum downward displacement is found by assessing the ULS criterion. The maximum upward and horizontal displacements are found by assessing the lift-off criterion.

Table 5.2: Summary of maximum allowable topside displacements, the maximum downward displacement is found by assessing the ULS criterion. The maximum upward and horizontal displacements are found by assessing the lift-off criterion. This assessment is performed without any form of heave compensation.

Water depth	Allowable downward	Allowable upward	Allowable horizontal
50 m	0.16 m	0.0061 m	0.38 m
100 m	0.81 m	0.018 m	1.5 m
200 m	2.0 m	0.089 m	2.8 m

5.2. Operational vessel motions

The occurring operational vessel motions are found by performing a 3-hour time simulation. The response is assessed for head waves (180°) and is found to be the same for all assessed water depths (50 m, 100 m, and 200 m). The time simulation results are presented in Table 5.3. Here it is visible that the maximum vessel motions follow the magnitude of the significant wave height for waves with a peak period of 8.0 s. The vertical vessel excitation for waves with a peak period of 4.0 s is much smaller, in the order of 15% of the significant wave height.

Table 5.3: Statistics of the vessel response for a JONSWAP spectrum with multiple wave characteristics. Measured at the drill-rig position, which is on the centreline at height of the CoF of the vessel (moonpool). Modelled using Orcina Ltd. Software and applicable for all water depths.

		Vertical			Horizontal	
T_p	H_s	Min.	Max.	Std.	Max.	Std.
4.0 s	1.5 m	−0.17 m	0.17 m	0.04 m	0.02 m	0.006 m
8.0 s	1.5 m	−0.66 m	0.69 m	0.19 m	0.66 m	0.171 m
8.0 s	2.0 m	−0.88 m	0.92 m	0.24 m	0.88 m	0.232 m

5.3. Operational drill-string time analysis

In this section, the operational drill-string analysis is performed. First, the occurring drill-string stresses are determined in a static situation with a constant penetration in multiple rock strengths. Here also the effect of torque on the system is analysed. Next, the occurring dynamic stresses at the before-mentioned measuring point are compared per water depth scenario and heave compensation method. Also, the displacements of the system are presented. Further, the stress statistics for multiple wave conditions are presented for the full-time series per heave compensation method. Finally, the operational parameters of fatigue damage and weight on bit are assessed.

5.3.1. Resonance analysis

Table 5.4 shows the resonance frequency results presented per heave compensation method per water depth. The resonance frequencies are determined under the pre-tensions described in Section 3.2.2. The results are used to interpret the motions and stresses that are presented in Section 5.3.3. Here the assumption is made that the mean pre-tension in the drill-string is equal to the target pre-tension. This assumption is validated using the stress statistics presented in Section 5.3.4.

The modal analysis used to find the results is performed on the passive configuration by considering both the drill-string and passive heave spring components. For the active configuration, only the drill-string is considered as the drill rig at the topside is connected rigidly to the vessel.

Table 5.4: Resonance frequency analysis per mode shape and per heave compensation method, for the three considered water depths. Computed by performing a modal analysis in OrcaFlex software.

Heave comp.	Mode	50 m	100 m	200 m
Passive	1^{st}	0.56 Hz	0.32 Hz	0.09 Hz
	2^{nd}	1.45 Hz	0.57 Hz	0.21 Hz
	3^{rd}	2.75 Hz	0.94 Hz	0.34 Hz
Active	1^{st}	0.82 Hz	0.43 Hz	0.10 Hz
	2^{nd}	2.13 Hz	0.77 Hz	0.23 Hz
	3^{rd}	4.04 Hz	1.12 Hz	0.37 Hz

As is visible in Figure 5.6, the vessel motions peak at a frequency of 0.09 Hz for z and 0.08 Hz for x. The vertical frequency is very close to the resonance frequency of the system operating at 200 m water depth. Thus, the occurrence of resonance is to be considered once evaluating the operational results in the following section.

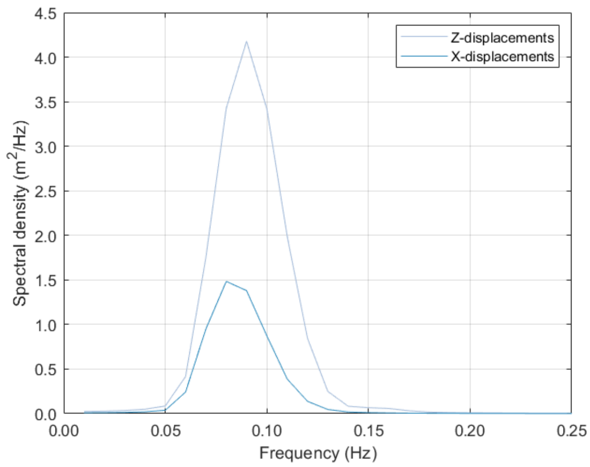

Figure 5.6: Spectral density of the vessel motions deconstructed in the vertical (z) and horizontal (z) motions.

Vortex-induced vibration

By determining the vortex-induced vibration (VIV) frequency, the relevance of the assessment is determined. Here a constant value for the dimensionless Strouhal number of 0.198 is used. By using this dimensionless number and the resonance frequencies determined in the previous subsection, the current velocities at vortex-induced resonance occur can be determined. These results are presented in Appendix G, Table G.2. The two modes which experience resonance are the second mode of the passive system at 50 m water depth and the third mode of the active system at 100 m water depth. The vortex-induced frequencies for a current of 0.5 m/s are within 35% of the resonance frequencies of the systems (12% and 14% respectively).

However, these modes carry little energy, and the effect on the total stresses for these modes is expected to be small with respect to the stresses induced by the vessel motion. Also, the resonance frequency constantly shifts due to the change in drill-string tension, making the lock-in resonance as a result of vortex shedding more unlikely. Further research, considering more current velocities will add to the understanding of VIV effects on the operation.

5.3.2. Effect of seabed conditions

As discussed a minimum drill-bit penetration of 1 mm is set to maintain production during operation. Therefore the minimum penetration force can be determined to achieve this 1 mm. Here it is assumed that a larger force only leads to a larger production, complications due to a sudden increase of the axial load or stick-slip phenomena of the bottom hole assembly are disregarded. Following the relation of [74], the torque matching the operational axial load can be determined. Both the axial and torsional load lead to stresses in the drill-string. The operational loads, torques, and stresses for a range of rock strengths that can be encountered in the field are presented in Table 5.5. The empirical study performed by [75] is used to determine the relationship between the axial, i.e. penetration, and tangential load. This empirical relation is subject to large insecurities during the examination. As this relation is highly dependent on the roller design and the sharpness/bluntness of the roller used. When comparing multiple studies the most found empirical value (3) is applied in this assessment. Thus it is assumed that the roller used during operations is sharp and follows the design presented in this study of [74]. Once the roller becomes blunt, the penetration and torsional loads are expected to become larger to maintain the same penetration depth.

Table 5.5: The required penetration force and torque to assure penetration of 1 mm. Also, the following shear stress at the outer diameter of the drill-string is provided.

Rock strength	Required force	Compressive stress	Required torque	Shear stress
5 MPa	48 kN	3.53 MPa	3.8 kNm	2.00 MPa
10 MPa	96 kN	7.06 MPa	7.7 kNm	4.06 MPa
25 MPa	240 kN	17.65 MPa	19.2 kNm	10.12 MPa
50 MPa	480 kN	35.29 MPa	38.4 kNm	20.24 MPa
100 MPa	960 kN	70.59 MPa	76.8 kNm	40.49 MPa

As visible in the above table, the shear stresses increase for rock surfaces with relatively large UCS values. Also, it is important to realise that the values presented are operational, torque variations due to stick-slip phenomena of the drill head are thus not taken into account. The shear stresses measured in operational conditions are not extremely large. However, for strong rock formations, the shear stresses are of significance once large torque variations occur in the order of 200% (empirical experience by Boskalis during comparable drilling operations). This is not expected in the operational conditions as described in Section 2.3.2.

5.3.3. Effect of wave conditions

The statistics per wave conditions are presented in Table G.3. It is visible that for wave spectra with peak periods of 4.0 s the occurring stresses decrease. For the wave conditions with a peak period of 8.0 s and a significant wave height of 2.0 m the stresses increase. The increase is most visible for systems using active heave compensation. In specific for the active heave compensator acting in 50 m water depth. This sensitivity is the result of a stiff system combined with larger vessel displacements. The passive systems show a relatively smaller increase in the stresses and the standard deviation of the total time series.

Finally, the last column shows the effect of an additional current. For all systems, the mean value of the stresses slightly shifts towards a more compressive situation. This is logical due to the constant directional load adding stress to the system over the full drill-string length. The active system experiences a larger standard deviation with respect to the passive system for water depths of 50 m and 100 m. Again the constant current adds energy and stresses to the system. However, for 200 m water depth, the standard deviation decreases. The systems both experience resonance in the scenario without a constant current. This resonance excitation is counteracted by hydrodynamic damping, which leads to a smaller standard deviation over the time series. During the simulation, it can be observed that the resonance modes are also less occurring. For each compensation method, the statistics are presented in Appendix E, Figures E.16, E.17, and E.18.

5.3.4. Effect of water depth

In this section, the probable wave conditions are determined using the environmental data provided in Section 2.3.2. Here the base case is set for wave conditions with a peak period and significant wave height of 8.0 s and 1.5 m respectively. This wave condition is used to analyse the drill-string response and in particular the effect of the heave compensation methods on the drill-string response.

Time analysis stress statistics

In this subsection, the statistics over the full-time series are presented for the base case wave condition, which is presented in Table 5.6. The statistics for all considered wave spectra and current scenarios are presented in Appendix G Table G.3 and discussed in the following section.

Table 5.6: Principal stress statistics measured above the bottom hole assembly for a DS300 drill-string with a target weight on a bit of 20 tonnes, for JONSWAP wave conditions with a T_p = 8.0 s, and a H_s = 1.5 m.

Water depth	Heave comp.	Mean	Std.	Max	Δ Std.
50 m	None	216.4 MPa	508.2 MPa	2743.6 MPa	-
	Passive	15.7 MPa	22.3 MPa	94.1 MPa	95%
	Active	17.4 MPa	13.6 MPa	-83.8 MPa	97%
100 m	None	157.2 MPa	253.3 MPa	1435.7 MPa	-
	Passive	15.2 MPa	8.2 MPa	37.3 MPa	97%
	Active	18.0 MPa	7.6 MPa	43.3 MPa	97%
200 m	None	71.5 MPa	139.8 MPa	751.1 MPa	-
	Passive	16.2 MPa	12.2 MPa	41.2 MPa	91%
	Active	19.4 MPa	18.1 MPa	63.1 MPa	88%

The main results following from the stress statistics are;

- The mean stresses per water depth are of the same magnitude when comparing the passive and active systems.
- The standard deviation of the measured stress increases when comparing the water depths of 100 m and 200 m. Whilst a decrease is expected.
- The drill-strings operating at 200 m water depth experience larger stress variations due to resonance in the first and third modes.

It is expected that the mean stresses are in the order of 14.4 MPa, as this corresponds to the target WOB which is fixed at 20 tonnes. Following the standard deviation, the stress variations over the period can be assessed. Also, a compensation factor, stylised as ΔStd., can be derived when compared to the uncompensated situation. As the stiffness of the drill-string decreases with increasing water depth, it is expected that the standard deviation decreases for larger water depths as the system shows less resistance to induced motion. The stress statistics are graphically presented in Appendix G.

In the frequency analysis presented in Section 5.3.1, the assumption is made that the target pre-tension equals the mean pre-tension in the drill-string during operation. This assumption can be validated using the stress statistics presented in Table 5.6. As mentioned the target weight on bit requires a mean tension of 14.4 MPa, and the mean stresses during operation are larger. This means that the drill-string experiences more tension than the target pre-tension for which the resonance frequencies are determined in the modal analysis. This larger mean tension leads to an increase in stiffness and an increase in the mean resonance frequency.

The resonance frequencies for the target pre-tension for the passive and active system are respectively 0.09 Hz and 0.10 Hz. Knowing that the mean tension is larger during operation, the frequency will increase slightly, and thus the period will decrease slightly. Even so, the resonance frequency of both systems is extremely close to the peak frequency of the vessel motions during operation, as presented in Section 5.3.1. Combining the larger standard deviation experienced at 200 m water depth and the resonance frequencies being so close to the peak period of the vessel motions, it can be stated that the increase in standard deviation is the result of first-order resonance in the drill-string.

Interpretation of motions and stresses

The response of the drill-string is assessed at the time section where the maximum vessel displacements occur. The physical drill-string response to extreme vessel displacements can not be derived by analysing the statistical stress values of mean and standard deviation. Every simulation is loaded by the same wave conditions, thus the same time interval is used for every simulation. In Figure 5.8, 5.9, and 5.10 the analyses for water depths of 50 m, 100 m, and 200 m are presented respectively. A dashed black line is plotted at the time when the vessel experiences the largest vertical upward displacement ($t = 5243.0$ s). The plot is subdivided into six subplots. These are schematically presented in Figure 5.7 and described below.

The top subplot shows the vertical (z) and horizontal (x) displacements of the vessel due to wave excitation. The second subplot shows the z-displacement of the top of the drill-string for both heave compensation methods. The horizontal displacements of the top node are not included in the figure as these are the same for both heave compensation methods and equal to the horizontal vessel motion. The third and fourth subplots show the vertical (z) and horizontal (x) displacement of the drill-strings mid-node respectively. The fifth subplot shows the drill-string stresses measured just above the bottom hole assembly. Here the axial stresses, shear stresses, and stresses due to the bending moment are incorporated. The bottom subplot shows the weight on bit for the drill head.

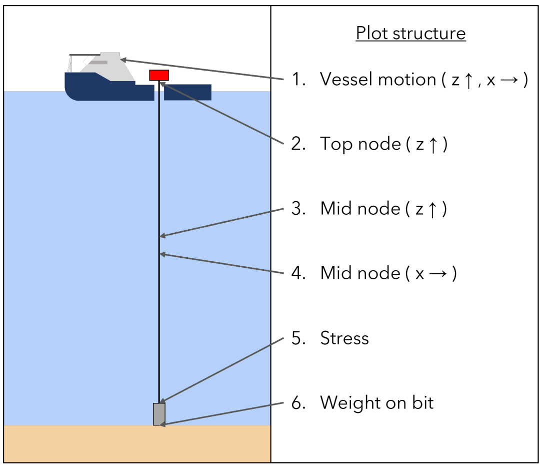

Figure 5.7: Schematic overview of the subplots and the measuring location in the total system.

50 m water depth
The following results are derived from Figure 5.8 for a water depth of 50 m and further analysis of the deconstructed motions and stresses. The resonance characteristics presented in Section 5.3.1 are referenced throughout.

- The compensated vertical (z) displacement experienced by the drill rig, i.e. the top node of the drill-string, is larger for the active system when compared to the passive system.
- The vertical (z) displacements at the middle of the drill-string are also larger for the active system in comparison to the passive system.
- The horizontal (x) displacements at the middle of the drill-string are in the same order for the two systems, the active system shows a vibration and slightly larger peaks.
- The active system shows a high-frequency response (0.88 Hz, corresponding to frequency analysis) which is not visible for the passive system.
- When deconstructing the measured stress above BHA, the predominant cause of stress increase during operation is the bending moment at the measuring point. Both due to horizontal topside displacements and drill-string deformations.
- The stiffer active heave system shows lower stress maxima in comparison to the passive system.
- The high-frequency vibration that the active system shows in the stresses is also translated to the WOB.

The z and x maxima at the top node are 0.032 m and 0.007 m for the active and passive heave systems respectively. The passive system shows a higher frequency of vertical displacements. This is the result of the spring in the PHC, the top node displaces with the natural frequency of the PHC. The z maxima at the mid node are 0.019 m and 0.003 m for the active and passive heave systems respectively. The peaks occur at the same time and with the same frequency as at the top node.

The x displacements at the topside are the same for the two heave compensation options, and the displacements at the middle of the drill-string are in the same order. This is expected as the topside horizontal motions of the vessel and thus the drill-string are identical. The high-frequency response of the active system shows a frequency of 0.88 Hz. This matches the first-order resonance frequency of the system under target pre-tension (0.82 Hz). The passive system does not show this high-frequency response due to the damper which is incorporated in the passive heave compensator.

The bending moment is the driver in the stresses measured above the BHA. The bending moment is the result of a horizontal topside displacement and a lateral modal excitation of the drill-string. For the active system, this modal excitation can be observed as a high frequent stress variation, which was also observed at the horizontal motion of the mid-node. Again this high-frequency response matches the first-order resonance frequency of 0.82 Hz. The z and x motions of the passive system peak a the same time, meaning that the maximum stresses as a result of axial load and bending moment occur simultaneously, leading to a larger maximum stress. This is not the case for the active system, the stresses as a result of the motions even counteract during the peak. Therefore, the stress maxima are smaller for the active system. Even though the larger system stiffness would lead to the assumption that the maximum stresses would be larger.

Finally, the WOB shows a minimum of zero tonnes, this is the point at which lift-off occurs. A negative weight on bit is not possible. As the WOB data is post-processed, the dynamic effects of lift-off and touchdown are not incorporated in the weight on bit data. The high frequent WOB signal will most likely be less visible during actual operation, as the BHA will experience hydrodynamic damping, damping due to drill-rock interaction, and an inertial component once accelerated.

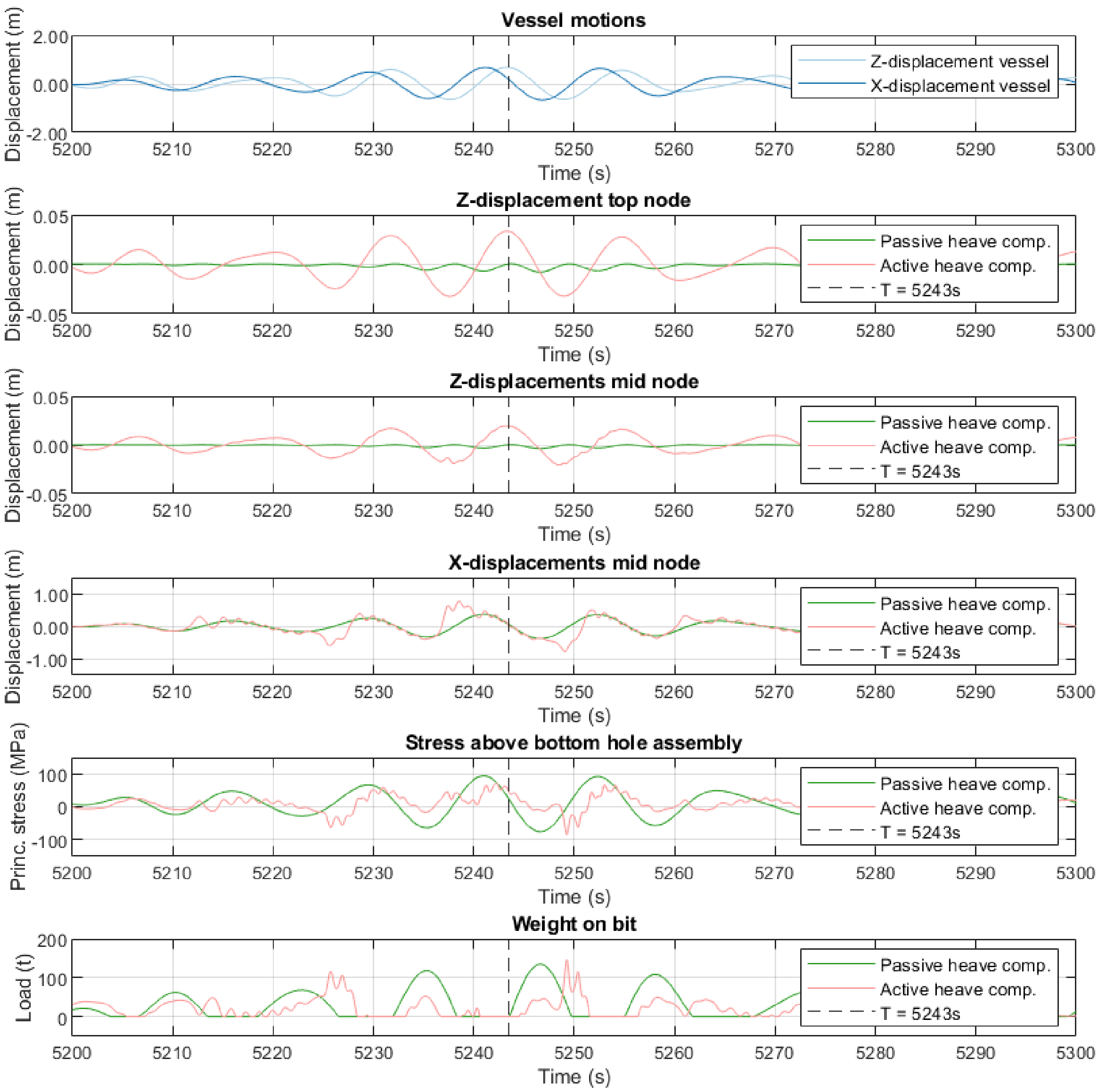

Figure 5.8: Multiple motions, stresses, and loads plotted to assess the drill-string dynamics during operation at *50 m water depth*. Both passive and active heave compensation options are presented in the same plot.

100 m water depth

The following results are derived from Figure 5.9 for a water depth of 100 m and further analysis of the deconstructed motions and stresses. The resonance characteristics presented in Section 5.3.1 are referenced throughout.

- The z and x displacements at the top node are the same as for 50 m water depth.
- The z displacements at the mid node are slightly smaller for both heave compensation systems.
- The horizontal displacements at the mid-node follow the same path for both heave compensation systems.
- The active system still shows a little high-frequency response in the horizontal motion.
- The second mode shape is dominantly observed for 100 m water depth.
- The stresses are predominantly the result of the bending moment experienced above the bottom hole assembly, the active system experiences more effect of axial stress as the vertical drill-string motions are larger.
- The stress data of the active system show larger variations in comparison to the passive system.

As the vessel is loaded by the same wave conditions as 50 m, the vessel motions remain the same. Showing absolute maxima for z of 0.017 m and 0.002 m for active and passive systems respectively. Which is in the same order as for 50 m water depth. Further, the horizontal (x) displacements at the mid-node are comparable in magnitude and path. Only a slight high-frequency response is visible in the horizontal direction for the active system.

The maximum measured resulting variations in displacement is in the order of 0.1 m. However, the active system shows large stress peaks just above the bottom hole assembly, the high-frequency vibration is very visible in the stress signal. The frequency of this vibration is 0.78 Hz, the determination presented in Figure G.10. The sensitivity to these extreme topside displacements is larger for the active system, while the stresses over other sections of the time series are similar in magnitude and path. This shows that the stress measured above the BHA is the result of both axial stress and a bending moment.

The bending moment is dominant in the final stress, however, the influence of the axial stress is visible in the stress data of the active system. When analysing the stress data of the active system, the signal shows large and steep stress peaks, this difference is not as clear in the displacements at the mid-node. However, when observing the simulation results and the drill-string shape during the presented time span, the drill-string shows deformation in the second order mode shape. This has as a result that the mid-node does not show the largest displacements, as visible in Figure G.8. The stresses at BHA follow from a bending moment which is the result of a second order deformation of the drill-string. As discussed in Section 5.1.1, the higher order mode-shapes are more present in larger water depths as the ratio of the drill-string stiffness over the hydrodynamic drag becomes smaller.

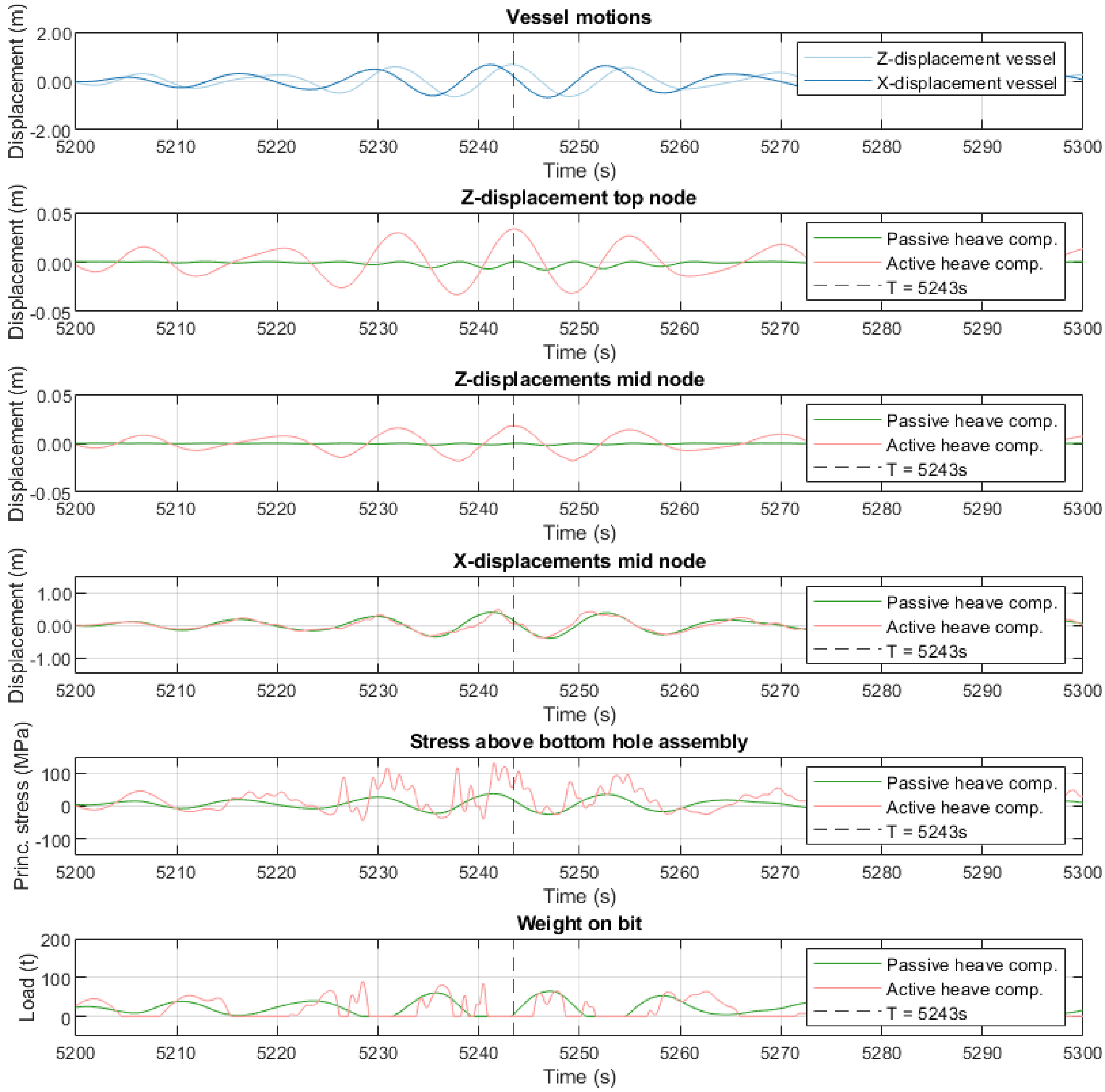

Figure 5.9: Multiple motions, stresses, and loads plotted to assess the drill-string dynamics during operation at *100 m water depth*. Both passive and active heave compensation options are presented in the same plot.

200 m water depth

The following results are derived from Figure 5.10 for a water depth of 200 m and further analysis of the deconstructed motions and stresses. The resonance characteristics presented in Section 5.3.1 are referenced throughout.

- The vertical (z) displacements at the middle of the drill-string are negligible for the passive system.
- There isn't a clear high frequent vibration visible on the horizontal displacement of the mid node.
- The horizontal displacements at the mid-nod experience larger peaks for the active system but generally follow the same path and have comparable magnitudes.
- The stress data for the active system show larger peaks as a result of larger bending moments in the drill-string.
- The weight on bit shows smaller variations over the time interval in comparison to shallower water and the two systems show comparable results.

When increasing the water depth to 200 m, the topside displacements remain the same as the same wave conditions and the vessel is considered. The magnitude of the horizontal displacements (x) at the middle of the drill-string is comparable. However, the active system shows a larger peak displacement and does not show the smooth sine shape as the passive system does.

When considering the stresses at BHA, two high-frequency responses can be derived which appear after each other in the stress data. The frequencies are in the order of 0.22 Hz and 0.41 Hz (determination presented in Figure G.11). These frequencies are very near the second and third-order resonance frequencies of the active system under target pre-tension. Once the drill-string is tensioned more or less, the resonance frequencies change due to the change in stiffness. During the simulation, it is observed that the second and third-order mode shapes are visible in the system.

The weight on bit shows a similar path with the stresses measured above BHA. The stress response of the two systems show less difference for an increasing water depth. The stiffness of the two systems move closer to each other.

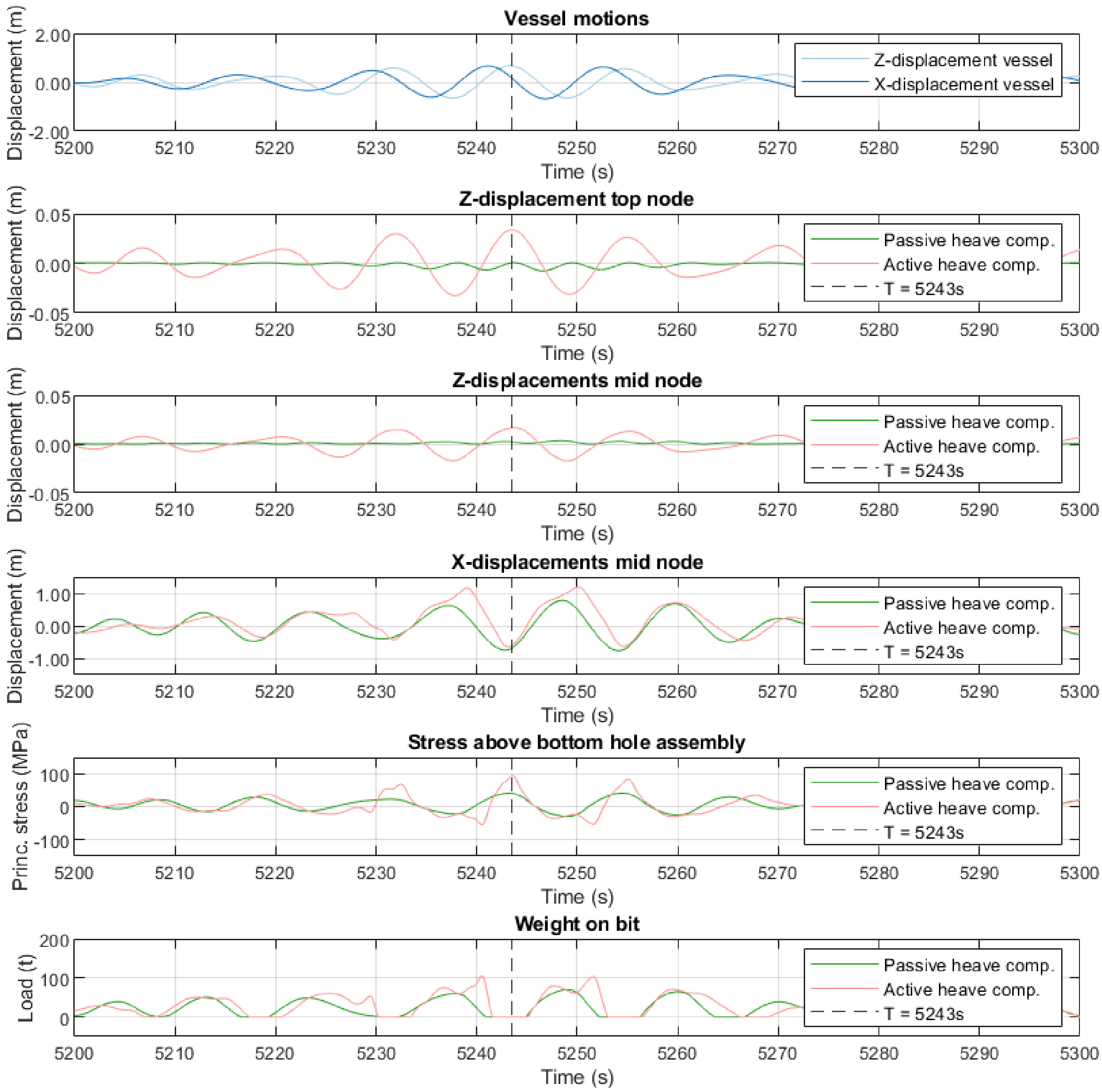

Figure 5.10: Multiple motions, stresses, and loads plotted to assess the drill-string dynamics during operation at *200 m water depth*. Both passive and active heave compensation options are presented in the same plot.

5.3.5. Fatigue damage

Following the DNV-GL-C203, Chapter 2, the fatigue damage can be constructed for a riser or steel pipe. The damages presented in Table 5.7 are determined using the time simulation which is presented in the previous section. A rainflow analysis is performed on the stress data at the location just above the bottom hole assembly, as the largest stresses appear at this location. The rainflow analysis performed uses stress range bins of 10 MPa. To construct the column days until failure, 24 hours is used per day.

Table 5.7: Fatigue damages for a 3-hour load cycle for a DS300 drill-string with a target weight on bit of 20 tonnes, a T_p = 8.0 s, and a H_s = 1.5 m (JONSWAP).

Water depth	Heave comp.	Damage	Days until failure
50 m	Passive	3.258e-4	383
	Active	2.952e-4	422
100 m	Passive	5.073e-6	24.6e3
	Active	9.362e-6	16.9e3
200 m	Passive	2.213e-5	5.6e3
	Active	3.346e-5	3.7e3

As expected, the damage is largest for drill-strings operating in 50 m water depth, as the absolute stresses are larger and the stiffness of the total system is larger. The damage is slightly larger for the passive heave compensation system in 50 m water depth. As with the stresses, an increase in the damage is visible for 200 m water depth when compared to 100 m water depth, this can again be attributed to the resonance of the drill-string as described in the previous section. It is visible that the fatigue damage is larger for the system using active heave compensation for water depths larger than 50 m. This can be because the high-frequency vibration also causes some damage in the rainflow calculation. However, the effect of these small load cycles is small on the total determined fatigue damage. As the total time, until failure is far beyond the time required to drill one borehole, the fatigue characteristic is assumed not to be of influence the workability of the operation.

5.3.6. Weight on bit and lift-off

As mentioned in the methodology chapter, each water depth and heave compensation scenario have the same target weight of bit of 20 tonnes. The statistics of the weight on bit results are presented in Table 5.8. Here the weight on bit data is analysed disregarding the zero values to find the mean and standard deviations. *Thus the values represent the weight on bit when the drill head is in contact with the seabed.* The zeros are represented in the lift-off percentage which is also presented in the table below.

Table 5.8: Weight on bit analysis of a 3-hour load cycle for a DS300 drill-string with a target weight on bit of 20 tonnes, a T_p = 8.0 s, and a H_s = 1.5 m (JONSWAP).

Water depth	Heave comp.	Mean WOB	Std. WOB	Lift-off percentage
50 m	None	164.4 t	274.9 t	64.2%
	Passive	21.7 t	23.1 t	30.8%
	Active	24.1 t	16.3 t	11.1%
100 m	None	50.9 t	117.8 t	70.1%
	Passive	21.1 t	11.1 t	3.1%
	Active	24.9 t	10.2 t	2.1%
200 m	None	41.8 t	74.2 t	59.7%
	Passive	22.4 t	15.9 t	1.7%
	Active	27.2 t	20.2 t	1.2%

The main results following from the weight on bit statistics are;

- For 50 m water depth, the active system shows favourable standard deviation in weight on bit and lift-off percentage.
- The mean weight on bit increases for the active system at 200 m water depth, larger target pre-tension is required during operation.
- The active heave compensation system shows a lower lift-off percentage for 50 m water depth.
- The lift-off percentages are similar for both heave compensation methods at 100 m and 200 m water depth.
- Due to the resonance frequency being close to the vessel motion frequency, the standard deviation increases at 200 m water depth. Relatively larger for the active system
- The lift-off percentage is never 0% for the time simulation, so the operation will experience some downtime for the considered wave condition.

At 50 m water depth, the standard deviation for the two compensation systems varies widely. The active system shows better results in weight on bit variation and lift-off percentage with respect to the passive system.

It is expected that for larger water depths, where the drill-string responds in a less stiff manner, the weight on bit variations (Std.) will become smaller. As is visible in the table this is the case. However, at 200 m water depth the standard deviation increases. As is discussed in Section 5.3.4, the drill-strings operating at 200 m water depth have resonance frequencies close to the period of the wave conditions. The vessel displacement (z and x) also shows a peak at this frequency when performing a Fast Fourier transformation. The active system is more sensitive to this resonance as there is no damping incorporated in the system.

Important to note is that the vertical drag, inertial component, and the added mass of the bottom hole assembly are not taken into account when determining the lift-off percentage. Thus the value determined in the analysis only indicates the performance. This value is used as a comparison for the two methods, it is expected that the effect of the above-mentioned phenomena is similar for the two methods. Here the assumption is made that the lift-off velocity and acceleration are similar in the two cases. The presented values in the table above are thus conservative. As each of the acting forces works against the vertical motion of the bottom hole assembly and will decrease the magnitude of the lift-off. The correlation between the stresses occurring above BHA and the WOB is presented in Appendix H Figure H.4.

6 Conclusions

In this research, a heave compensated pile-top drill rig has been dynamically analysed in ranging water depths of 50 m, 100 m, and 200 m under relevant wave conditions. Firstly, the maximum allowable topside displacements have been assessed before the drill-string reached an operational limit. Secondly, the operational vessel motions under the relevant wave conditions have been assessed to determine the requirement of heave compensation in the drilling configuration. Third and finally, the passive and active heave compensation methods have been assessed using the performance criteria, during a 3-hourly time simulation under the before-mentioned environmental conditions. These steps have been taken to answer the following research question:

What is the most effective heave compensation method for anchor pile drilling from a construction support vessel?

Overall conclusions:

- The research revealed that the model generates critical data input which can be used in a heave compensation selection tool. This enables the user to more efficiently construct floating wind foundations, accelerating the energy transition.
- The research shows that heave compensation is required for the full range of considered water depths and wave conditions. Without the use of heave compensation, passive or active, the ULS is exceeded during all time simulations, considering the full range of water depths and wave conditions.
- The operational vessel data also shows that the active and passive heave compensation methods operate within their stroke length during all dynamic time analyses. Verifying the modelling assumption for the active system.
- The vessel displacement which limits the operation under heave compensated conditions is the vertical upward motion, with BHA lift-off as the limiting criterion. This displacement is limiting for the full range of water depths and wave conditions.
- The operational analysis shows that the bending moment in the drill-string is the predominant source of the occurring drill-string stresses. The occurring bending moment is the result of horizontal (uncompensated) vessel motions and drill-string deformations over its full length due to vertical topside displacements.
- The unconfined compressive strength of the bedrock is the main driver which determines the required weight on bit during operation. The weight on bit influences which BHA

mass and related drill-string pre-tension are to be applied during operation, to maintain the most constant WOB.

For 50 m water depth:

- The drill-string configuration mounted with passive heave compensation experiences a decreased stiffness in comparison to the active configuration. Leading to a smaller standard deviation of the stresses.
- For the considered wave conditions with a peak period of 8.0 s, the active configuration shows favourable results for both researched performance criteria of weight on bit and the lift-off percentage.
- For the considered wave condition with a peak period of 4.0 s, the passive and active configurations show comparable results for both researched performance criteria.

For 100 m and 200 m water depth:

- For all considered wave conditions, the active and passive heave configurations show comparable results for both researched performance criteria.
- The stiffness of both systems becomes comparable for larger water depths, as the effect of the passive heave compensation spring in the total system is found to become smaller.
- The output of this research can effectively be used to perform a final economic assessment using the availability, day rate, and mobilisation complexity of the heave compensation equipment. Which will determine which configuration is most effective per site.

For 200 m water depth:

- For the wave conditions with a peak period of 8.0 s, resonance is experienced in the drill-string. As the displacement frequency of the vessel locks in with the resonance frequency of the drill-string.
- Due to the modelling method of the active system, the compensating effect of the system on a high frequent resonance motion can not be researched.

Finally, Table 6.1 summarises the applicability of the two heave compensation methods per selected European floating offshore wind site.

Table 6.1: Representation of which heave compensation method is workable per European offshore location. Determined using the wave spectra present and the bathymetry data.

Site	Active heave comp.	Passive heave comp.
The West of Orkney	+	−
Bretagne Sud	+	−
Baltic Offshore Delta	+	+
Heimdall	+	+
INTOG WoSa	+	−

7 Recommendations

7.1. Design recommendations

- Both the active and passive heave compensation methods show favourable characteristics, being respectively the small remaining topside displacements and the systems stiffness decrease. When combining these methods into a hybrid system and performing an optimisation, it is expected that the workability rates will improve even further. Therefore, a combined analysis of the workability increase versus the cost increase of such a design choice is to be performed.
- The operational analysis shows that the bending moment in the drill-string is the predominant source of the occurring drill-string stresses. By compensating the horizontal motions of the drill rig, which is the partial cause of the bending moments, the resulting stresses will decrease and the workability of the operation is expected to increase. Therefore, a combined analysis of the workability increase versus the cost increase of such a design choice is to be performed.
- The research shows that an increase in pre-tension, increases the mean stress to become more tensional, however, the standard deviation also increases. In the research, operational values for BHA mass and WOB have been used to assess workability. Analysis shows a clear correlation between the applied pre-tension and the occurring stress variations. Therefore, further optimisation research into the pre-tension leading to the most favourable occurring stresses for the DS300 drill-string under operational conditions is to be performed.
- In this research the drill-string connection is modelled as clamped at the top and bottom, as is the case in reality. This design choice leads to the system having a larger stiffness in comparison to another connection type, leading to large occurring drill-string stresses and stress variations. Designing a system with alternative topside and BHA connections, such as a hinge, is expected to have a positive effect on the occurring stresses and the workability of the operation. The effect of this design choice on the weight on bit and drill-string dynamics is to be further researched.
- The research shows that a decrease in drill-string stiffness leads to a decrease in the occurring stress standard deviation. Therefore, design improvements which mitigate the bending moment in the steel drill-string as a result of the drill-string deformation are to be further researched. As an example, the use of thick rubber gaskets between the segments could decrease the occurring bending moments as it decreases the local stiffness in the drill-string, it is important to note that the torque can still be transferred over the drill-string length to the rotating drill head.

- The research shows that VIV is of relevance for certain drill-string modes at 50 m and 100 m water depth. Mitigating design methods which decrease the effect of VIV are to be researched. Such as changing the drill-strings dimensions, stiffness, or surface roughness.

7.2. Modelling recommendations

- The research shows that the stresses increase when including a directional wave spreading around the main wave direction. Further research into the workability of the heave compensation systems for beam wave states and stern quartering wave states is to be performed.
- In this research the current is considered to be constant over the full length during the dynamic analysis. By considering a multi-directional current or a non-constant current over the drill-string length, the stresses working on the drill-string will differ, this effect is expected to be small. However, the multi-directional waves can influence the mode shape in which the drill-string reacts to topside displacements. Therefore a specific analysis of this effect is recommended.
- Vortex-induced vibrations are found to play a role for the drill-string operating in 50 m and 100 m water depth, locking in with the second and third modes of the drill-string. This leads to extra stresses in the drill-string which are not considered in the research, making the results optimistic. Further analysis including the effects of VIV during the drilling operation is recommended.
- In this research, the effect of torsion on the total experienced drill-string stresses was determined to be minimal for the considered bedrock strength. Therefore, the effect of torsional loading was neglected. However, when drilling in harder bedrock at water depths larger than 200 m, the torsion and torsion variations show relevance. Therefore, this relation under extreme conditions holds interest to be researched further for large-diameter drills.
- In this research, the efficiency of the passive heave compensator is tuned to mimic the workings of an actual passive heave compensator, following information provided by CraneMaster [20]. When altering the modelled spring and damping coefficient characteristics to displacements and velocities, the reaction of the drill-string to vessel motions will change. In reality, this is done by changing the cylinder diameter and the piston pressure. When changing the slope of the spring coefficient over its displacement, larger WOB variations are expected. However, further optimisation into the damping coefficient slope can lead to smaller occurring stresses.
- In this research, the efficiency of the active heave compensator is assumed to be constant for all peak periods and significant wave heights researched at an efficiency of 95%, following information provided by BargeMaster [7]. When decreasing this efficiency, for selected or all wave periods, the occurring drill-string stresses will increase as result. In further research, the effect of smaller efficiencies and variable efficiencies over the incoming wave periods and heights, related to the system's actual performance, is to be researched. In this sense, the active heave compensation model approaches reality more.
- The understanding of the bottom hole assembly motion holds relevance for the workability of the drilling operation. As the lift-off point is a limit in this study, the bottom hole assembly is modelled as clamped to the seabed. For further analysis, the modelling of the bottom hole assembly as freely moving in the z-direction will add to the understanding of the lift-off behaviour. This is of relevance to better understand the hydrodynamic load working on the bottom hole assembly during lift-off.

References

[1] 4C Offshore. *Global Offshore Renewable Map*. Mar. 2022. URL: https://map.4coffshore.com/offshorewind/.

[2] R. Abumandour, M. Kamel, and M. Nassar. "Application of the GDQ Method to Vibration Analysis". In: *International Journal of Mathematics and Computational Science* 1 (June 2015), pp. 242–249.

[3] A.M. Al-Ajmi and R.W. Zimmerman. "Stability analysis of vertical boreholes using the MogiCoulomb failure criterion". In: *International Journal of Rock Mechanics and Mining Sciences* 43.8 (2006), pp. 1200–1211.

[4] Aktis Hydraulics. *Aktis Hydraulics Offshore Waves*. Mar. 2022. URL: https://aktishydraulics.com/capabilities/waves/waves-2/.

[5] *Ampelmann Systems*. Mar. 2022. URL: https://www.ampelmann.nl/systems/.

[6] C. Balci. "Estimation of optimum specific energy based on rock properties for assessment of roadheader performance". In: *Journal of the Southern African Institute of Mining and Metallurgy* 104.11 (2004), pp. 633–641.

[7] *Bargemaster Products*. Mar. 2022. URL: https://www.barge-master.com/products/bm-t700/.

[8] N. Barton, R. Lien, and J. Lunde. "Engineering classification of rock masses for the design of tunnel support". In: *Rock mechanics* 6.4 (1974), pp. 189–236.

[9] R. Bekkers. "Modelling of the drilling rates for large diameter offshore foundation piles". MA thesis. Delft, NL: Delft University of Technology, Sept. 2018.

[10] S. Biao and M. Baosong. "The return of drilling fluid in large diameter horizontal directional drilling boreholes". In: *Tunnelling and Underground Space Technology* 52 (2016), pp. 1–11.

[11] Z.T. Bieniawski. "Classification of rock masses for engineering: the RMR system and future trends". In: *Rock Testing and Site Characterization*. Elsevier, 1993, pp. 553–573.

[12] N. Bilgin, H. Copur, and C. Balci. *Mechanical excavation in mining and civil industries*. CRC press, 2013.

[13] N. Bilgin et al. "Dominant rock properties affecting the performance of conical picks and the comparison of some experimental and theoretical results". In: *International Journal of Rock Mechanics and Mining Sciences* 43.1 (2006), pp. 139–156.

[14] R.D. Blevins. "Flow-induced vibration". In: *New York, Harvard journal* (1977).

[15] F. Burel, R. Taccani, and N. Zuliani. "Improving sustainability of maritime transport through utilization of Liquefied Natural Gas (LNG) for propulsion". In: *Energy* 57 (2013), pp. 412–420.

[16] B. Butler and E. Larralde. "Motion compensation on drilling vessels". In: *Offshore Technology Conference*. OnePetro. 1971.

[17] B.V. Butler. "Heave compensation". In: *SPE European Meeting*. OnePetro. 1973.

[18] S.L. Chen, K. Blackwood, and E. Lamine. "Field investigation of the effects of stick-slip, lateral, and whirl vibrations on roller-cone bit performance". In: *SPE drilling & completion* 17.01 (2002), pp. 15–20.

[19] L. Cheng. *Novel coal-cutting bits and their wear resistances*. Vol. 8791. US Department of the Interior, Bureau of Mines, 1983.

[20] *Cranemaster Passive Heave Compensator*. Mar. 2022. URL: https://www.cranemaster.com/products/passive-heave-compensators/.

[21] R.A. Cunningham. "Analysis of Downhole Measurements of Drill String Forces and Motions". In: *Journal of Engineering for Industry* 90.2 (May 1968), pp. 208–216. eprint: https://asmedigitalcollection.asme.org/manufacturingscience/article-pdf/90/2/208/6497975/208_1.pdf.

[22] *Developments in XL Drilling for Monopiles/Shafts used in the offshore energy sector*. June 2014. URL: https://www.sut.org/wp-content/uploads/2014/06/SUT_140625_OSIG-SWI_FSC_SWGeoforum_Presentation.pdf.

[23] J.S. Dodgson et al. "Multi-criteria analysis: a manual". In: (2009).

[24] C.H. Dowding and D. Siebert. "Control of Construction Vibrations with an Autonomous Crack Comparometer". In: *Explosives and Blasting Techniques* (2000), pp. 103–110.

[25] M.W. Dykstra, D.C.K. Chen, and T.M. Warren. "Experimental evaluations of drill bit and drill string dynamics". In: *SPE Annual Technical Conference and Exhibition*. OnePetro. 1994.

[26] EMODnet Bathymetry. *Bathymetry Map*. Dec. 2021. URL: https://www.emodnet-bathymetry.eu/.

[27] Wind Europe. "Floating offshore wind energy: a policy blueprint for Europe". In: *Position Paper* 10 (2018).

[28] I. Evans. "Theory of the cutting force for point-attack picks". In: *Int. J. Min. Eng.;(United Kingdom)* 2.1 (1984).

[29] I. Evans and C.D. Pomeroy. *The strength, fracture and workability of coal: a monograph on basic work on coal winning carried out by the Mining Research Establishment, National Coal Board*. Elsevier, 1966.

[30] V. Eyring et al. "Emissions from international shipping: 1. The last 50 years". In: *Journal of Geophysical Research: Atmospheres* 110.D17 (2005).

[31] *Fleet and Equipment*. Mar. 2022. URL: https://boskalis.com/about-us/fleet-and-equipment.html#view/grid.

[32] *Flydrill Kelly-Pile-Top Drilling Unit*. 2021. URL: https://www.efebauer.com/products/overview-other-products/fly-drill/.

[33] K.H. Gehring. "A cutting comparison". In: *Tunnels and Tunnelling;(UK)* 21.11 (1989).

[34] A. Ghasemloonia, R.D. Geoff, and S.D. Butt. "Vibration analysis of a drillstring in vibration-assisted rotary drilling: finite element modeling with analytical validation". In: *Journal of Energy Resources Technology* 135.3 (2013).

[35] N. Goktan R.M. & Gunes. "A semi-empirical approach to cutting force prediction for point-attach picks". In: *Journal of the southern African institute of mining and metallurgy* 105.4 (2005), pp. 257–263.

[36] K. Hiscock, H. Tyler-Walters, and H. Jones. "High level environmental screening study for offshore wind farm developments–marine habitats and species project". In: (2002).

[37] E. Hoek and E.T. Brown. “The Hoek–Brown failure criterion and GSI–2018 edition”. In: *Journal of Rock Mechanics and Geotechnical Engineering* 11.3 (2019), pp. 445–463.

[38] E. Hoek and P. Kaiser. *Support of Underground Excavation in Hard Rock*. Mining Research Directorate and Universities Research Incentive Fund, Jan. 1995.

[39] L.H. Holthuijsen. *Waves in oceanic and coastal waters*. Cambridge university press, 2010.

[40] L.W. Home. “Limiting factors on economical use of a raise drill”. In: *Proceeding of 3rd Australian tunnelling conference, Sydney*. 1978, pp. 90–98.

[41] *Jiansui Rock Roller Cutters*. Jan. 2021. URL: http://www.rock-cutters.com/rcd-roller-cutters/.

[42] A. Joshi et al. “Likert scale: Explored and explained”. In: *British journal of applied science & technology* 7.4 (2015), p. 396.

[43] Y. Kallinderis, K. Schulz, and W. Jester. “Application of Navier-Stokes Methods to Predict Vortex-Induced Vibrations of Offshore Structures”. In: *Parallel Computational Fluid Dynamics 2000*. Ed. by C.B. Jenssen et al. Amsterdam: North-Holland, 2001, pp. 13–30.

[44] D. Kim and N. Ku. “Heave Compensation Dynamics for Offshore Drilling Operation”. In: *Journal of Marine Science and Engineering* 9.9 (2021), p. 965.

[45] X. Li et al. “A theoretical model for estimating the peak cutting force of conical picks”. In: *Experimental Mechanics* 58.5 (2018), pp. 709–720.

[46] M.A. Abdel N. Mahmoud. “Correlation of sandstone rock properties obtained from field and laboratory tests”. In: *International Journal of Civil and Structural Engineering* 4.1 (2013), p. 1.

[47] K.R. Massarsch, B.H. Fellenius, and A. Bodare. “Fundamentals of the vibratory driving of piles and sheet piles”. In: *geotechnik* 40.2 (2017), pp. 126–141.

[48] M. Mellor. *Mechanics of Cutting and Boring: Dynamics and energetics of indentation tools*. Vol. 76. The Laboratory, 1975.

[49] Microsoft Bing. *Microsoft Bing Maps*. Apr. 2022. URL: https://www.bing.com/maps.

[50] S.A. Miedema. *The Delft sand, clay and rock cutting model*. IOS Press, 2014.

[51] M.H. Miller and D.L. Sikarskie. “On the penetration of rock by three-dimensional indentors”. In: *International Journal of Rock Mechanics and Mining Sciences & Geomechanics Abstracts* 5.5 (1968), pp. 375–398.

[52] J. Nedwell and D. Howell. “A review of offshore windfarm related underwater noise sources”. In: *Cowrie Rep* 544 (2004), pp. 1–57.

[53] Y. Nishimatsu. “The mechanics of rock cutting”. In: *International Journal of Rock Mechanics and Mining Sciences & Geomechanics Abstracts*. Vol. 9. 2. Elsevier. 1972, pp. 261–270.

[54] E.K. Norlund and I. Gribkovskaia. “Reducing emissions through speed optimization in supply vessel operations”. In: *Transportation Research Part D: Transport and Environment* 23 (2013), pp. 105–113.

[55] *Offshore Foundation Drilling*. Jan. 2021. URL: https://www.herrenknecht.com/en/products/productdetail/ofd/.

[56] *Offshore Foundations - BSD3000 & Dive Drill*. 2021. URL: https://www.bauer-renewables.co.uk/en/offshore-foundations/.

[57] *Orcina Ltd. - the home of OrcaFlex*. Nov. 2022. URL: https://www.orcina.com/.

[58] B. Paul and D.L. Sikarskie. "A preliminary theory of static penetration by a rigid wedge into a brittle material". In: *SME Transactions* 372 (1965), p. 383.

[59] *Pick-points and Adapters*. Jan. 2022. URL: `https://www.diomar.gr/pick-points-and-adapters/`.

[60] *Reverse Circulation Pile-Top Drillig Rigs*. 2021. URL: `https://hmhw.com/service/rcd-rigs/`.

[61] *Reverse circulation pile-top drills*. July 2021. URL: `https://www.lddrill.com/equipment/rcd-pile-top-drills/`.

[62] *Reverse circulation pile-top drills*. 2021. URL: `http://www.ddcbv.com/what-we-do/pile-top-rigs/`.

[63] E.R Rhee et al. "A study on the inverse kinematic analysis of the casing oscillator". In: *ISIE 2001. 2001 IEEE International Symposium on Industrial Electronics Proceedings (Cat. No.01TH8570)*. Vol. 1. 2001, 666–671 vol.1.

[64] *ROC Drilling Equipment*. June 2022. URL: `http://www.rocequipment.com/`.

[65] F.F. Roxborough and H.R. Phillips. "Rock excavation by disc cutter". In: *International Journal of Rock Mechanics and Mining Sciences & Geomechanics Abstracts* 12.12 (1975), pp. 361–366.

[66] A.R. Shahani and S.M.H. Sharifi. "Contact stress analysis and calculation of stress concentration factors at the tool joint of a drill pipe". In: *Materials & Design* 30.9 (2009), pp. 3615–3621.

[67] G. Spagnoli and L. Weixler. "Alternative Offshore Foundation Installation Methods". In: *Offshore Technology Conference*. OnePetro. 2013.

[68] G. Spagnoli and L. Weixler. "New technologies for offshore piles installation". In: *Offshore Mediterranean Conference and Exhibition*. OnePetro. 2013.

[69] R. Teale. "The concept of specific energy in rock drilling". In: *International Journal of Rock Mechanics and Mining Sciences & Geomechanics Abstracts* 2.1 (1965), pp. 57–73.

[70] K. Terzaghi. "Rock defects and loads on tunnel supports". In: *Rock tunnelling with steel supports* (1946).

[71] J. Tian et al. "Rock breaking mechanism in percussive drilling with the effect of high frequency torsional vibration". In: *Energy Sources, Part A: Recovery, Utilization, and Environmental Effects* 44.1 (2022), pp. 2520–2534.

[72] T.M. Warren. "Factors affecting torque for a roller cone bit". In: *Journal of petroleum technology* 36.09 (1984), pp. 1500–1508.

[73] G.E. Wickham and H.R. Tiedemann. *Ground support prediction model (RSR concept)*. Tech. rep. JACOBS ASSOCIATES INC SAN FRANCISCO CA, 1974.

[74] G. Wijk. "A model of tunnel boring machine performance". In: *Geotechnical & Geological Engineering* 10.1 (1992), pp. 19–40.

[75] G. Wijk. "Rotary drilling prediction". In: *International journal of rock mechanics and mining sciences & geomechanics abstracts*. Vol. 28. 1. Elsevier. 1991, pp. 35–42.

[76] G. Wijk. "The stamp test for rock drillability classification". In: *International Journal of Rock Mechanics and Mining Sciences & Geomechanics Abstracts*. Vol. 26. 1. Elsevier. 1989, pp. 37–44.

[77] P.J. Willard, G. Neumann, and R.W. James. *Practical methods for observing and forecasting ocean waves by means of wave spectra and statistics*. Tech. rep. NAVAL OCEANOGRAPHIC OFFICE NSTL STATION MS, 1971.

[78] Wind Europe. “Wind Energy in Europe (2021-2025)”. In: (Feb. 2021).

[79] *Field Measurements of Downhole Drillstring Vibrations*. Vol. All Days. SPE Annual Technical Conference and Exhibition. Sept. 1985. eprint: `https://onepetro.org/SPEATCE/proceedings-pdf/85SPE/All-85SPE/SPE-14330-MS/2075870/spe-14330-ms.pdf`.

[80] WW3 NOAA. *Wavewatch III Environmental Modelling Centre*. Apr. 2022. URL: `https://polar.ncep.noaa.gov/waves/wavewatch/`.

[81] D. Zhang and L. Wang. “Investigation of chip in vibration drilling”. In: *International Journal of Machine Tools and Manufacture* 38.3 (1998), pp. 165–176.

[82] J.B. Zhang and X.H. Lu. “Fatigue analysis of the drill string according to multiaxial stress”. In: *Advanced Materials Research*. Vol. 418. Trans Tech Publ. 2012, pp. 993–996.

[83] L.H. Zhu et al. “A mathematical model of the motion of cutting particles in reverse circulation air drilling”. In: *Applied Mathematics and Computation* 256 (2015), pp. 192–202.

A

Appendix - Theoretical background

In this appendix the theoretical background to the research is presented. This theory is used to understand and interpret the results which are presented in Chapter 5.

Rock excavation methods

In order to excavate rock and create the desired anchor pile hole, multiple drilling methods can be used. The largest distinction is made between rock cutting and rock indenting. Which show different excavation types during operation.

Rock cutting

When drilling using a cutting method, rock is probable to fail due to shear or cataclastic failure [50]. This is the result of large cutting angles and small excavation depths. The type of failure is dependant on the ductility number of the rock. To assess the cutting forces and specific energy required to excavate rock, multiple models are developed. Here it is important to distinguish brittle tensile and brittle shear failure. [53] and [50] theoretically describe brittle shear failure. [29], [28], [35], [45] and [50] theoretically describe brittle tensile failure. Ductile failure of rock is described by [50]. Finally an empirical cutting model is described by [13].

Table A.1: Rock classification based on UCS [38]

Grade*	Term	Uniaxial Comp. Strength (MPa)	Point Load Index (MPa)	Field estimate of strength	Examples**
R6	Extremely Strong	> 250	>10	Rock material only chipped under repeated hammer blows, rings when struck	Fresh basalt, chert, diabase, gneiss, granite, quartzite
R5	Very strong	100 - 250	4 - 10	Requires many blows of a geological hammer to break intact rock specimens	Amphibolite, sandstone, basalt, gabbro, gneiss, granodiorite, limestone, marble, rhyolite, tuff
R4	Strong	50 - 100	2 - 4	Hand held specimens broken by a single blow of geological hammer	Limestone, marble, phyllite, sandstone, schist, shale
R3	Medium strong	25 - 50	1 - 2	Firm blow with geological pick indents rock to 5 mm, knife just scrapes surface	Claystone, coal, concrete, schist, shale, siltstone
R2	Weak	5 - 25	***	Knife cuts material but too hard to shape into triaxial specimens	Chalk, rocksalt, potash
R1	Very weak	1 - 5	***	Material crumbles under firm blows of geological pick, can be shaped with knife	Highly weathered or altered rock
R0	Extremely weak	0.25 - 1	***	Indented by thumbnail	Clay gouge

* Grade according to ISRM (1981).
** All rock types exhibit a broad range of uniaxial compressive strengths which reflect the heterogeneity in composition and anisotropy in structure. Strong rocks are characterised by well interlocked crystal fabric and few voids.
*** Rocks with a uniaxial compressive strength below 25 MPa are likely to yield highly ambiguous results under point load testing.

Table A.2: Examples of ductility numbers per rock type [38]

Rock type	Class	Group	Texture: Course	Texture: Medium	Texture: Fine	Texture: Very fine
SEDIMENTARY	Clastic		Conglomerate (22)	Sandstone 19	Siltstone 9	Claystone 4
SEDIMENTARY	Clastic			← Greywacke (18) →	← Greywacke (18) →	
SEDIMENTARY	Non-Clastic	Organic		← Chalk 7 →	← Chalk 7 →	
SEDIMENTARY	Non-Clastic	Organic		← Coal (8-21) →	← Coal (8-21) →	
SEDIMENTARY	Non-Clastic	Carbonate	Breccia (20)	Sparitic Limestone (10)	Micritic Limestone 8	
SEDIMENTARY	Non-Clastic	Chemical		Gypstone 16	Anhydrire 13	
METAMORPHIC	Non Foliated		Marble 9	Hornfels (19)	Quartzite 24	
METAMORPHIC	Slightly foliated		Migmatite (30)	Amphibolite 31	Mylonites (6)	
METAMORPHIC	Foliated*		Gneiss 33	Schists (10)	Phyllites (10)	Slate 9
IGNEOUS	Light		Granite 33		Rhyolite (16)	Obsidian (19)
IGNEOUS	Light		Granodiorite (30)		Dacite (17)	
IGNEOUS	Dark		Diorite (28)		Andesite 19	
IGNEOUS	Dark		Gabbro 27	Dolerite (19)	Basalt (17)	
IGNEOUS	Dark		Norite 22			
IGNEOUS	Extrusive pyroclastic type		Agglomerate (20)	Breccia (18)	Tuff (15)	

* These values are for intact rock specimens tested normal to foliation. The value of m_i will be significantly different if failure occurs along a foliation plane.

When performing rock cutting, the drill-head is equipped with cutting bits, the most encountered forms are the chisel and conical pick-point. Improved cutting bit inserts, which decrease wear are described by [19]. Cutting bits move through the excavation layer in a horizontal, dragging manner. Often chisels are used for soft and non-abrasive rock. Due to the shape of a pick-point, it experiences a smaller contact surface with the excavation material. Resulting in a increase in local stress when cutting. Thus pick-points are more favourable when excavating harder rock. Cutting methods are workable for rock with strengths up to 100.0 MPa [50], making it relevant. The spacing between the cutting bits are optimised to increase excavation rates. Examples of a pick-point and chisel cutter bit are provided in Figure A.1a and A.1b.

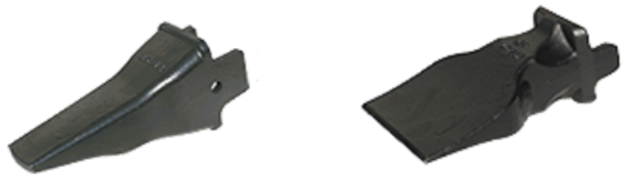

(a) Pick-point cutter **(b)** Chisel cutter

Figure A.1: Examples of different cutter bit types [59]

Rock indentation

When excavating rock using an indentation method, rock is crushed under high local pressure. [12] states that the penetration indeces are often in the order of 15 - 35 kN/mm. When excavating ductile rock, a relatively constant cutting forces is observed, when excavating brittle rock a more saw-toothed profile is observed [48]. To describe the relation between indentation forces and penetration depth for brittle rock, theoretically models are described by [58], [29], [51], and [65] for multiple roller bits. Empirical models are described by [76], [72], and [40].

Indentation drill heads are equipped with rollers, these rollers are modified to toothed rollers, v-shaped discs, or button rollers. When hard rock is excavated, Indentation methods are most often used. Due to it's design, the roller can exert a higher local pressure, which leads to a crushed failure type in brittle rock. During loading, cracks form and propagate through the material forming chips which break out. The three main roller types are presented in Figure A.2a, A.2b, and A.2c.

(a) Toothed roller **(b)** V-shaped disc roller **(c)** Button roller

Figure A.2: Examples of different roller bit types [41]

Vibration

An alternative method to excavate rock is through the use of vibrations. Vibratory tools are often used in combination with cutters or indenters. A comprehensive model of the effect of vibration in the practice of steel cutting is described by [81]. Note that steel and rock can react differently due to difference in plasticity or brittleness. The effect of vibration on the already existing cutting and indentation techniques, is described by [71]. Here the effect of vibrations on the rate of penetration (ROP) is found positive. The effect is largest when the vibration reaches the natural frequency of the excavated rock. For the experimental set-up, an increase of the ROP of 150 % is measured at this resonance point.

Transportation of cuttings

Once the rock is fractured, the cuttings must be transported out of the borehole. In the case of no transport, the cuttings would remain at the drilling interface and decrease the drill-rate.

The main methods used in offshore operations are direct circulation drilling (DCD), reverse circulation drilling (RCD) and bucket drilling.

DCD is used in oil and gas drilling, pumping pressurised drilling fluid, called *mud*, down along the drill-string in a hose and releasing it at the bottom of the borehole. Once released, the mud travels upwards through the borehole and escapes at the seabed surface. A flow is created in which the cuttings are transported. For small diameter boreholes this is a workable approach. However, when increasing the diameter of the borehole, the total volume which must be filled with mud increases exponentially. The flow velocity drops with the increase in diameter, making this transport method unattractive for anchor pile drilling. Also the large volumes of drilling fluid makes it a more expensive option. An improved DCD approach is discussed by [10], however not applicable in the researched situation.

Reverse circulation drilling

When using RCD, a hose or pipe which is located within the drill string is used to transport the cuttings to sea level. By creating an upward flow in this hose or pipe, the seawater and cuttings surrounding the drill-head are sucked into the pipe. Finally, the cuttings are disposed into the open sea at water level, or caught and filtered in tanks. The flow in the hose or pipe can be created using an airlift system or a hydraulic pump. The behaviour of cuttings is described by [83], which studies the effect of particle size on particle velocity. The transport of cuttings is one of the limiting conditions which determine the drill rate of a drill. Due to the presence of seawater during anchor pile drilling, RCD is an interesting technique for anchor pile drilling. In Figure A.3 an example of an airlift RCD method is presented.

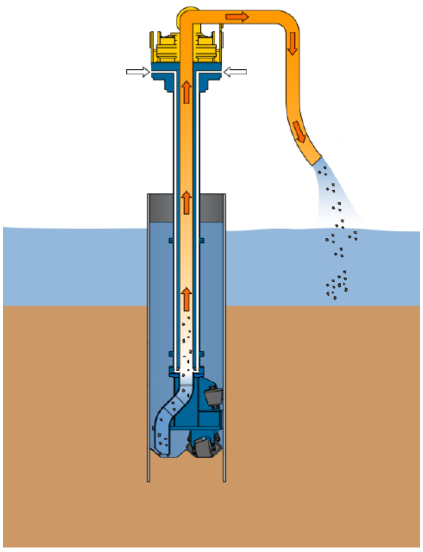

Figure A.3: Reverse Circulation Drilling method, modified from [22]

Bucket drilling

Finally, another method to transport cuttings is to collect them and periodically, this is often done using a bucket. The bucket drilling method works for a drill head with cutter bits. During the cutting of the soil, the loose material is directly scooped into the bucket. By applying a downward force on the rock, more material is forced into the bucket every rotation. Once the bucket is full of soil, it is lifted to sea level and disposed either into a collection tank, or at a specified location. The use of this transportation method is used for softer soils such as clay or sand and is not recommended for rock cutting. The logistic task of lifting the complete bucket to sea level makes this a unfavourable option when drilling deeper. However, when removing an overburden layer, it is of interest.

Rate of penetration

To determine the performance of a drill, the rate of penetration (ROP) in selected rock strengths must be determined. As is discussed in previous work by [9], the drilling rate has two limits. These limits are the;

- Maximum achievable WOB
- Transportation rate of cuttings

- Maximum deliverable torque
- Maximum deliverable power
- Maximum rotational speed.

To determine the ROP, a simplified model based on the specific energy is determined. The specific energy is expressed in the amount of energy required to excavate a volume of soil or rock [50]. By translating the specific energy to operational parameters, a ROP can be approximated. The rotational and thrust specific energy is provided in Equation A.1 [69].

$$e = e_t + e_r = \left(\frac{F}{A}\right) + \left(\frac{2\pi}{A}\frac{NT}{u}\right) \tag{A.1}$$

with:

e_t	Thrust specific energy	[N/m^3]
F	Thrust exerted	[N]
A	Surface drill head	[m^2]
e_r	Rotary specific energy	[N/m^3]
N	Rotational speed	[rpm]
T	Torque exerted	[Nm]
u	Penetration rate	[m/min]

The specific energy can be expressed following the model described by [6]. Here a combination of the models of [13] and [33] is made and tested to measured experimental data. An empirical relation is found to determine the optimum specific energy based on the UCS and BTS of a rock sample.

The efficiency of rock excavation is dependant on the type of drill, rock, and gearing. This is again dependant on the drilling rig. This simplified ROP model is used to compare drilling rigs, thus assumptions are made to make this comparison. As shown in Table A.3.

Table A.3: Assumptions in drill rate model

Parameter	Value	Unit
Ratio $P_{op.}$ / P_{max}	50.0	%
Ratio $T_{op.}$ / T_{max}	50.0	%
Airlift velocity	4.0	m/s
Concentration airlift	0.05	-
Ratio F_H / F_V (cutter)	1.5	-
Ratio F_H / F_V (indenter)	10.0	-

Two examplar ROP plots for drill heads fitted with rollers, are provided in Figure A.4. The limits stated above all lead to individual ROP for different compressive strengths. The lowest of the limits is governing as normative ROP.

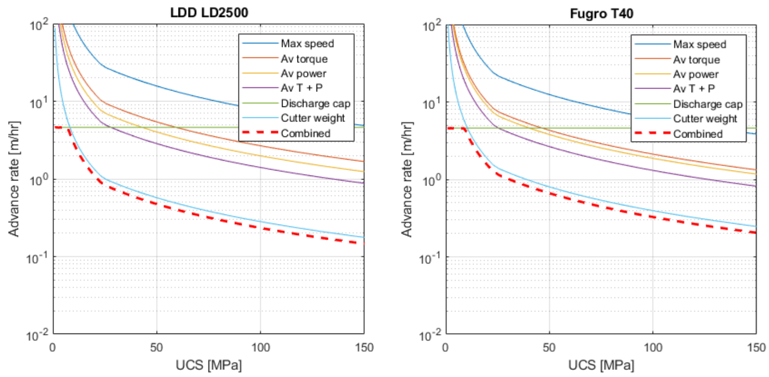

Figure A.4: Modelled drill rates for three drill rigs

Borehole stability

When drilling a borehole it is important to assess the stability of the wall, to make a decision on the use of wall-stabilising measures during operation. In the essence borehole stability can be divided in micro stability and macro stability. By assessing if there is a shear plane present that might lead to macro failure of borehole wall.

Slope failure

A cross-section of a borehole can be viewed as a vertical wall with a specified depth. Assessing the slope stability in soils using the Mohr-Coulomb failure envelope is a proven method. This criterium states that their is a linear relation for the failure due to a combination of compressive and shear loading. Pore pressure is an important aspect to this assessment leading to cohesion is sand soil. In submerged conditions the pore pressure is equal to the surrounding pressure. Making the pressure difference zero. Clay experiences cohesion due to electrostatic forces, Rock due to the chemical cementation of minerals and sediment [50]. Heavily fractured rock, i.e. a low RQD, experiences less cohesion when assessed at macro scale. This lack of cohesion can form a slope stability issue. The Mohr-Coulomb failure envelop assumes soils to be homogeneous and in tact, making it unreliable for the cause of heavily fractured rock. An alternative to the Mohr-Coulomb failure criterium is the Mogi-Coulomb failure criterium . Which is used in the assessment of vertical boreholes [3].

Casing use

A casing consists of a steel pipe which is installed as bracing measure. Casings can be utilised to reinforce the borehole during operation or permanently. The installation of casings can be done using a casing oscillator [63]. This oscillator turns the casing back and forth until the target depth is reached. Another method to install a casing is by using a vibrohammer, similar to the installation of a monopile. The outer diameter of the casing is often slightly smaller than the inner diameter of the borehole to ensure good connection. Another method is the vibratory casing driving. This technique is similar to sheet pile driving which is broadly used in the civil industry [47]. Here it is important to note that the vibration must be monitored when sensitive structures or wildlife are present. The vibrations which are emitted and the effect of mitigation measures are described by [24]. Casings are not necessarily required when drilling, only when a borehole is sensitive to collapse. The risk of collapse is lower for anchor pile drilling when comparing to deep oil and gas exploration boreholes.

Rock mass rating evaluation

A method to assess the stability of a borehole and the need for stability measures is the so-called Rock Mass Rating (RMR) rating principle, here rock properties such as RQD, UCS, and joint spacing are given point ratings. This method is often used in the tunnelling industry to asses which reinforcement techniques must be used per RMR rating. The first model to describe this rating has been determined empirically by [11]. Next to the classic RMR system multiple other rating methods have been developed to assess tunnelling and borehole support measures. These are the; rock load classification system [70], rock structure rating classification [73], Q-classification system [8], geological strength index (GSI) [37]. The models are broadly used, however are applicable to rock formation on dry land, incorporating a parameter for groundwater present or pore pressure. The model of Hoek [37] shows the opportunity to use the GSI in a submerged manner following the Hoek-Brown criterium. The downside to this approach, is the freedom of interpretation in the determination of the GSI value. Which is sensitive to a human error and must be determined by one who is experienced in the rock mechanics field.

Effect of RQD on stability

The RMR approach discussed in the Section A takes the Rock Quality Designation (RQD) into account. The RQD parameter is a way to describe the fracturing of a rock sample. This is a parameter that is often assessed in on site sample testing. Emperical relations between the RQD and UCS of a sandstone sample have been found in an onshore experimental set-up [46]. This approach has not been proven applicable to all rock types and strengths. However, when the RQD value becomes very low, the rock particles may act as unconsolidated, making it prone to instability issues.

Ocean waves

When describing the motion of a vessel, it is important to first understand the waves which load it. The commonly used way to describe ocean waves is by means of the ocean wave theory. This theory is based on the assumption that an irregular ocean wave can be dividing into multiple regular, harmonic waves. Each single harmonic component has it's own amplitude, wave length, frequency, and direction. By following the superposition principle, all regular waves combined make it possible to predict the irregular and complex behaviour of ocean waves by means of regular harmonics [39]. This superposition principle is graphically represented in Figure A.5. A single harmonic wave follows the shape and characteristics of a regular sine function. The profile of a harmonic wave propagating in the positive x direction following time steps t can be described by the Equation A.2.

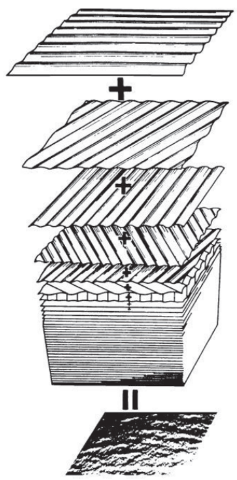

Figure A.5: Superposition principle on an irregular ocean [77]

$$\zeta = \zeta_a \cos(kx - \omega t) \tag{A.2}$$

with:

ζ_a	Wave amplitude	[m]
k	Wave number	[m^{-1}]
ω	Wave frequency	[rad/s]
x	Position	$[m]$
t	Time step	$[s]$

Morison Equation

The hydrodynamic force on a slender structure consist of two parts (f_d & f_i). The first is the loading by waves, the second is the loading by current. Current is assumed to be a constant force, due to the constant velocity at which the water flows. Variations in the current velocity are generally small and happen slowly. The loading by waves is non-constant and can be described following the orbital motion at which the water particles move.

The total loading on the structure can be subdivided in a drag and an inertia component. The steady drag force f_d is expressed in terms of a quadratic relation to water particle velocity. In the drag expression a drag coefficient C_D is present. When a body is shaped more hydrodynamic, a lower coefficient is used. For a sphere the general coefficient is 1.20. The drag component of the Morison Equation is provided in Equation A.3

$$f_d(z) = \frac{1}{2}\rho C_D D u(z)\left|u(z)\right| \tag{A.3}$$

with:

ρ	Density of sea water	[kg/m^3]
C_D	Drag coefficient	$[-]$
D	Diameter of tubular	[m]
u	Particle velocity	[m/s]

The inertial component of the Morison equation is quadratically related to the diameter of the member and linearly related to the acceleration of the water particle velocities. The expression is provided in Equation A.4.

$$f_i(z) = \frac{1}{4}\pi\rho C_M D^2 \dot{u}(z) \tag{A.4}$$

with:

C_M	Inertia coefficient	$[-]$
$\dot{u}$	Particle acceleration	[m/s^2]

Finally the drag and inertia part of the Morison equation can be combined to form the final form, which is presented in Equation A.5.

$$f(z) = f_d(z) + f_i(z) \tag{A.5}$$

The inertial wave force is strongly dependant on the Keulegan-Carpenter (KC) number. Due to the fact that the added mass coefficient vary significantly when a change in KC number occurs.

The expression for the KC number is presented in Equation A.6. A structure is drag dominated when the KC number is smaller than 10, and inertia dominated when the KC number is larger than 40. In these situations, the other part of the Morison equation becomes redundant. In the case the KC number is within the range of 10 and 40, both parts must be taken into account.

$$KC = \frac{u_a T}{D} \tag{A.6}$$

with:

KC	Keulegan Carpenter number	$[-]$
u_a	Flow velocity	[m/s]
T	Wave period	[s]
D	Diameter tubular	[m]

B

Appendix - Drilling method risk assessment

In this appendix the risk of the project has been assessed. This must be done in order to finally come to a correct and all-inclusive concept methodology. Below the risks are subdivided into health & safety hazards and environmental hazards. After these hazards are identified, measures can be selected to decrease or remove the impact it has on the crew or operation.

Hazardous activities

During the following activities, mechanical hazards are present;

- Loading / Unloading
- Transport
- Assembly / Disassembly
- Positioning of machinery
- Work with hydraulics
- Drilling operation
- Cleaning & Inspection
- Exchange of components.

These activities will be assessed per hazard subdivision. There the causes, consequences, probabilities, and impacts are taken into account. In this stage the hazards with the largest impact are taken into account for consideration. Meaning that the hazards which affect the crew in a health or safety manner are considered.

Health & safety

First the health and safety hazards will be elaborated. These are the hazards which affect the crew and all people involved in the drilling operation. Per group the most hazardous activities will be touched upon and the possible mitigation measures will be discussed.

Mechanical hazards

Mechanical hazards are hazards which occur due to the failure or misuse of mechanical equipment or parts. Due to the fact that a drill rig is a large piece of mechanical machinery, the mechanical hazards are the largest group of hazards. The most hazardous activities are in the assembly operation and disassembly. Collision of a part with another part or crew member are the most probable risks. Mitigating measures which must be taken are correct briefing and debriefing of the crew, correct use of PPE, and clear communication between crew members during the activity. Also area's which are to hazardous must be marked and elaborated in the briefing.

Electrical hazards
Electrical hazards are hazards which occur due to the failure or misuse of a electrical parts or equipment. This could be a short-circuiting power tool or the failure of a fuse. The most hazardous activities are the assembly/disassembly and the exchange of components. During these activities parts can be live which can lead to crew being shocked and short-circuiting of the circuit. The short circuit can on it's turn lead to equipment break down. By frequent maintenance and surveying of the system, the leakage of current could be monitored and discovered. Next to monitoring, live parts can be marked to warn the crew of the hazard. Correct training of crew can decrease the change of these electrical hazards.

Thermal hazards
Thermal hazards are hazards which occur due to a change in thermal properties. This could be an explosion or fire but also an unexpected change in temperature leading to burning or injury. Within this group the most hazardous activities are within the drilling operation and the exchange of components. When exchanging, parts can still be of a high or low temperature. During maintenance and exchange of components, the machinery must be turned off in advance, to allow the machinery to cool down and relieve the pressure in the system. The system must remain down during the maintenance, a sign "Maintenance performed" can be an effective manner to mitigate the system being turned on by accident. By correct briefing of the crew, this information can be shared and elaborated further.

Substance hazards
Substance hazards are hazards which occur due to (mostly) leakage of substances. This could be a fuel leakage leading to a fire but also slipping due to a grease stain. The most hazardous operation is during drilling operations. Substance hazards can escalate fast, making it an important hazard to view. By correct recognition of these failures, the hazard can be decreased. This can be obtained by correct training of crew to recognise the first signs of a failure. Also training can make sure certain hazardous systems are not overloaded, which can increase the probability of failure. Also by informing crew on the hazards during operation can decrease the probability of occurrence, again by briefing and debriefing.

Noise hazards
Noise hazards are hazards which occur due to an excess of noise. This could be through loud exhaust systems or rubbing surfaces. The most hazardous activity for noise is during drilling operation. The personal consequences of frequent exposure to loud noise is hearing loss, which is a high impact on the well-being of the crew. The use of correct PPE and a warning when noisy equipment is turned on can minimise the exposure of the crew. During operation, communication between crew members can be hampered due to the noise. One can argue that a decrease of efficient communication can lead to more hazardous situations. With correct training and briefing of crew this communication gap can be closed.

Ergonomic hazards
Ergonomic hazards are hazards which occur due to (mostly) heavy work. This could be a issues with tool usage or visibility, or even lifting improperly. During drilling operation and during

maintenance the ergonomic hazards are highest. Managing a drill rig is heavy work, which can lead to strain, fatigue, and pain when exercised incorrectly. The use of correct clothing and footwear is a way to mitigate some of the hazards. Also by focusing on a correct working posture and health consultants on board can decrease the escalation of small issues.

Environmental

During offshore operations, the effect on marine flora and fauna must be taken into account. This topic is gaining more traction in the tendering process of new operations. It is therefore necessary to consider. The environmental risks discussed are; noise, emissions, and spillage of toxic substance.

Noise

Little research has been performed into the noise which is emitted during offshore pile drilling. In practice, it is likely sound will be transmitted into the water through air, ground and directly via the structure. Through the movement of the drill-head at the drill-rock interface, ground borne vibrations will be transmitted to the water. Also mechanical vibrations that are generated by the drilling rig can be transmitted through the air or directly to the water through it's parts. Also the disposal of cuttings at the water surface can create noise once entering the water. Next to the noise during the drilling operation, the noise and disturbance during transport is important to consider.

The available information states that drilling noise is often of a low level [52], and consisting of low frequency tones. However, the measurements have been implemented from comparable oil and gas drilling champagnes of a different scale to the foundation drilling assessed in this research. There is some evidence that the drilling noise could be enough to invoke behavioural reactions by some types of cetacea (whales). However, this is not yet proven in a published study. A mitigation option which could be researched is the use of a bubble curtain. This practice is occasionally used when pile-driving to decrease the noise transmission. This method is mainly focussed on the transmission through structure, which is not expected to be the main driver when drilling. When a casing is required during drilling, a vibro-hammer might be used. This operation is comparable to the installation of monopiles.

Due to the lack of information regarding the noise each drilling asset emits, no difference can be stated. However, due to the fact that the In-pile and Subsea drill have all mechanical machinery situated below water level, more sound may be transmitted directly to the surrounding water.

Emissions

During offshore pile drilling both vessel and drilling equipment are powered through diesel or LNG engines and generators. By using these engines CO_2, CH_4, SO_x, and NO_x are emitted into the environment [30]. Yearly a Construction vessel emits more than 9 000 tonnes of CO_2 [54], which is one of the highest contributing green house gasses. At this moment green alternatives are not yet commercially applied in the field. A shift towards electric or sustainable fuel propulsion is required to decrease the footprint of an offshore operation. The sustainable fuels which are considered and are in development are hydrogen (H_2) and e-methanol. Also a shift to the use of Liquefied Natural Gas (LNG) is noticeable in the industry. However, this is not a step towards the use of fossil free fuel. The transition to LNG can decrease the emission of a vessel up to 15% [15].

Substance spillage & turbidity

The spillage of toxic substance is a hazard to marine life. In comparison to offshore oil and gas operations, the amount of substances which can spill is relatively low. As no oil or gas is exploited from the subsurface. However, hydraulic fluids, fuel, lubricants, and grout can be spilled. [36] shows that the spillage of these substances affects the benthos present in the area. Benthos are a group of small organisms living at the seabed. These organisms are eaten by the fish and crustations present, which are on their turn eaten by seabirds and marine mammals. Thus the harmfull chemical substances which affect the benthos travel up the food chain to finally reach the larger animals present in the area. Eventually the spillage of toxic substances affects the whole ecosystem.

Next to the spillage, turbidity can occur due to the cuttings being disposed at sea level. These cuttings consist of small rock particles, sand, or clay. As with spillage, turbidity affects the benthos most. The turbidity at the surface leads to a decrease in sunlight reaching the seabed. Also the the cuttings will eventually land on the seabed, covering the living environment of the benthos. However, [36] shows that the effect is relatively low for these organisms. Only when a large change in water depth or seabed morphology is the result of the disposed cuttings.

C

Appendix - Asset specifications

In this appendix the considered assets are presented, these assets form the basis on which the economic assessment has been performed. The economic assessment lead to the determination of the most cost-effective drilling configuration. The most cost-effective drilling configuration has been assessed in this research.

Drilling methods

Pile-top drills

Large diameter drilling

Large Diameter Drilling, *LDD* in short, is a drilling contractor, designer, and manufacturer that is specialised in RCD drills using roller drill-heads. The drilling assets offered by LDD are summarised in Table C.1 with the corresponding characteristics. Only assets that are compatible with the design requirements set in Section 2.3.1 are considered.

Table C.1: LDD RCD asset overview [61]

Asset	Diameter range		Max. torque	Max. WOB	Mass
LD612	2000 mm	3000 mm	119 kNm	55 t	24 t
LD818	2000 mm	2500 mm	180 kNm	80 t	28 t
LD2500.1	2000 mm	5000 mm	119 kNm	100 t	30 t
LD2500.2	2000 mm	5000 mm	539 kNm	100 t	34 t

HMH

HMH is a RCD drilling asset designer and manufacturer specialised in roller drill-heads. The drilling assets offered by HMH are summarised in Table C.2 with the corresponding characteristics. Only assets that are compatible with the design requirements set in Section 2.3.1 are considered.

Table C.2: HMH RCD asset overview [62]

Asset	Diameter range		Max. torque	Max. WOB	Mass
PBA 615	1200 mm	2700 mm	150 kNm	60 t	19 t
PBA 818	1500 mm	3000 mm	180 kNm	90 t	27 t
PBA 936	2000 mm	6500 mm	360 kNm	120 t	32 t
PBA 1042	2500 mm	7500 mm	420 kNm	120 t	34.5 t

Fugro

Fugro is a RCD drilling asset contractor, designer, and manufacturer specialised in roller drill-heads. Fugro also specialises in soil surveys. The drilling assets offered by Fugro are summarised in Table C.3 with the corresponding characteristics. Only assets that are compatible with the design requirements set in Section 2.3.1 are considered.

Table C.3: Fugro asset overview [22]

Asset	Diameter range		Max. torque	Max. WOB	Mass
T10	1000 mm	2600 mm	267 kNm	100 t	30 t
T40	2000 mm	4000 mm	457 kNm	120 t	46 t

ROC

ROC is a RCD drilling asset contractor, designer, and manufacturer specialised in roller drill-heads. The drilling assets offered by ROC are summarised in Table C.4 with the corresponding characteristics. Only assets that are compatible with the design requirements set in Section 2.3.1 are considered.

Table C.4: ROC asset overview [64]

Asset	Max. diameter	Max. torque	Max. WOB	Mass
R3025	2500 mm	300 kNm	120 t	36 t
R3030	3000 mm	300 kNm	120 t	40 t
R3733	3300 mm	372 kNm	120 t	42 t

In-pile drills

Herrenknecht

Herrenknecht is a drilling asset designer and manufacturer. They have developed the Offshore Foundation Drilling (OFD) [55] asset using knowledge learned in onshore tunnelling. The OFD can be fitted with cutting teeth or a full face roller bit. The OFD asset is tailor made to a contractors dimensions, a general design for the requested pile design is provided in Table C.5. Herrenknecht states that the drill is able to operate in all rock types up to 150.0 MPa.

Table C.5: Herrenknecht drilling assets [55]

Asset	Diameter	Max. torque	Max. WOB	Mass
OFD	2500 mm	540 kNm	120 t	50 t

Bauer

Bauer is a drilling asset designer and manufacturer. One of the concepts they have developed is the so-called "Dive drill" [56]. The dive drill (DD C40) can be fitted with cutting teeth or a full face roller bit, depending on the to be excavated material. In the process a template must be installed on the seabed to ensure a stable and correct drilling location and angle. Another concept Bauer has developed is the so-called "Fly Drill" (BFD 3500) as discussed in Section C. The specification of these drilling assets are given in Table C.6. The maximum operational depth at which these assets can operate is 200 m. [67] states that the drill is used to remove soft soils up to 20.0 MPa using the auger drill-head.

Table C.6: Bauer Dive Drill assets [56]

Asset	Diameter range		Max. torque	Max. WOB	Mass
DD C40	1750 mm	3500 mm	275 kNm	100 t	35 t
BFD 3500	1850 mm	3500 mm	360 kNm	24 t	15 t

Subsea drills

Table C.7: Bauer Subsea drilling asset overview [56]

Asset	Diameter range		Max. torque	Max. WOB	Mass
BSD 3000	2000 mm	3000 mm	110 kNm	100 t	270 t

Casing fastening

A casing can be fastened using a casing oscillator, this is a machine which is able to rotate a large casing back and forth. In this way the casing is installed deeper into the borehole after more depth is reached with the drill-head. Another option is to use a vibro hammer, which is similar to a vibrating hammer used for monopile installation. The in-pile drill must be operated using a casing under in all scenarios. The pile-top drill and subsea drill use a casing when the seabed consists of cohesionless soils or an overburden layer is present. The subsea drill has an integrated casing oscillator in it's design [68]. Which can reach a total depth of 11.0 meters.

Generalised drilling assets

Table C.8: Generalised drilling assets

Drill type	Technique	Max. torque	Max. WOB	Power	Mass	Max. WD
Pile-top drill	RCD	306 kNm	100 t	350 kW	35 t	-
In-pile drill	RCD	408 kNm	110 t	300 kW	40 t	200 m
Subsea Drill	RCD	110 kNm	100 t	250 kW	270 t	-

Vessels

The drilling assets must be operated from a floating "platform". Each vessel has it's own characteristics, from possible locations for a drilling asset to it's reaction to wave heights and wave lengths. In the following parts the different types will be discussed. To assess the different types and there characteristics, the fleet of *Boskalis* will be used. As this contains a broad spectrum of options. In the assessment of different vessels the expected deck space required for a construction operation is taken into account. By following this step, four general vessel types can be distinguished;

1. Barge
2. Sheerleg
3. Construction support vessel
4. Heavy-lift vessel.

Barge

The first considered vessel type is the barge, a barge is a non-propelled vessel which is often used for it's large deck area. A barge can be equipped with a heavy-lift crane, making it a versatile and interesting option. Because the barge is non-propelled, a tugboat is required for the barge to move from port to site. A barge can maintain it's position through the use of anchors, these anchors are installed and relocated using anchor handling vessels. The available barges considered are presented in Table C.9. Once a barge does not have a crane installed, and this is required for an operation, an additional sheerleg barge can be mobilised. This extra option is elaborated in Section C.

Table C.9: Available Boskalis barges [31]

Asset	Deck area	Crane capacity	Moonpool	Positioning	Length
Giant 6	4 500 m^2	None	None	Anchors	137.0 m
Giant 7	4 500 m^2	1 000 t	None	Anchors	137.0 m

Tugboat

A tugboat, or tug in short, is generally used to move floating assets which are non-propelled. This could be a barge as described above, but could also be a semi-submersible floating platform. Another application for tugs is the handling of anchors as also described above. A typical bollard pull for an oceangoing tug is in the order of 200 t. For an anchor handling tug the bollard pull can be in the range of 70 t up to 180 t.

Sheerleg

A sheerleg is a heavy-lift barge which can be deployed as addition to a barge or other vessel. It is a heavy-lift asset which has no deck space available for a drilling spread. The sheerlegs presented in Table C.10 are self-propelled, however anchor handling vessels are required to install and relocate the anchors at the correct position. Through this way the sheerleg can maintain it's position during operation. A disadvantage to the use of a sheerleg is that the crane may only be operated in wave conditions where the significant wave height is smaller or equal to 1.5 m. This has to do with certifications on the vessel.

Table C.10: Available Boskalis sheerleg heavy-lift barges [31]

Asset	Deck area	Crane capacity	Positioning	Length
Taklift 4	None	2 200 t	Anchors	72.6 m
Taklift 7	None	1 200 t	Anchors	83.2 m
Asian Hercules III	None	1 000 t	Anchors	106.4 m

Construction support vessel

The second vessel type is the construction support vessel, *CSV* in short. This type of vessel is often used for offshore construction and has a combination of a medium sized deck and an installed crane, making it a versatile option. Within the CSV's one can make a subdivision in "small" CSV's which have a smaller deck space and generally a lower crane capacity, and "large" CSV's which have a larger deck space and generally a larger crane capacity. The distinction between small and large is based on the total length of the vessels in combination with the crane capacity. The small CSV is not able to provide enough deck space for the drilling spread and the foundation piles. It must be combined with a barge to increase the available deck space. The small and large CSV's are presented in Table C.11 and C.12 respectively.

Table C.11: Available Boskalis small CSV's [31]

Asset	Deck area	Crane capacity	Moonpool	Positioning	Length
BOKA Pegasus	810 m^2	6 t	None	DP2	91.0 m
BOKA Fulmar	850 m^2	20 t	7.0 m x 7.0 m	DP2	93.4 m
BOKA Falcon	1 015 m^2	150 t	7.0 m x 7.0 m	DP2	93.4 m

Table C.12: Available Boskalis large CSV's [31]

Asset	Deck area	Crane capacity	Moonpool	Positioning	Length
BOKA Tiamat	1 000 m^2	120 t	7.2 m x 7.2 m	DP2	98.1 m
BOKA Atlantic	1 405 m^2	140 t	7.2 m x 7.2 m	DP2	115.4 m
BOKA Ocean	2 400 m^2	250 t	7.2 m x 7.2 m	DP2	136.6 m

Heavy-lift vessel

The last vessel type is the heavy-lift vessel, this vessel is used to lift large and heavy constructions in offshore construction operations. These vessels typically have a large deck space to accommodate the large constructions during transport. Due to the size of the vessel, the reaction to wave loading is relatively lower than the previous vessel types. The available heavy-lift vessels considered are presented in Table C.13.

Table C.13: Available Boskalis heavy-lift vessels [31]

Asset	Deck area	Crane capacity	Moonpool	Positioning	Length
Bokalift 1	6 300 m^2	3 000 t	None	DP2	216.0 m
Bokalift 2	7 500 m^2	4 000 t	None	DP2	231.0 m

Generalised vessels

To perform a conceptual analysis on the best fitting type of vessel for this operation, generalised vessels are produced. In the determination of the generalised vessels, the data of the vessels mentioned in the parts above are used.

Table C.14: Generalised vessels to consider in design

Asset	Deck area	Crane capacity	Moonpool	Positioning	Length
Barge	4 500 m^2	None	None	Anchors	137.0 m
Sheerleg	None	1 700 t	None	Anchors	87.0 m
Heavy lift barge	4 500 m^2	1 000 t	None	Anchors	137.0 m
Small CSV	890 m^2	20 t	7.0 m x 7.0 m	DP2	93.0 m
Large CSV	1 450 m^2	165 t	7.2 m x 7.2 m	DP2	115.0 m
Heavy lift vessel	7 000 m^2	3 500 t	None	DP2	220.0 m

Boskalis

EQUIPMENT SHEET

SOUTHERN OCEAN
CONSTRUCTION SUPPORT VESSEL

CONSTRUCTION / CLASSIFICATION	
Built by	Metalships & Docks, Vigo, Spain
Year of construction	2010
Classification	DNV +1A1, DYNPOS-AUTR, EO, DK(+), CLEAN, CLEAN DESIGN, COMF-V(3), NAUT-OSV, HELDK.
Flag	Malta
Port of registry	Valletta

FEATURES	
Accommodation	120 berths, 50 x single cabins and 35 x double cabins
Client & office facilities	1 x offline office on 01 ACC 1 x online office on 04 ACC 1 x conference room 1 x briefing room/cinema
Hospital	2 berths
Mess room	60 seats
Recreation room	50 seats
Conference room	12 seats
Reception room	Reception room for helideck
Recreation facilities	Gymnasium, sauna and cinema

CAPACITIES	
Bunker capacity	Approx. 1,700 m^3
Other tanks for cargo	Potable water: approx. 600 m^3 Ballast water: approx. 7,400 m^3
Freshwater gen.	2 of each 25 m^3 per day

MAIN DATA	
Length overall	136.6 m
Length BP	120.4 m
Beam	27.0 m
Draft max	6.85 m
Depth main deck	9.7 m
Deadweight	Approx. 10,000 t
Main deck area	Approx. 2,400 m^2
Deck strength over all	10 t/m^2
Deck hatches	Two 4 m x 3 m hatches

PROPULSION AND MAIN SYSTEM	
Main engine (electric driven)	Wärtsilä, 4 x 3,360 kW
Propulsion	Kongsberg, two Azipull thrusters each 3,500 kW
Bow thruster	1 x RR swing up thruster 1,500 kW 2 x RR tunnel thrusters 1,500 kW each

Figure C.1: BOKA Ocean equipment sheet, provided by [31]

D

Appendix - Economic drilling methodology development

In this appendix the economic criteria to form a concept drilling method are presented. These criteria and their weight have determined which drilling concept has been assessed in this research. The scores per criterion are also presented in this Appendix, leading to the formation of the final concept drilling configuration. Being, the pile top drill operated from a large construction support vessel using a form of heave compensation.

Cost per pile

To assess the cost-effectiveness per configuration, the cost per pile is of importance. The operational day-rate is built up considering the cost of; the vessel or vessel combination, drilling equipment, grouting equipment, possible motion compensation unit, and the personnel operating all equipment. The ROP per drilling asset is determined to find the total duration per pile and combined to find the total cost per pile.

For the pile-top and in-pile drill motion compensation is required and generalised to a single addition in day rate. For the subsea drill no motion compensation is required for drilling, only for the lifting and lowering to the seabed. Each drill-head is assumed to be fitted with roller bits. In the use of the simplified model, the effect of the RQD is not incorporated. Thus the UCS of fully intact rock is assessed, giving a conservative outcome in the weak and medium drill-rates. The drill rates are presented in Table D.3 and graphically presented in Figure D.3.

In Table D.4 the costs per pile for each configuration are summarised. The information is retrieved from quotations offered by the drilling contractors discussed in Appendix C. Within the quotations, the preparation costs vary widely. Even for the same drilling asset. Therefore it is assumed that the preparation costs for all drilling assets are similar and are not taken into account in the drilling costs per pile. Finally, the presence of an overburden layer is assumed to have little to no effect on the scores each drilling asset achieves. Due to the similar drill-rates achieved in the soft overburden soil.

The rating of the drilling assets is done following a linear scaling approach. The configuration with the lowest costs per pile scores highest (5). From this point the score will decrease by 1 point per 20% increase in cost. A minimum rating of 0 is set. In Table D.4 the scores per configuration and soil type are summarised.

Cycle time

The cycle time of a drilling asset is an important parameter to asses. It is a driving component in the total time spent, which is determining for the total cost of the operation. As the time spent drilling is assessed in the previous criterion, there must be corrected for this. Therefore, the drilling time is chosen to be fixed as 24 hours in the cycle time assessment. In this way the time required to mobilise, install, de-install, and demobilise the drilling asset can be assessed.

For the pile-top drilling rig, it is possible to not fully de-install the drill-string when travelling between drilling locations, this translates to relative short periods being possible between drilling locations. Also, the subsea drill has a relatively fast installation time because the unit is already built up correctly, this has as result that the asset only has to be lifted over board and lowered to the seabed, making sure the umbilicals follow correctly and safe. When an overburden layer is present, an increase of 6 hours is expected in the drilling time for the pile-top and subsea drill. When increasing the water depth, the total cycle time of the pile-top drill is expected to increase more relative to the subsea drill. The time advantage of a partial lifting is not larger than the time taken to install a template at more than 200.0 m water depth. The pile-top drill is expected to have an additional 3 hours per borehole to position the template and/or casing. For the subsea drill this is an additional 2 hours to lower and position.

The deconstructed cycle times per water depth scenario and seabeds with and without overburden are presented in Table D.5 and D.7. Next, also the cycle times per water depth scenario are provided for 2, 10, and 50 drilling locations in Table D.6 and D.8 respectively.

When considering the rates for multiple drilling locations, the differences become more clear between drilling assets. The cycle time for 50 locations is used as rating point. The rating of the drilling assets is done following a linear scaling approach. The configuration with the lowest cycle time scores highest (5). From this point the score will decrease by 1 point per 20% increase in cycle time.

Risk of operation

The risks during drilling create an uncertainty in the operation, which is favourably minimised as much as possible. Risks can be split in to two components, the first is the probability of an event, the second is the impact or consequence this event has. To assess the operational risks, a subdivision is made between;

- Risk of stagnation during drilling
- Risk of mechanical failure.

Stagnation can lead to a delay of multiple days or even abandonment of equipment. Both cases lead to an increase in total costs, thus this is an important criterion to consider in the design. By limiting this risks in the process, a reliable planning can be made for the operation. A high risk of mechanical failure also is a high risk on delay. For the considered drilling assets this risk differs due the nature of the design. In the case of a pile-top drill, most of the mechanical components are situated above the sea level and are easier to reach in case of failure. Which makes the impact of such a failure smaller than when the full set of mechanical components is situated on the seabed (in case of an in-pile and subsea drill). When increasing the water depth, the risk for the subsea drill also increases for each soil type. This is due to the lack in track record of such a drill design.

In the concept phase of the methodology design, the risks are not calculated as monetary values. In Table D.9 the risks per drilling asset are provided. For clarity the risk is split in the probability and the impact to finally form the risk. The rating of the risks are done following a qualitative Likert scale [42] presented below.

Logistical complexity

For each methodology, there are certain logistical steps which have to be taken in order for the drilling operation to succeed. As some steps are successive, making the total time to to prepare the operation longer. For instance, the use of multiple vessels is a larger logistical challenge.

The need for anchor handling tugs to locate the vessel correctly or the requirement to install a casing regardless the soil conditions (as is the case for in-pile drills) add to the complexity of the operation. In the ideal situation, there would be a minimal amount of logistical steps, creating a robust planning and operation.

When rating the concepts on logistical complexity, multiple elements play a role as described above. For each drilling asset and vessel the logistical complexity is presented in Table D.10 and D.11.

The logistical complexity is scored for the vessel options and drilling assets. Ranging between High, Medium, and Low. The rating of the logistical complexity is done following a Likert scale [42]. For the use of multiple vessels, a deduction of 1 point is applied in the final score.

Vessel response

The vessel response relates to the workability rate for which the drilling operation can be performed. Next to this, the possible need of motion compensation measures in the methodology can be determined. Both the workability and the need for a motion compensation both lead to an increase of total costs.

Because linear wave theory is used, the response can linearly be extrapolated to specific wave conditions. A H_s of 1.0 m and a JONSWAP wave spectrum are used. Also the design draught of the vessel is used, as the drilling spread is an average weighing load. Note that for a specific site, the wave spectrum might differ and thus the response characteristics might differ slightly. For the qualitative assessment this method suffices.

On each vessel, multiple locations for the drilling assets are possible. Each vessel is tested on multiple locations; location 1 is present at the stern on the centreline, location 2 at port side at the height of the Centre of Gravity, location 3 is at port side at one-third of the total length of the vessel measured from the stern, finally location 4 is located at the moonpool where present (CSV's). The responses of each vessel for locations 1 and 3 are presented in Figure D.1. The individual vessel responses for all locations are presented in Figure D.4.

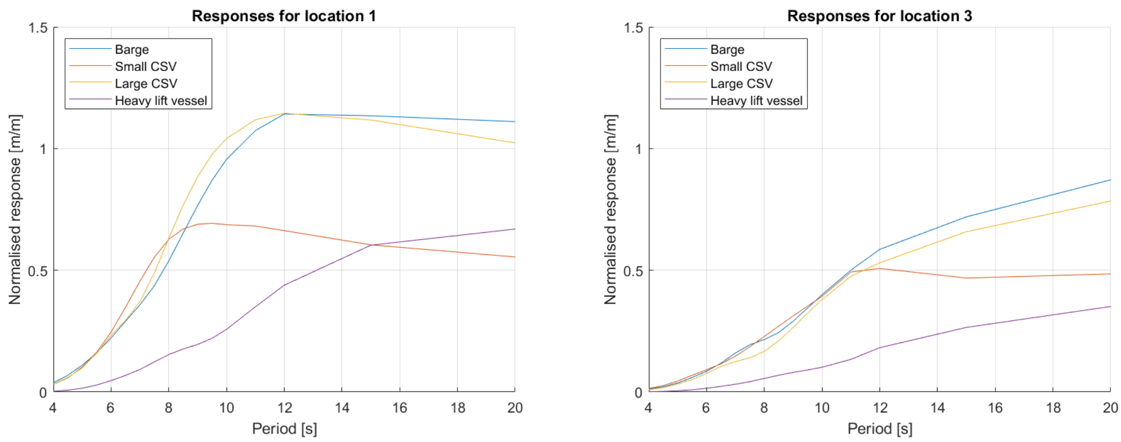

(a) **(b)**

Figure D.1: Comparison of vessel responses for location 1 and 3

To rate the vessels, the typical wave periods at the selected European sites are assessed, as mentioned in Section 2.3.2. An angle of incidence range of 165° to 180° is used. This represents a spread around the design angle of the vessel (which is 180°). This orientation has favourable response characteristics for the vessel. However, it also shows the sensitivity of the vessel to waves under a slight angle with respect to the head angle. Location 3 shows favourable responses for each vessel, thus this location will be used for rating. As is visible in the Figure D.1b the barge, small CSV, and large CSV respond comparable up to wave periods of approximately 11.0 s. When increasing the period beyond 11.0 s, the small CSV shows better responses. The heavy-lift vessel shows smaller responses for all considered wave periods.

For the *In-land sea* peak period, the responses for all vessels are low, the response of the heavy-lift vessel is significantly smaller. For the *Open sea* peak period the barge, small CSV and large CSV responses are increasing more relative to the response of the heavy-lift vessel. The heavy-lift vessel scores highest (5), due to the favourable responses for all wave periods. The barge and large CSV, score 2 points due to the response being more than double that of the heavy-lift vessel for all wave periods. The small CSV scores 3 for the improving relative response for wave periods larger than 11.0 s.

Required deck space

The area of a spread is an important criterion, for a smaller required deck space more construction material can be housed on the vessel deck. This makes the need for additional transport from the harbour smaller. It also leads to a flexibility in vessel options, might an option be unavailable. Drilling assets with larger spreads, require larger vessels. Larger vessels are more expensive to operate and tend to have low availability, making the option to operate on a smaller vessel more attractive in the design process.

For the total spread, the pile installation equipment, grouting equipment, and grout tanks are simplified to a single area of approximately 500 m^2. Which is extracted from previous Boskalis projects. This value is used for all drilling assets, because the positioning and grouting of the anchor piles will be performed in a similar way, regardless of the pile drilling technique. The drilling spread area's are presented in Table D.12.

The rating of the required deck space is done following a linear scaling approach. The method with the smallest drilling spread area will receive the highest score (5). The score will decrease by one point per 20 % increase in total required deck space (drilling, positioning & grouting spread). A minimum score of 0 points is set. The final scores for each drilling asset is 5 points. As the differences in required deck space are marginal.

Mass ratio

The mass ratio has effect on the stability and efficiency of a vessel. When a vessel is loaded with a relatively light spread, favourable sailing conditions can be created and a vessel can sail at design draught. When a relatively heavy spread is required to operate a drilling asset, a vessel will thus be loaded heavier and it may be more sensitive for stability issues during sailing. Also, a heavily loaded vessel requires more fuel to travel the same distance. Making it a more expensive and unfavourable option.

In the determination of the mass of the spread the pile installation equipment, grouting equipment, and grout tanks are not incorporated. This is due to the same reason mentioned in Section D. It is assumed that this equipment will not differ between the different drilling options. The spreads and mass ratio's per combination are provided in Table D.13.

The range in mass ratio's is large. The minimum ratio in the configurations is 0.25% of the vessel mass, which is experienced as a very light weight to carry on deck. Again a linear scaling with steps of 20% will be used to determine the scores. The smallest mass ratio scores the maximum amount of points (5). A minimum score of 0 points is set. The heavy-lift vessel scores 5 points due to the large self-weight the vessel has, all other configurations score 0 points due to the large difference in vessel mass.

Morph chart

#	Function	Option 1	Option 2	Option 3	Option 4	Option 5	Option 6
Vessel	Sailing	Fossil fuel engine	Electric engine	Hydrogen engine	Hybrid engine	Tugboat	
	Lifting	Mount. crane	Crawler crane	Add. sheerleg	Add. heavy lift barge	Add. large CSV	Add. heavy lift vessel
	Position keeping	Anchors + Tugs	DP1	DP2	DP3		
	Transport drilling & grout spread	Own deck	External vessel				
	Transport piles	Own deck	External vessel				
	Equipment positioning	Stern	Portside	Starboard	Moonpool	Crane	
	Template positioning	Install. ROV	External ROV	Diver	Camera on crane hook		
Pile	Pile installation	Upending on deck	Lower to the seabed and upend	Roll overboard			
	Grouting	From vessel	From external vessel				
Drilling	Power transmission	Seabed (gravity/friction)	Casing (friction)	Vessel (power)			
	Power generation	Fossil fuel generator	Hybrid generator	Hydrogen generator	Electric battery		
	Transport method	DCD	RCD: Airlift	RCD: Pump	Bucket		
	Drill-head type	V-shaped roller	Button roller	Toothed roller	Pick point cutter	Chisel cutter	Combination
	Casing use	Complete water and borehole depth	Complete borehole depth	Overburden depth	None		
	Template use	Template (Full time)	Template (Beginning)	None			
	Noise Mitigation	Bubble Screen	Sleeve	None			

Figure D.2: Morphological chart leading to the defined drilling configurations, filled for the Piletop drilling method in combination with a Large construction support vessel and a form of heave compensation.

Weight determination
Scoring matrix

Table D.1: Weight determination matrix criteria 1

		1	2	3	4	5	6	7	Total	Normalised factor
1	Cost per pile	1	1	1	1	1	1	1	7	1,000
2	Cycle time	0	1	1	1	0	1	1	5	0,714
3	Risk of operation	0	1	1	0	1	1	1	5	0,714
4	Logistical complexity	0	0	0	1	1	1	1	4	0,571
5	Vessel response	0	0	1	1	0	1	1	4	0,571
6	Required deck space	0	0	0	0	0	1	1	2	0,286
7	Mass ratio	0	0	0	0	0	0	1	1	0,143

Table D.2: Weight determination matrix criteria 2

		1	2	3	4	5	6	7	Total	Normalised factor
1	Cost p pile	1	1	1	1	1	1	1	7	1,000
2	Cycle time	0	1	1	0	1	1	1	5	0,714
3	Risk of operation	0	0	1	1	1	1	1	5	0,714
4	Logistical complexity	0	1	0	1	1	1	1	5	0,714
5	Vessel response	0	0	0	0	1	1	1	3	0,429
6	Required deck space	0	0	0	0	0	1	1	2	0,286
7	Mass ratio	0	0	0	0	0	0	1	1	0,143

Best-Worst method

$$a_B = \begin{pmatrix} 1 & 3 & 4 & 6 & 7 & 8 & 9 \end{pmatrix}$$

$$a_W = \begin{pmatrix} 9 & 7 & 7 & 6 & 5 & 3 & 1 \end{pmatrix}^T$$

$$\xi^* = 0.4747$$

optimise for:

$$\left| \frac{\mathrm{w}_{B1}}{\mathrm{w}_{j1}} - a_{Bj} \right| \leq \xi^*$$

and:

$$\left| \frac{\mathrm{w}_{W2}}{\mathrm{w}_{j2}} - a_{Wj} \right| \leq \xi^*$$

giving optimised weight w_j^*:

$$w_j^* = \text{average}\left(w_{j1}, w_{j2}\right)$$

Cost per Pile

Table D.3: Drill rate per drilling asset, per soil type

Drilling asset	Drill rate		
	Weak soil	Medium soil	Strong soil
Pile-top drill	3.2 m/h	0.82 m/h	0.24 m/h
In-pile drill	2.6 m/h	0.71 m/h	0.20 m/h
Subsea drill	2.8 m/h	0.60 m/h	0.12 m/h

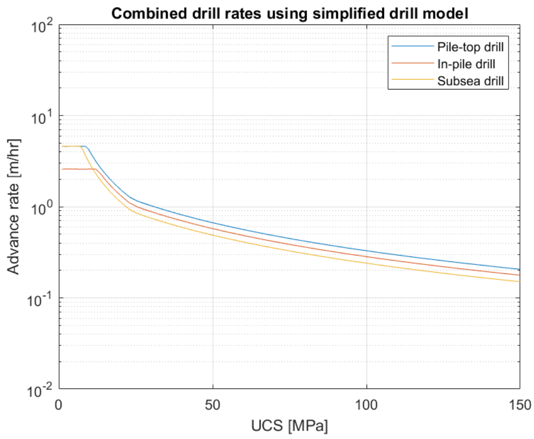

Figure D.3: Drill rates compared for generalised drilling assets, RQD 100%

Table D.4: Cost per pile including vessel(s), drilling asset and optional motion compensation, rounded per 5 kEUR

		Weak soil		Medium soil		Strong soil	
Vessel(s)	Drilling technique	kEUR	Score	kEUR	Score	kEUR	Score
Barge + Sheerleg	Pile-top drill + MC	20	3	80	3	280	3
	In-pile drill + MC	30	0	100	1	360	0
	Subsea drill	25	1	115	0	570	0
Barge + Crawler	Pile-top drill + MC	15	5	50	5	180	5
	In-pile drill + MC	20	3	70	4	240	4
	Subsea drill	15	5	75	3	370	0
Heavy lift barge	Pile-top drill + MC	20	3	75	3	260	3
	In-pile drill + MC	25	1	95	1	340	1
	Subsea drill	25	2	105	0	535	0
Small CSV + Barge	Pile-top drill + MC	15	4	65	4	225	4
	In-pile drill + MC	25	2	85	2	300	2
	Subsea drill	20	3	95	1	465	0
Large CSV	Pile-top drill + MC	15	5	50	5	180	5
	In-pile drill + MC	20	4	65	4	240	4
	Subsea drill	15	5	75	3	365	0
Heavy lift vessel	Pile-top drill + MC	35	0	135	0	465	0
	In-pile drill + MC	45	0	165	0	585	0
	Subsea drill	40	0	190	0	940	0

Cycle time

Table D.5: Cycle time per drilling asset WD_{50-200}

Overburden	Asset	Mob.	Drill	Transport		Drill	Demob.
				Install.	De-install.		
No	Pile-top drill	16 hrs	24 hrs	5 hrs	7 hrs	24 hrs	14 hrs
	In-pile drill	12 hrs	24 hrs	10 hrs	12 hrs	24 hrs	10 hrs
	Subsea drill	8 hrs	24 hrs	6 hrs	8 hrs	24 hrs	6 hrs
Yes	Pile-top drill	16 hrs	30 hrs	5 hrs	7 hrs	30 hrs	14 hrs
	In-pile drill	12 hrs	24 hrs	10 hrs	12 hrs	24 hrs	10 hrs
	Subsea drill	8 hrs	28 hrs	6 hrs	8 hrs	28 hrs	6 hrs

Table D.6: Total time for multiple drilling locations WD_{50-200}

Overburden	Asset	Total time			Score
		n=2	n=10	n=50	
No	Pile-top drill	3.75 day	15.75 day	75.75 day	5
	In-pile drill	3.83 day	19.17 day	95.83 day	4
	Subsea drill	3.17 day	15.83 day	79.17 day	5
Yes	Pile-top drill	4.25 day	18.25 day	88.25 day	5
	In-pile drill	3.83 day	19.17 day	95.83 day	5
	Subsea drill	3.67 day	18.33 day	91.67 day	5

Table D.7: Cycle time per drilling asset $WD_{200-1000}$

Overburden	Asset	Mob.	Drill	Transport		Drill	Demob.
				Install.	De-install.		
No	Pile-top drill	19 hrs	24 hrs	8 hrs	10 hrs	24 hrs	17 hrs
	Subsea drill	10 hrs	24 hrs	8 hrs	10 hrs	24 hrs	8 hrs
Yes	Pile-top drill	19 hrs	30 hrs	8 hrs	10 hrs	30 hrs	17 hrs
	Subsea drill	10 hrs	28 hrs	8 hrs	10 hrs	28 hrs	8 hrs

Table D.8: Total time for multiple drilling locations $WD_{200-1000}$

Overburden	Asset	Total time			Score
		n=2	n=10	n=50	
No	Pile-top drill	4.25 day	18.25 day	88.25 day	5
	Subsea drill	3.50 day	17.50 day	87.50 day	5
Yes	Pile-top drill	4.75 day	20.75 day	100.75 day	5
	Subsea drill	3.83 day	19.17 day	95.83 day	5

Risk of the Operation

Table D.9: Risk of the drilling asset in multiple soil scenario's

		Stagnation			Mechanical failure		
	Drilling asset	Prob.	Impact	Risk	Prob.	Impact	Risk
Weak soil	Pile-top drill	−	+/−	Low	−	+/−	Low
	In-pile drill	−	+/−	Low	+/−	+/−	Medium
	Subsea drill	−	+	Medium	+/−	+	High
Medium soil	Pile-top drill	+/−	+/−	Medium	−	+/−	Low
	In-pile drill	+/−	+/−	Medium	+/−	+/−	Medium
	Subsea drill	+/−	+	High	+/−	+	High
Strong soil	Pile-top drill	+/−	+/−	Medium	+/−	+/−	Medium
	In-pile drill	+/−	+/−	Medium	+/−	+/−	Medium
	Subsea drill	+/−	+	High	+	+	Very high

Logistical complexity

Table D.10: Logistics score per drilling method

Drilling asset	Logistical steps	Logistical complexity
Pile-top drill	Installation of template	Medium
	Assembly drill-string per 3m	
	Removal of template	
	Partial disassembly drill-string	
In-pile drill	Installation of template	High
	Installation of casing	
	Lowering of drill installation	
	Removal of casing	
	Removal of template	
	Lifting of drill installation	
Subsea drill	Lowering of subsea drill	Low
	Leveling of subsea drill	
	Lifting of subsea drill	

Table D.11: Logistics score per vessel or vessel combination

Vessel or vessel combination	Positioning	Logistical complexity
Barge & sheerleg	Anchor	Very high
Barge & crawler crane	Anchor	High
Heavy lift barge	Anchor	High
Small CSV & Barge	DP2 & Anchor	High
Large CSV	DP2	Low
Heavy lift vessel	DP2	Low

Vessel response

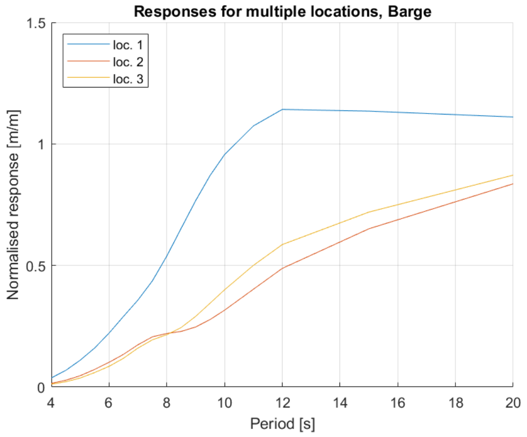

(a)

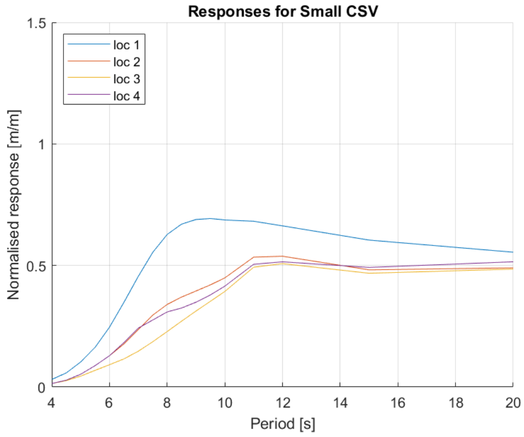

(b)

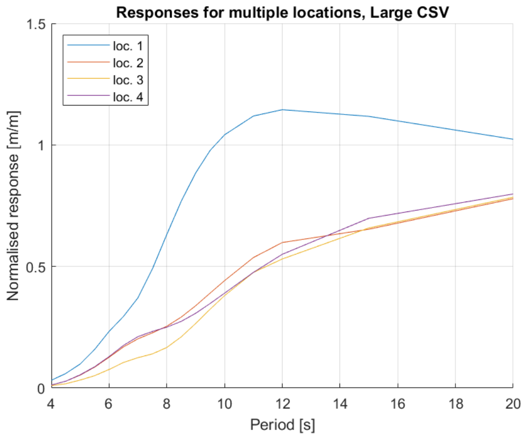

(c)

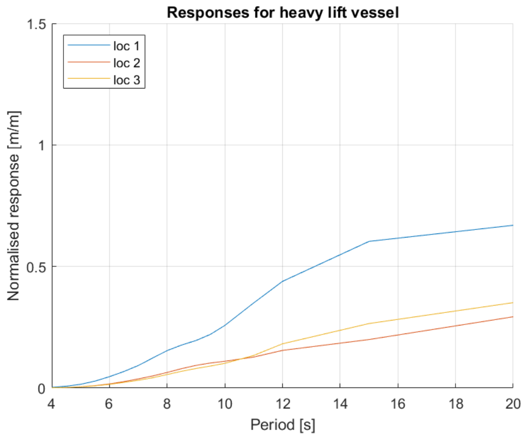

(d)

Figure D.4: Individual vessel responses

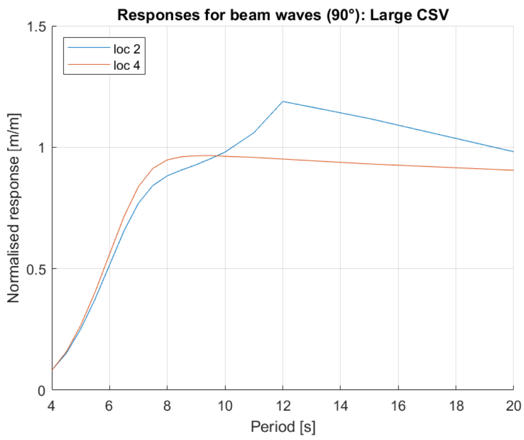

Figure D.5: Moonpool response comparison beam waves (90°)

Required deck space

Table D.12: Area of the drilling spread

Asset	Area of spread	Main driver(s)
Pile-top drill	±350 m^2	Template
		Drill rig
In-pile drill	±315 m^2	Template
		Casing pile
Subsea drill	±385 m^2	Subsea drill
		Umbilical reel
Other equipment	±500 m^2	Grout tanks
		Positioning gripper

Mass ratio

Table D.13: Mass ratio of spread

Drilling Asset	Vessel	Mass			Ratio
		Drill spread	Grout spread	Vessel	
Pile-top drill	Barge	135 t	30 t	13 500 t	0.012
Pile-top drill	Heavy lift barge	135 t	30 t	15 500 t	0.011
Pile-top drill	Small CSV	135 t	30 t	10 500 t	0.016
Pile-top drill	Large CSV	135 t	30 t	14 000 t	0.012
Pile-top drill	Heavy lift vessel	135 t	30 t	65 000 t	0.003
In-pile drill	Barge	140 t	30 t	13 500 t	0.013
In-pile drill	Heavy lift barge	140 t	30 t	15 500 t	0.011
In-pile drill	Small CSV	140 t	30 t	10 500 t	0.016
In-pile drill	Large CSV	140 t	30 t	14 000 t	0.012
In-pile drill	Heavy lift vessel	140 t	30 t	65 000 t	0.003
Subsea drill	Barge	270 t	30 t	13 500 t	0.022
Subsea drill	Heavy lift barge	270 t	30 t	15 500 t	0.019
Subsea drill	Small CSV	270 t	30 t	10 500 t	0.029
Subsea drill	Large CSV	270 t	30 t	14 000 t	0.021
Subsea drill	Heavy lift vessel	270 t	30 t	65 000 t	0.005

Final Rating

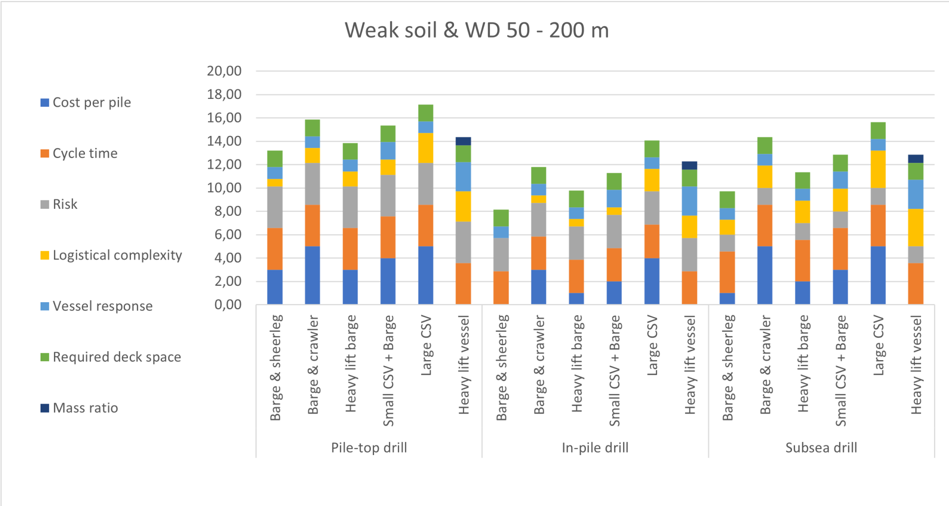

(a)

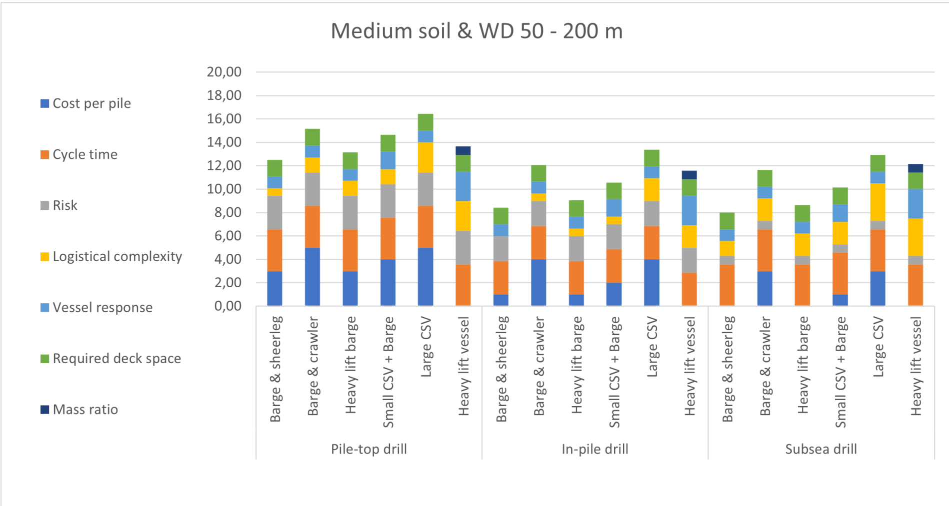

(b)

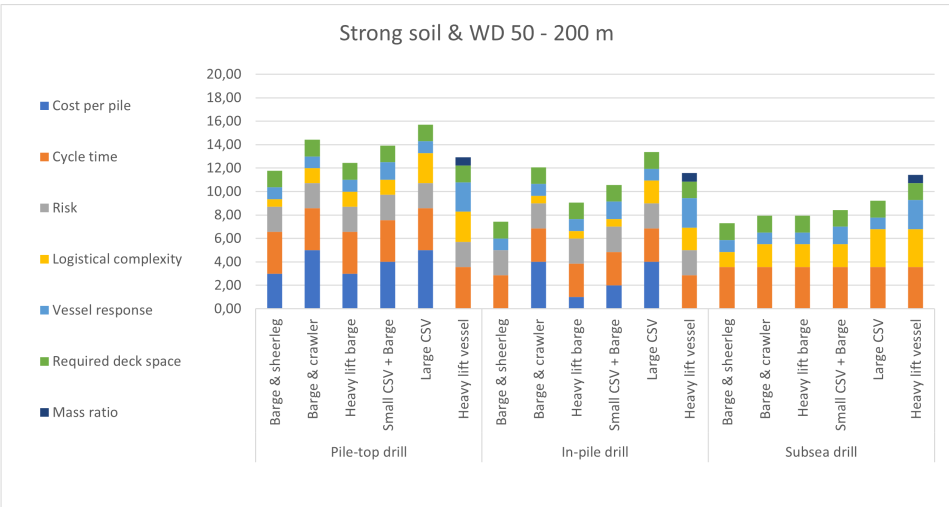

(c)

Figure D.6: Score composition per rock type for water depth range 50 - 200 m

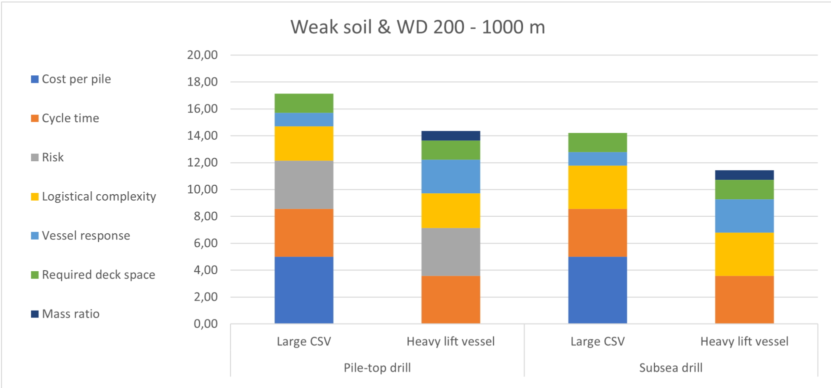

(a)

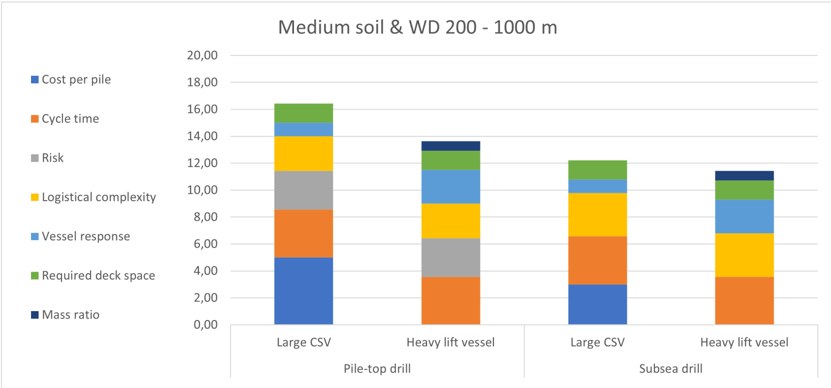

(b)

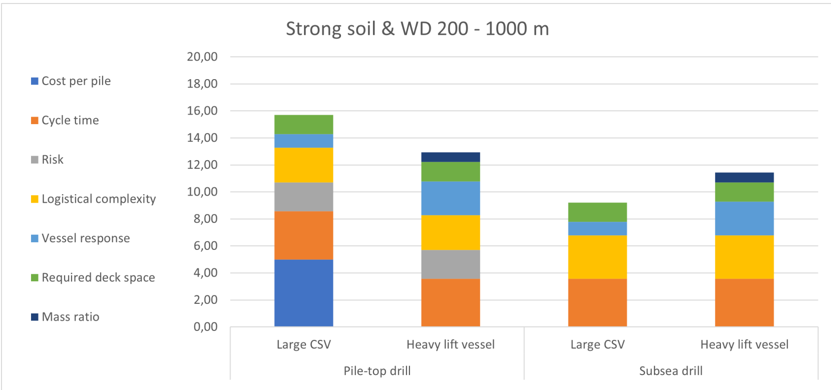

(c)

Figure D.7: Score composition per rock type for water depth range 200 - 1000 m

Table D.14: Weight determined for the drilling assets, following two methods

#	Criterion	Weight
1	Cost per pile	1.00
2	Cycle time	0.71
3	Risk of operation	0.71
4	Logistical complexity	0.65
5	Vessel response	0.50
6	Required deck space	0.29
7	Mass ratio	0.14

E

Appendix - European FOW site analysis

In this appendix the European sites are presented. Both the metocean data, bathymetry, and seabed conditions are presented in the tables below. This information forms the input of the research and creates the boundaries within the drilling configuration must operate.

Locations for design input

In this section, the site information is presented. This information is used to determine the relevant design conditions for which the configurations must operate and be optimised.

Table E.1: Water Depth ranges of selected sites [26]

#	Site	WD_{min}	WD_{max}
1	The West of Orkney	45 m	100 m
2	Bretagne Sud	90 m	100 m
3	Baltic Offshore Delta	110 m	140 m
4	Heimdall	140 m	200 m
5	Norde Phase 1	270 m	390 m
6	INTOG (WoSa)	480 m	1500 m

Table E.2: Significant wave heights and peak wave periods of selected sites in the *summer months*

#	Site	H_s	T_p
1	The West of Orkney	1.90 m	8.49 s
2	Bretagne Sud	1.38 m	9.51 s
3	Baltic Offshore Delta	0.76 m	4.12 s
4	Heimdall	0.99 m	5.34 s
5	Nordes Phase 1	1.70 m	8.90 s
6	INTOG (WoSa)	1.90 m	8.49 s

Table E.3: Bedrock conditions for three sites

#	Site	Bedrock			Overburden	
		UCS_{min}	UCS_{max}	RQD	Type	Thickness
1	Bretagne Sud	5.0 MPa	35.0 MPa	Medium	Clay	15.0 m
2	Neart na Gaoithe	5.0 MPa	25.0 MPa	Medium	Clay & Sand	8.0 m
3	Wikinger Süd	0.1 MPa	5.0 MPa	Low	Clay, Sand & Gravel	12.0 m

F

Appendix - Overview OrcaFlex model

In this appendix the OrcaFlex model is presented. A water depth of 50 m is used to present the configuration. As discussed in the method chapter, the active heave compensation is modelled by manipulating the RAOs of the modelled vessel. The passive heave compensation is modelled by a spring-damper combination presented in Figure F.1.

Snapshots model setup

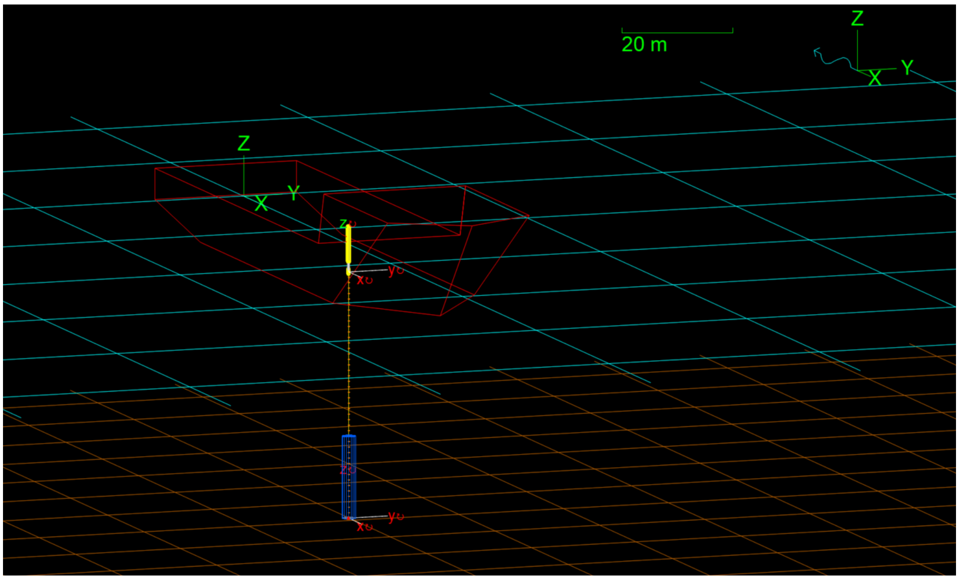

Figure F.1: Passive heave compensation model in OrcaFlex.

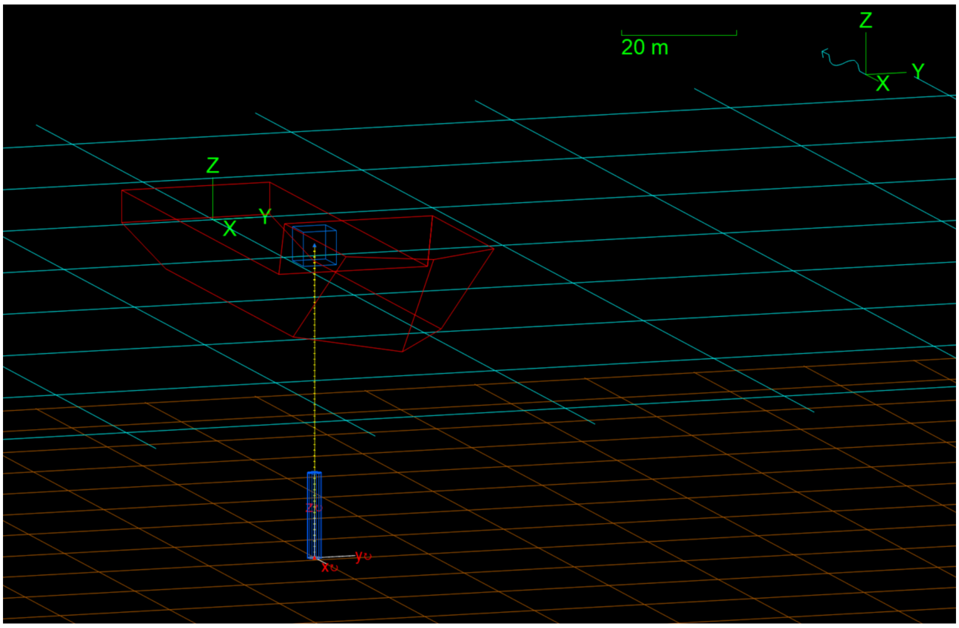

Figure F.2: Active heave compensation model in OrcaFlex.

Passive heave compensation characteristics

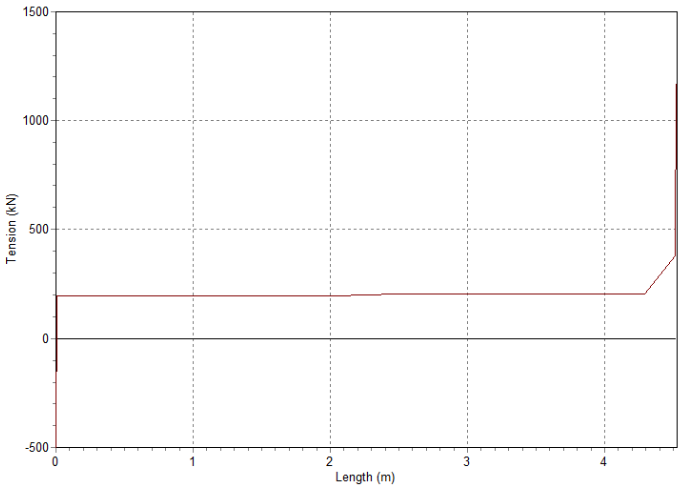

Figure F.3: Spring relation of the passive heave compensation model in OrcaFlex, at 50m waterdepth

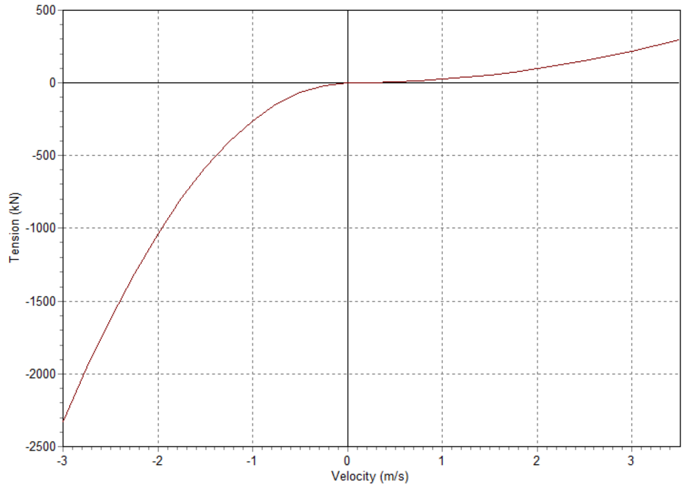

Figure F.4: Damping relation of the passive heave compensation model in OrcaFlex, at 50m waterdepth

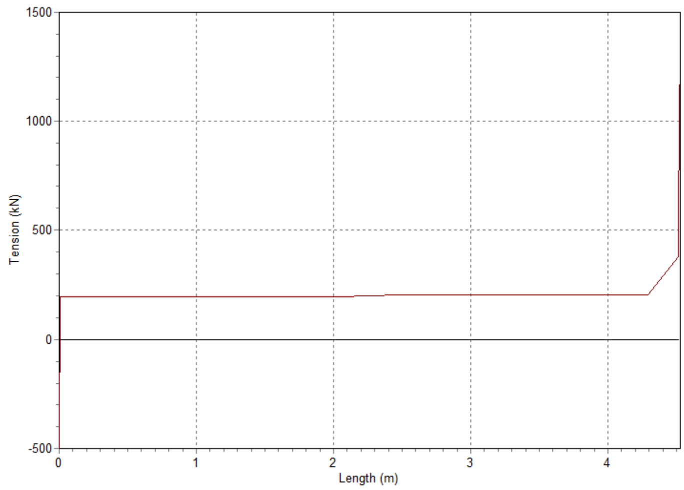

Figure F.5: Spring relation of the passive heave compensation model in OrcaFlex, at 100m waterdepth

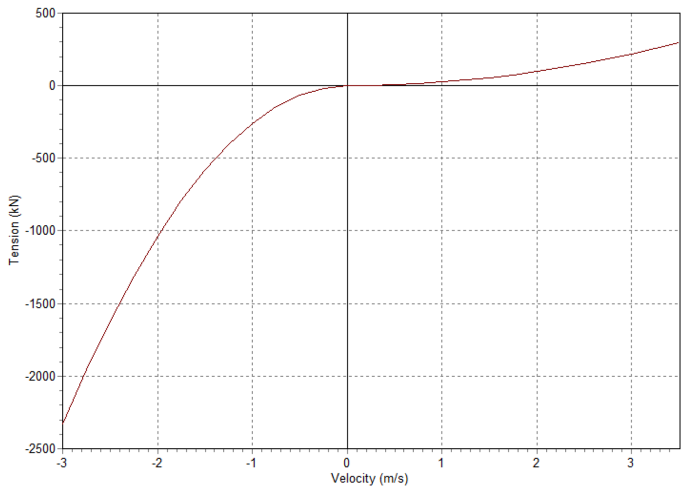

Figure F.6: Damping relation of the passive heave compensation model in OrcaFlex, at 100m waterdepth

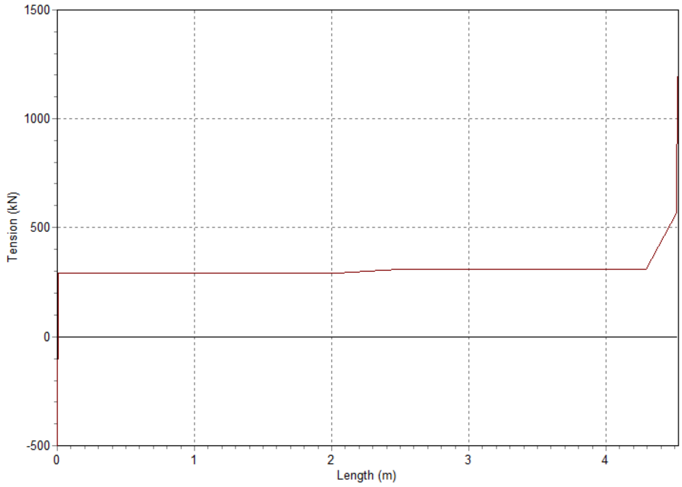

Figure F.7: Spring relation of the passive heave compensation model in OrcaFlex, at 200m waterdepth

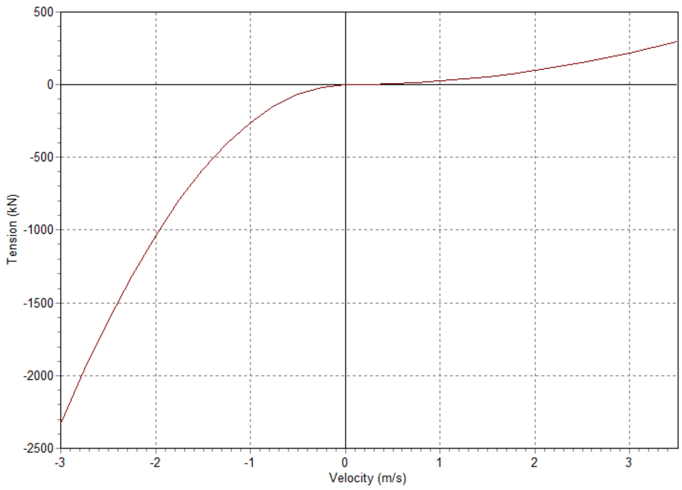

Figure F.8: Damping relation of the passive heave compensation model in OrcaFlex, at 200m waterdepth

Active heave compensation characteristic

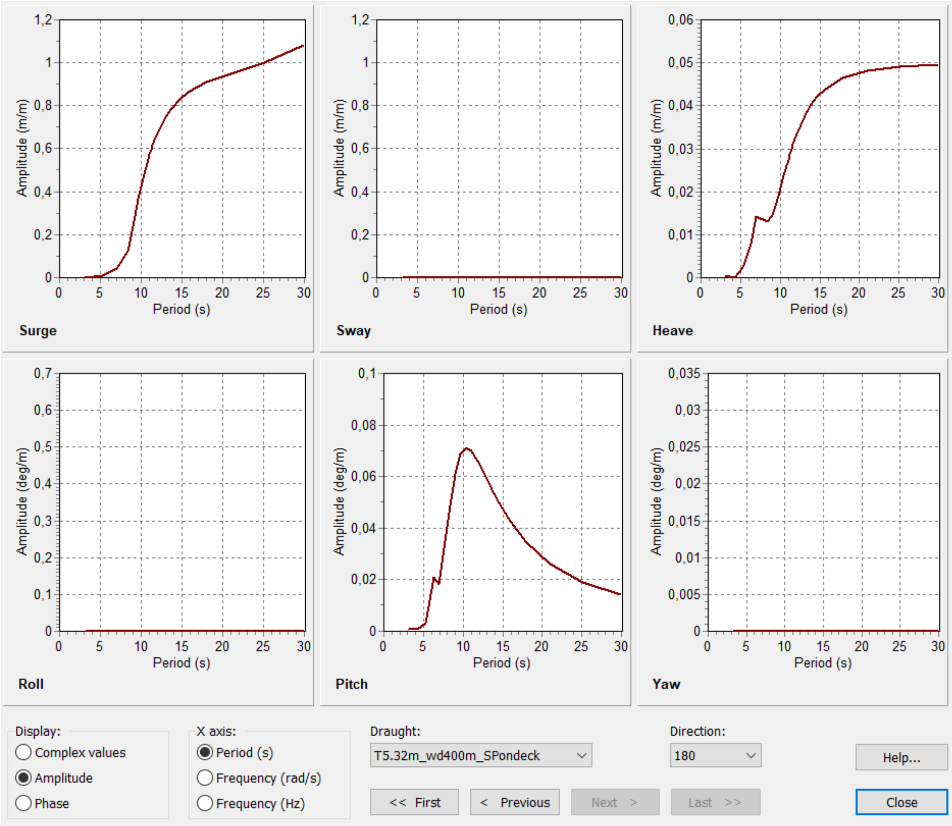

Figure F.9: Modified RAOs for the BOKA Ocean, for the wave direction of 180°.

Drill-string characteristics

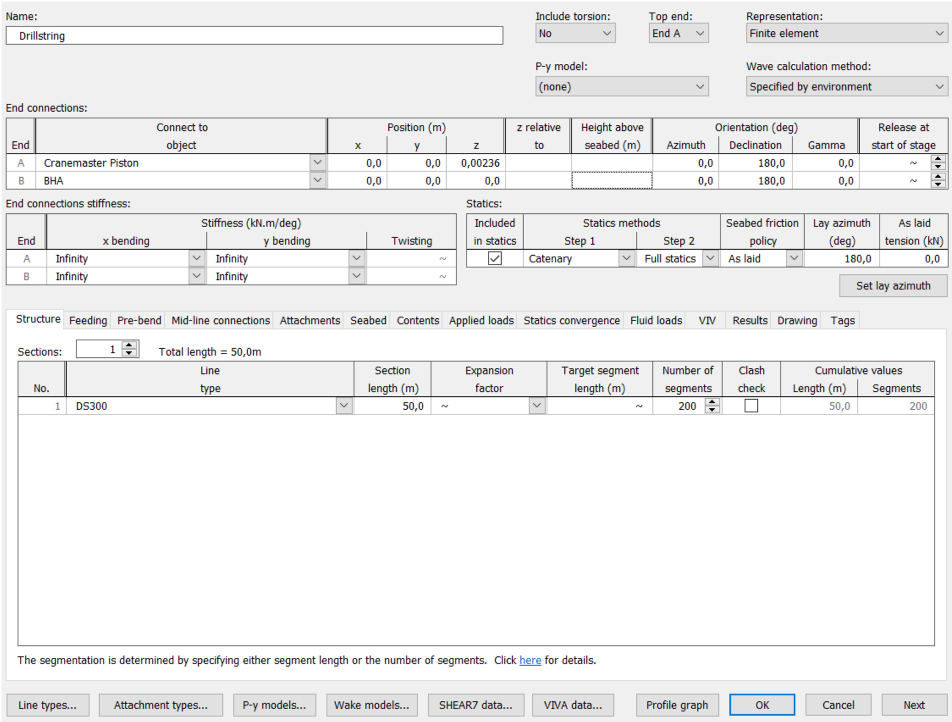

Figure F.10: Input screen DS300 drill-string for a 50m water depth situation.

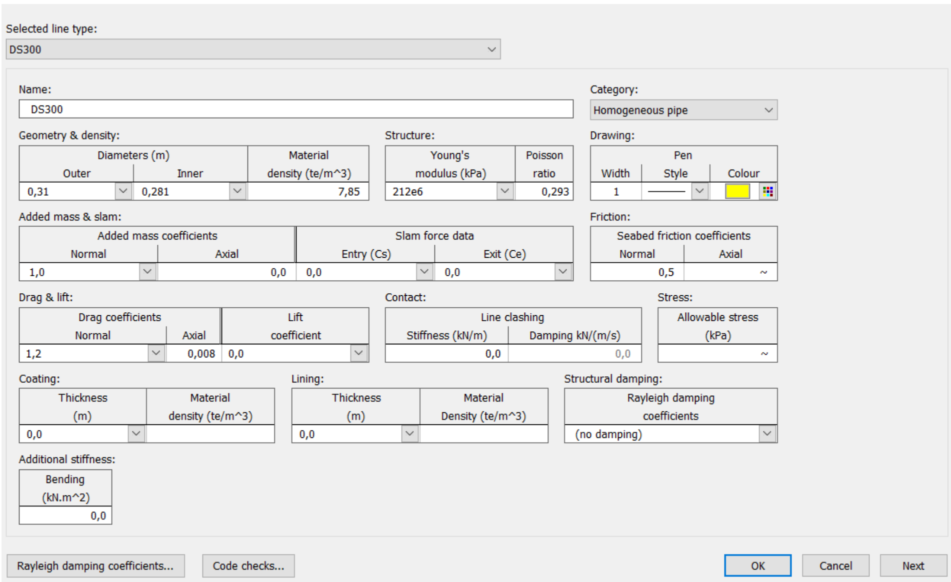

Figure F.11: DS300 drill-string characteristics.

RAOs BOKA Ocean

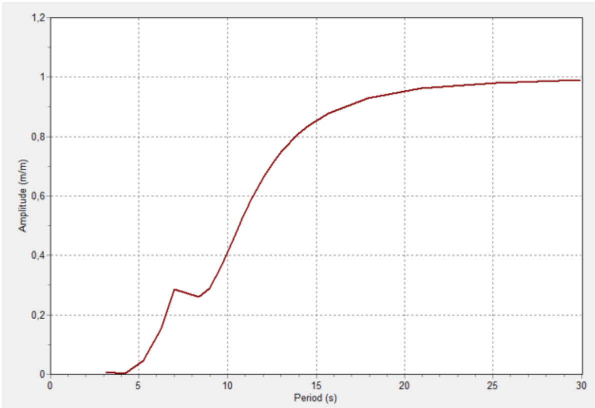

Figure F.12: Response amplitude operator for multiple wave periods in the heave DOF, for the vessel BOKA Ocean.

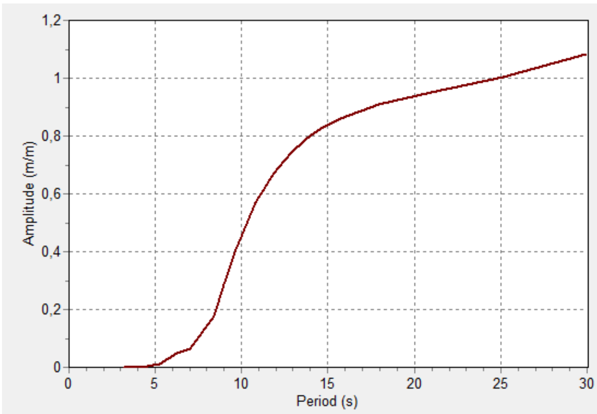

Figure F.13: Response amplitude operator for multiple wave periods in the surge DOF, for the vessel BOKA Ocean.

G

Appendix - Results dynamic drilling analysis

In this appendix the results of the dynamic drilling analysis are further presented.

Validation model nodes

In this section the amount of nodes is determined, by measuring the ULS exceedance point in the drill-string for multiple amount of nodes and for the three considered water depths. The assumption is made that an infinite amount of nodes will provide the most accurate results.

Table G.1: Intersection with ULS for different amount of drill-string nodes. Leading to the determination of 200 nodes used in the analysis.

# Nodes	WD_{50}	WD_{100}	WD_{200}
2	0.22 m	1.10 m	3.09 m
5	0.19 m	1.08 m	2.68 m
10	0.21 m	1.01 m	2.34 m
20	0.18 m	0.95 m	2.10 m
50	0.15 m	0.82 m	1.97 m
100	0.16 m	0.81 m	2.00 m
200	0.16 m	0.81 m	2.00 m
500	0.16 m	0.81 m	2.01 m
1000	0.16 m	0.81 m	2.00 m
2000	0.16 m	0.81 m	2.00 m
5000	0.16 m	0.81 m	2.00 m

Limiting horizontal topside displacements

Below the limiting horizontal topside displacement is again presented with the addition of passive heave compensation.

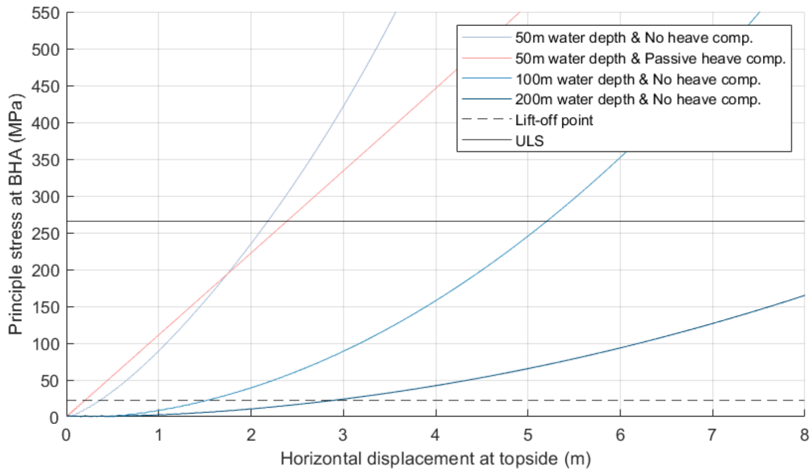

Figure G.1: The local **tensile** stress of a DS300 drill-string above the bottom hole assembly as a result of a horizontal displacement at the topside, intersecting the factorised yield strength of the drill-string material (steel). The passive heave compensation option is added

Vortex-induced vibrations

Below the VIV on the drill-string is analysed.

Table G.2: Velocities leading to lock-in for the vortex-induced vibrations.

Heave comp.	Mode	50 m	100 m	200 m
Passive	1st	1.14 m/s	2.00 m/s	7.10 m/s
	2nd	0.44 m/s	1.12 m/s	3.04 m/s
	3rd	0.23 m/s	0.68 m/s	1.88 m/s
Active	1st	0.78 m/s	1.49 m/s	6.39 m/s
	2nd	0.30 m/s	0.83 m/s	2.78 m/s
	3rd	0.16 m/s	0.57 m/s	1.73 m/s

Table G.3: Statistic values for multiple wave conditions.

Water depth	H.c.	T_p	H_s	Current	Mean	Std.	Max
50 m	None	4.0 s	1.5 m	0.0 m/s	50.3 MPa	153.7 MPa	698.4 MPa
		8.0 s	1.5 m	0.0 m/s	226.4 MPa	531.2 MPa	2743.6 MPa
		8.0 s	2.0 m	0.0 m/s	300.0 MPa	704.0 MPa	3666.4 MPa
	Passive	4.0 s	1.5 m	0.0 m/s	10.3 MPa	1.1 MPa	14.2 MPa
		8.0 s	1.5 m	0.0 m/s	10.3 MPa	22.3 MPa	94.1 MPa
		8.0 s	2.0 m	0.0 m/s	10.3 MPa	29.8 MPa	122.4 MPa
	Active	4.0 s	1.5 m	0.0 m/s	9.9 MPa	7.2 MPa	44.3 MPa
		8.0 s	1.5 m	0.0 m/s	15.2 MPa	13.6 MPa	-83.8 MPa
		8.0 s	2.0 m	0.0 m/s	21.5 MPa	55.7 MPa	-320.0 MPa
100 m	None	4.0 s	1.5 m	0.0 m/s	31.1 MPa	92.1 MPa	-471.3 MPa
		8.0 s	1.5 m	0.0 m/s	157.2 MPa	253.3 MPa	1435.7 MPa
		8.0 s	2.0 m	0.0 m/s	Unstable	Unstable	Unstable
	Passive	4.0 s	1.5 m	0.0 m/s	6.5 MPa	1.3 MPa	10.9 MPa
		8.0 s	1.5 m	0.0 m/s	6.5 MPa	8.2 MPa	37.3 MPa
		8.0 s	2.0 m	0.0 m/s	6.5 MPa	11.0 MPa	47.7 MPa
	Active	4.0 s	1.5 m	0.0 m/s	9.3 MPa	5.1 MPa	29.6 MPa
		8.0 s	1.5 m	0.0 m/s	10.8 MPa	7.6 MPa	43.3 MPa
		8.0 s	2.0 m	0.0 m/s	14.4 MPa	30.0 MPa	164.5 MPa
200 m	None	4.0 s	1.5 m	0.0 m/s	12.5 MPa	53.2 MPa	250.7 MPa
		8.0 s	1.5 m	0.0 m/s	71.5 MPa	139.8 MPa	751.1 MPa
		8.0 s	2.0 m	0.0 m/s	98.1 MPa	178.3 MPa	991.5 MPa
	Passive	4.0 s	1.5 m	0.0 m/s	6.0 MPa	1.2 MPa	9.9 MPa
		8.0 s	1.5 m	0.0 m/s	5.9 MPa	12.2 MPa	41.2 MPa
		8.0 s	2.0 m	0.0 m/s	5.9 MPa	14.8 MPa	48.5 MPa
	Active	4.0 s	1.5 m	0.0 m/s	4.4 MPa	3.5 MPa	21.0 MPa
		8.0 s	1.5 m	0.0 m/s	4.0 MPa	18.1 MPa	63.1 MPa
		8.0 s	2.0 m	0.0 m/s	4.0 MPa	22.8 MPa	122.9 MPa

Convergence check for multiple displacement velocities in the first mode shape

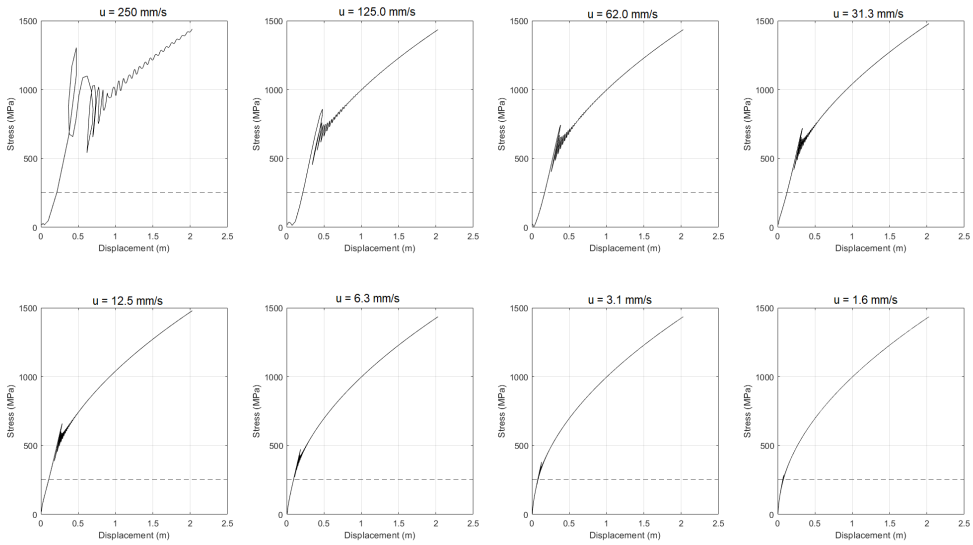

Figure G.2: Stress results for the first buckling mode shape, examined for multiple velocities in a water depth of 50 m.

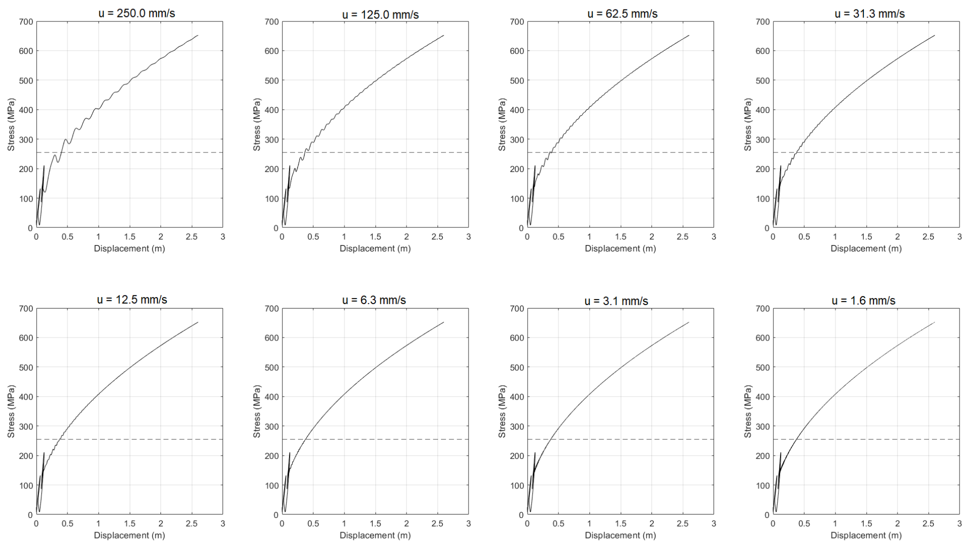

Figure G.3: Stress results for the first buckling mode shape, examined for multiple velocities in a water depth of 100 m.

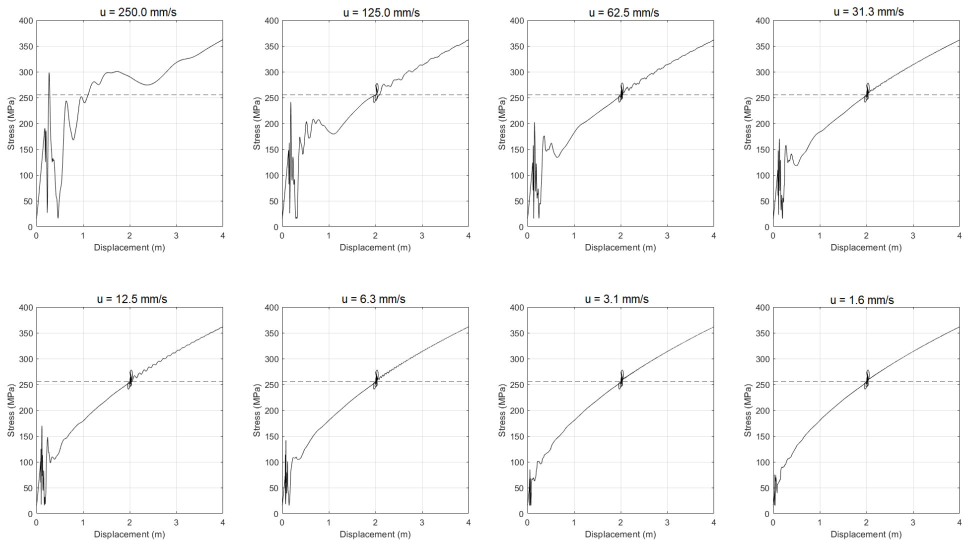

Figure G.4: Stress results for the first buckling mode shape, examined for multiple velocities in a water depth of 200 m.

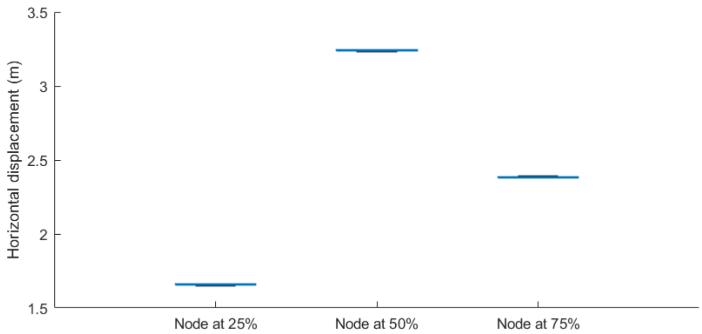

Figure G.5: Lateral displacement of three nodes for 50 m water depth

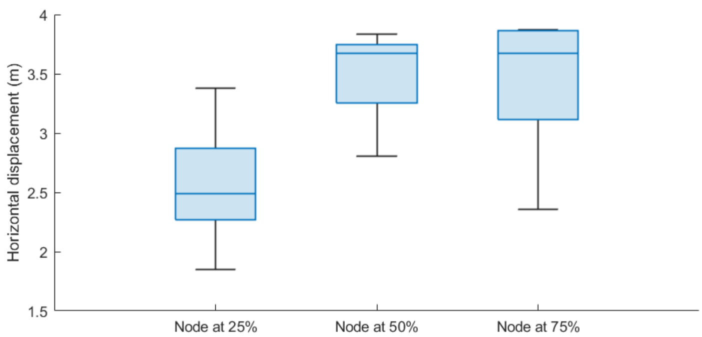

Figure G.6: Lateral displacement of three nodes for 100 m water depth

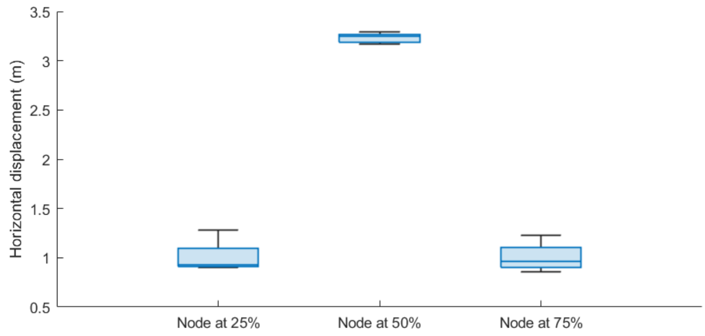

Figure G.7: Lateral displacement of three nodes for 200 m water depth

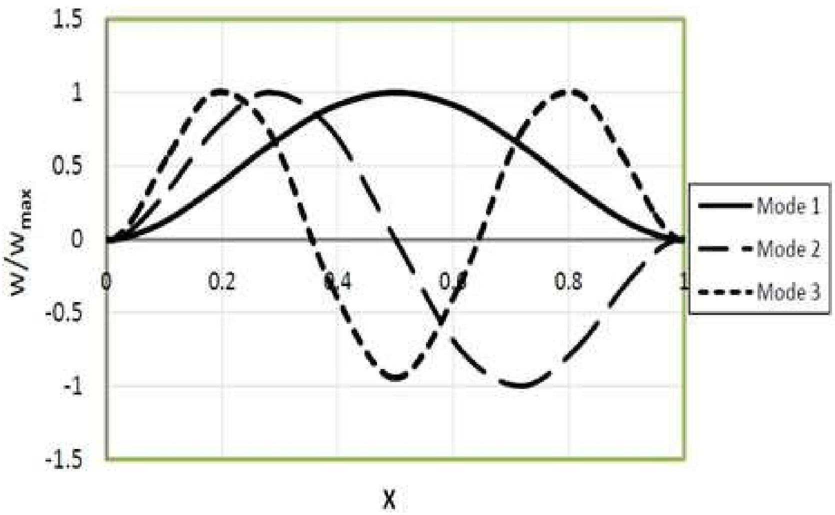

Figure G.8: Mode shapes for a clamped beam (n=1,2,3), [2].

Table G.4: ULS exceedence point for multiple displacement velocities, respectively for 50, 100, and 200 m water depth.

Simulation	Water depth	u	Intersect f_y
E50.1	50 m	250.0 mm/s	0.22 m
E50.2	50 m	125.0 mm/s	0.24 m
E50.3	50 m	62.5 mm/s	0.18 m
E50.4	50 m	31.3 mm/s	0.15 m
E50.5	50 m	12.5 mm/s	0.16 m
E50.6	50 m	6.3 mm/s	0.16 m
E50.7	50 m	3.1 mm/s	0.16 m
E50.8	50 m	1.6 mm/s	0.16 m
E100.1	100 m	250.0 mm/s	0.61 m
E100.2	100 m	125.0 mm/s	0.73 m
E100.3	100 m	62.5 mm/s	0.79 m
E100.4	100 m	31.3 mm/s	0.81 m
E100.5	100 m	12.5 mm/s	0.80 m
E100.6	100 m	6.3 mm/s	0.81 m
E100.7	100 m	3.1 mm/s	0.81 m
E100.8	100 m	1.6 mm/s	0.81 m
E200.1	200 m	250.0 mm/s	1.12 m
E200.2	200 m	125.0 mm/s	1.99 m
E200.3	200 m	62.5 mm/s	2.00 m
E200.4	200 m	31.3 mm/s	2.00 m
E200.5	200 m	12.5 mm/s	2.00 m
E200.6	200 m	6.3 mm/s	2.00 m
E200.7	200 m	3.1 mm/s	2.00 m
E200.8	200 m	1.6 mm/s	2.00 m

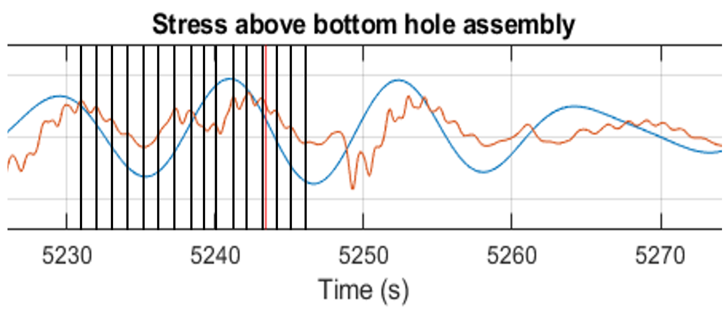

Figure G.9: Frequency determination for the stress response of an active compensated system for a water depth of 50 m

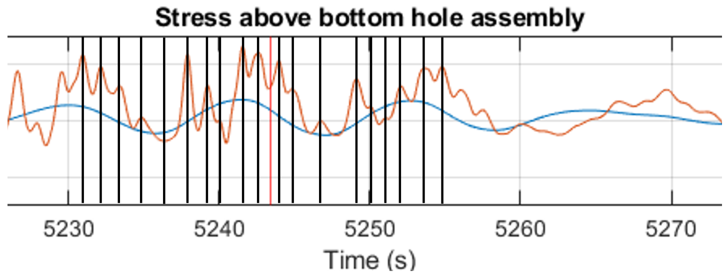

Figure G.10: Frequency determination for the stress response of an active compensated system for a water depth of 100 m

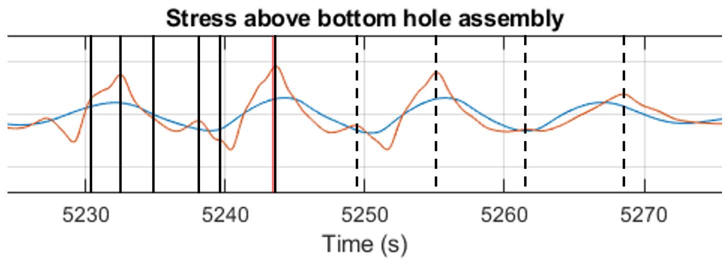

Figure G.11: Frequency determination for the stress response of an active compensated system for a water depth of 200 m

H

Appendix - Validations and verifications

Validation of stress measuring point

The figures below show the bandwidth in which the stresses occur over a 3-hourly time series. Presented over the length of the drill-string. The vertical axes shows the length as positioned during operation. Where 0.0 is the topside position.

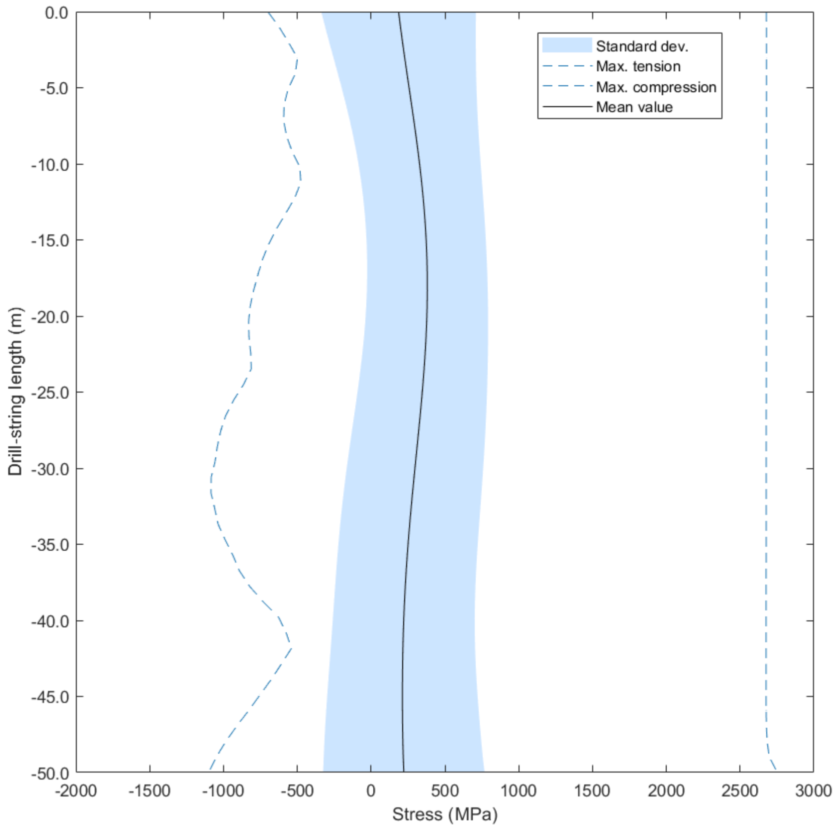

Figure H.1: Stress bandwidth over the full length of the drill-string during a 3-hourly time series performed for a JONSWAP wave spectrum with T_p = 8.0 s and H_s = 1.5 m and a water depth of 50 m.

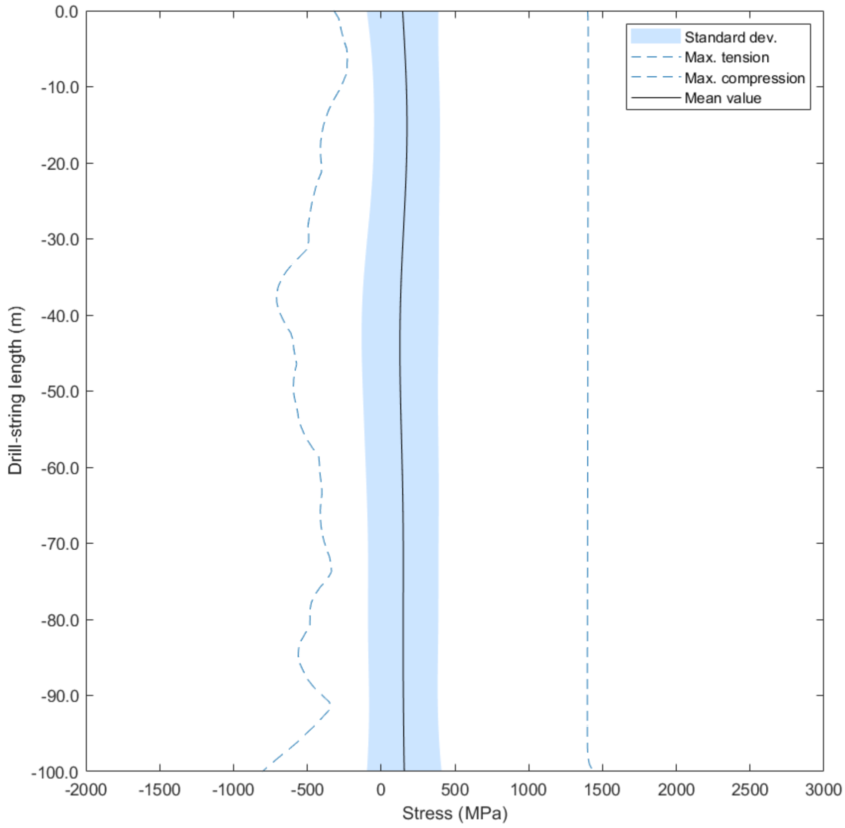

Figure H.2: Stress bandwidth over the full length of the drill-string during a 3-hourly time series performed for a JONSWAP wave spectrum with T_p = 8.0 s and H_s = 1.5 m and a water depth of 100 m.

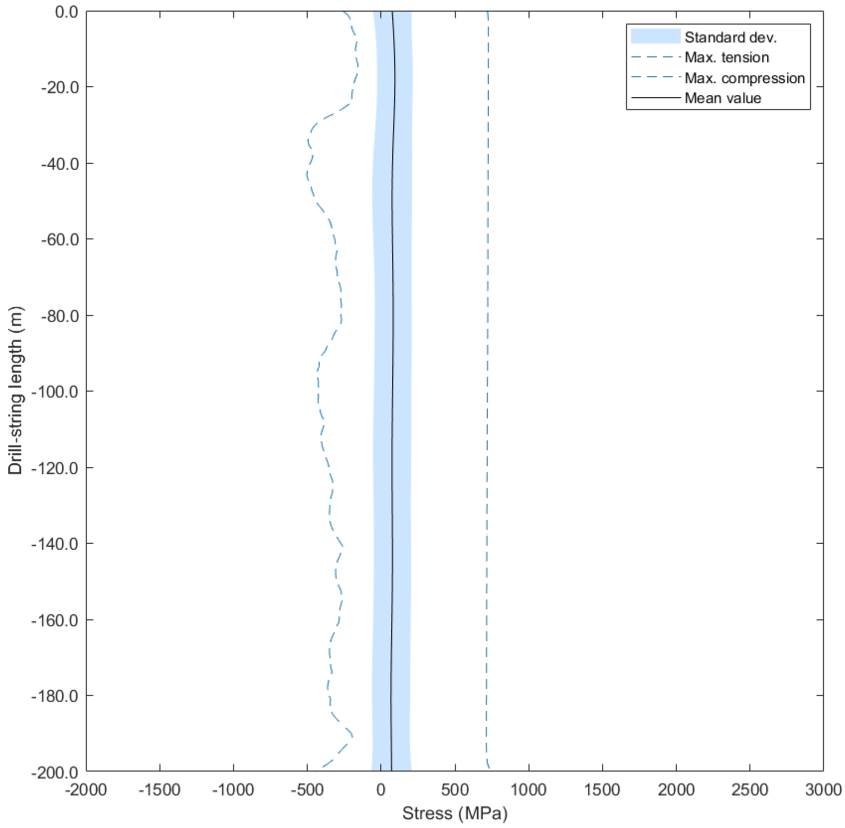

Figure H.3: Stress bandwidth over the full length of the drill-string during a 3-hourly time series performed for a JONSWAP wave spectrum with T_p = 8.0 s and H_s = 1.5 m and a water depth of 200 m.

Verification weight on bit results

To validate the weight on bit results, the correlation between the WOB and BHA stresses are assessed. As is visible in Figure H.4, there is a linear correlation between the stress above the bottom hole assembly and the weight on bit. This is expected as the stress vector above the bottom hole assembly is directed vertically. And thus the correlation can be described as the translation of stress to load through the cross-sectional area. At zero stress above the bottom hole assembly, the weight on bit corresponds with just a little less than 30 tonnes, which is the weight of the bottom hole assembly subtracted by the buoyant force working on it.

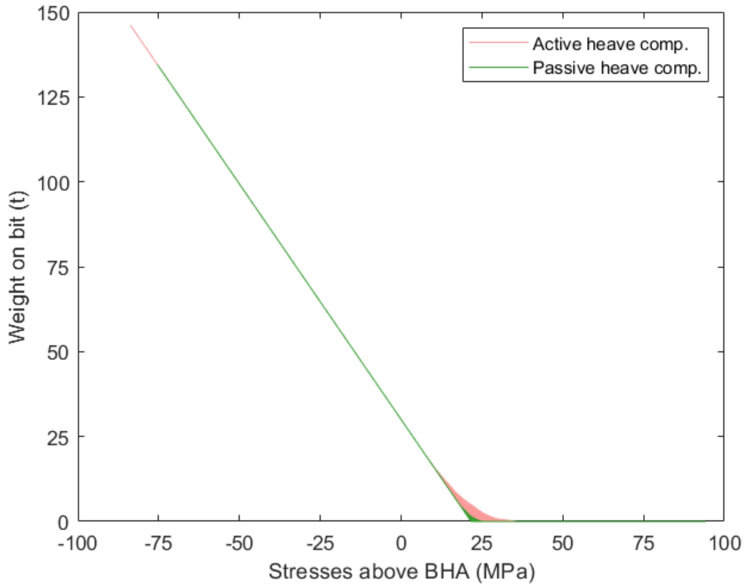

Figure H.4: Correlation between the stresses above the bottom hole assembly and the weight on bit acting on the seabed for a water depth of 50 m. When the bottom hole assembly leaves the seabed, the weight on bit becomes zero.

When approaching the zero weight on bit the correlation shows non-linear behaviour. The weight on bit data is manipulated during post-processing to never become negative and have zero as a minimum, as is visible in Figure 5.8. This leads to a discrepancy when describing the correlation. Here the higher frequency vibrations which are visible for the system with active heave compensation results in a larger scatter in this transition zone. This scatter is smaller for the system with passive heave compensation due to the more regular stress response in the drill-string around zero. Thus this scatter is the result of post-processing, without post-processing the relation is fully linear.

I

Appendix - Sensitivity analysis

In this appendix a sensitivity analysis is presented to the assumptions made in the research. In this sense the assumptions are validated or recommendations are substantiated for further research.

Wave loading under an angle

To assess the sensitivity of the operation to wave loading under an angle, a wave spreading is added to the model. This wave spreading is model using a spreading function in the form of $\cos^n$. Here n is the spreading component, which is selected to be 24. This gives a spreading up to approximately 35 degrees on both sides of the target wave direction, which is 180°. The stress statistics for each scenario are presented in Table I.1. It is visible that for all water depths there is less tension in the drill-string and larger standard deviations occur for both systems. The active systems relatively reacts more sensitive to the wave loading under an angle than the passive system. The effect becomes smaller for larger water depths. The increase of stress standard deviation is expected as the vessel experiences motions in more degrees of freedom. As the drill-rig in positioned at the moonpool, the effect of the motions is kept as mimimal as possible.

Table I.1: Stress statistics as result of directional wave spreading with a spreading exponent of 24 for a $\cos^n$ spreading function. Assessed for both heave compensation methods and all three considered water depths and a wave condition with T_p = 8.0 s and H_s = 1.5 m.

Water depth	Heave comp.	Mean	Std.
50 m	Passive	10.8 MPa	24.7 MPa
	Active	12.3 MPa	17.1 MPa
100 m	Passive	10.7 MPa	8.5 MPa
	Active	11.4 MPa	8.0 MPa
200 m	Passive	14.5 MPa	12.2 MPa
	Active	15.7 MPa	18.4 MPa

Drill-string stiffness

The mean stress over the time series decreases for a drill-string with increased stiffness, meaning it shifts more to the compressive domain. This is expected for the stiffer system and the relative change in mean is largest for 50 m water depth. The standard deviation increases slightly for the stiffer system. The percentual change in mean and standard deviation is not in the same order as the stiffness increase. The wall thickness is increased as presented in Table I.2.

Table I.2: New inner diameters of the drill-string required for a stiffness increase or decrease.

Stiffness change	D_{inner}	D_{outer}
+20 %	0.2740 m	0.310 m
0 %	0.2810 m	0.310 m
−20 %	0.2876 m	0.310 m

Table I.3: Stress statistics as result of a stiffness change in the drill-string. Assessed for the situation without heave compensation for all three considered water depths and a wave condition with T_p = 8.0 s and H_s = 1.5 m.

Water depth	Stiffness change	Mean	Δ	Std.	Δ
50 m	+20 %	208.7 MPa	-3.6 %	510.7 MPa	0.5 %
	0 %	216.4 MPa	-	508.2 MPa	-
	−20 %	224.7 MPa	3.8 %	502.9 MPa	-1.0 %
100 m	+20 %	155.2 MPa	-1.3 %	255.5 MPa	0.9 %
	0 %	157.2 MPa	-	253.3 MPa	-
	−20 %	158.2 MPa	0.6 %	252.5 MPa	-0.4 %
200 m	+20 %	72.1 MPa	0.8 %	142.1 MPa	1.7 %
	0 %	71.5 MPa	-	139.8 MPa	-
	−20 %	70.8 MPa	-1.0 %	139.3 MPa	-0.4 %

Variation in pre-tension

In this section, a variation in the drill-string pre-tension is applied and the effects of this modification is assessed by analysing the drill-string stresses and the drill-string stress statistics.

Table I.4: WOB statistics as result of a pre-tension increase in the drill-string. Assessed for the two heave compensation situations for all three considered water depths and a wave condition with T_p = 8.0 s and H_s = 1.5 m.

Water depth	Pre-tension variation	Mean	Δ	Std.	Δ
50 m	$+50$ %	224.1 MPa	3.6 %	516.0 MPa	1.5 %
	0 %	216.4 MPa	-	508.2 MPa	-
	-50 %	206.8 MPa	-4,4 %	502.8 MPa	-1.1 %
100 m	$+50$ %	160.5 MPa	2.1 %	256.7 MPa	1.3 %
	0 %	157.2 MPa	-	253.3 MPa	-
	-50 %	153.0 MPa	-2.7 %	251.8 MPa	-0.6%
200 m	$+50$ %	75.3 MPa	5.3 %	141.6 MPa	1.3 %
	0 %	71.5 MPa	-	139.8 MPa	-
	-50 %	67.0 MPa	-6.3 %	137.6 MPa	-1.6 %